Design and Control of Household CHP Fuel Cell System

Korsgaard, Anders Risum

Publication date:
2008

Document Version
Accepted author manuscript, peer reviewed version

Design and Control of
Household CHP Fuel Cell System

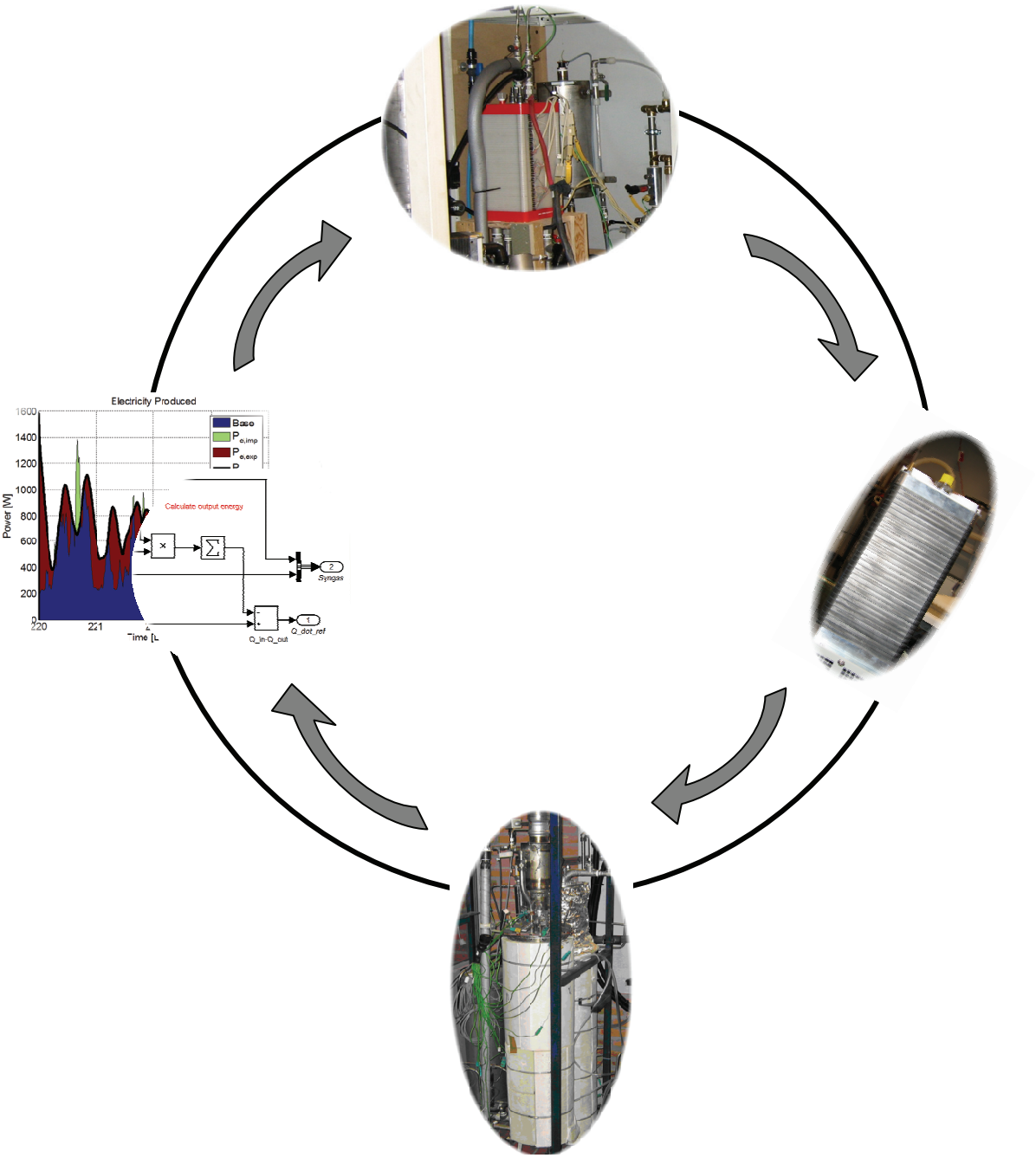

PhD. project Dissertation

Anders Risum Korsgaard

Institute of Energy Technology

Aalborg University

Autumn 2003 - Autumn 2006

Aalborg University

Institute of Energy Technology, Pontoppidanstræde 101, 9220 Aalborg East

Title: *"Design and Control of Household CHP Fuel Cell System"*

Anders R. Korsgaard, M.Sc. Mechanical Engineering, e-mail: ark@serenergy.dk. Department of Thermal Energy Systems, AAU, IET. September 2007.

Supervisors:

Søren Knudsen Kær (in the period 2003-2006)
(Associate Professor, AAU, IET)

Mads Pagh (in the period 2004-2006)
(Assistant Professor, AAU, IET)

Members of the Assessment Committee:

Mads Pagh Nielsen
Assistant Professor, Department of Fluids and Combustion Engineering, AAU, IET.

Soeren K. Kær
Associate Professor, Department of Fluids and Combustion Engineering, AAU, IET (Chairman)

Pages: 122

Publications: 6 included of which 3 were submitted to journals, 2 to conferences and 1 is still unsubmitted.

Front Page Photos : Illustration of the work flow in the Ph.D. project containing some of the laboratory test components and Matlab®Simulink simulations.

Abstract

The objective of this doctoral thesis was to design a simple, flexible and robust fuel cell system for micro combined heat and power (μCHP) systems for local households.

Several components in the PEM fuel cell systems were tested and modeled. During the first part of the Ph.D. main focus was put on the low temperature PEM fuel cell technology, but as the system complexity needed for this technology was high, focus shifted towards the high temperature PEM technology. This technology offers increased resistance toward impurities in the reformat stream such as carbon monoxide.

Laboratory tests on both technologies were performed and an empirical model was developed for the HTPEM technology. The model take into account variations in operating temperature, cathode stoichiometry, CO content in reformat stream and current density.

The fuel cell model forms the basis of the transient Matlab®Simulink model which, beside the fuel cell, takes into account fuel processor components such as steam reformer, heat exchangers and water gas shift reactor.

A novel system layout was invented and simulated for a whole year cycle taking as input the transient energy consumption of 25 single family houses and timely dependent grid electricity and natural gas prices. A total efficiency of 85-94%$_{LHV}$ was obtained with a variable cost margin, compared to a traditional natural gas furnace, of app. 400-600€ per household.

Indholdsfortegnelse

1 Introduction

In this chapter the fuel cell based micro combined heat and power system will be explained, starting with the general overview of such a system. This is followed by a brief introduction to the major technical system components.

1.1 Introduction to the fuel cell technology

1.1.1 Introduction to μCHP

In the recent years the energy sector has received increased attention due to the concern for oil shortage and the present dependency on politically unstable foreign nations. Additionally, concerns such as the green house effect and a general depletion of our energy reserves have played a significant role in the debate.

This has caused the development of a range of new energy technologies such as windmills, solar cells, bio-fuels and fusion energy. All of them have inherent weaknesses and strengths and in general they must be thought of as a piece of the puzzle. This also counts for Micro Combined Heat and Power (μCHP) systems dealt with in this thesis.

While most of the technologies mentioned above supply or harvest energy, combined heat and power should be thought of as an efficient way of converting these (or more traditional energy resources) at the right time and place to the energy form needed. By combining the generation the heat loss typically associated with electricity production can be used for heating or even cooling purposes under certain circumstances. By taking this conversion system into local households or larger building complexes the word micro comes into play. So why is this interesting, considering that most of us trust in "big is better" (or at least cheaper)?

In Denmark, as many other countries, small to large scale combined heat and power plants have been widely spread for decades. However, in general the transmission losses associated with the transport of energy from the central and even decentralized power plants to the domestic households is of major concern. By repositioning the energy conversion step to the location of the end consumer, it is believed that significant savings can be achieved. However, it must also be considered that the co-generation of heat and power tends to introduce problems for the grid. What is causing these problems?

The answer is that heat and power consumption is offset, meaning that when producing heat, the electricity is not always required. This weakness is amplified when combined with most stochastic renewal energy sources, which produces energy when the sun or wind is available (of course with the exception of hydro power).

So besides producing heat and electricity μCHP should also aim to improve this situation and maybe even increase grid stability.

Besides fuel cell technology which is treated in this thesis, there has been performed extensive work on other technologies for μCHP purposes. These include systems based on the traditional internal combustion engine, which have used in various projects including [1]. It was seen however that the electrical efficiency was rather low (20-30%). A number of companies supplying these kinds of systems exist including EC-power, Senertec and Ecopower.

In recent years the Stirling engine has been receiving more focus even though the efficiency, this technology can offer, is relatively low. This is mainly due to the relatively low cost and simplicity of the system making it fairly easy to introduce to the market. Moreover also issues such as a very long lifetime, silent operation, low maintenance cost and high fuel flexibility makes it attractive. On of the most dominant players (at least on the European Market) is the company Whisper Tech, which signed a contract with the British energy company E.ON in 2004.

The fuel cell based CHP systems offer a range of advantages over the competing technologies which include:

- Higher efficiencies ranging from 30-50% for the overall system should be possible depending on the system configuration and fuel cell type used.
- A high turn down ratio, so the system can accommodate the consumption at any given time.
- In some cases a rapid startup and quick transient response in order to play a role in grid stabilization.
- Potentially low cost even though this still has to be proven.

Today most believe that μCHP will be spread through larger fleet owners who lease systems to the end users in domestic households. These companies will negotiate terms for gas delivery and electricity import/export conditions to the grid.

1.1.2 Fuel cell basics

Fuel cells are electrochemical devices, which efficiently convert energy in the form of hydrogen directly into electricity without combustion and with no moving parts. The process is the opposite of electrolysis and can be compared with the reaction taking place in batteries. The basic reaction is shown in equation:

$$2H_2 + O_2 \rightarrow 2H_2O + 4e- \quad (1)$$

The following figure illustrates the principle of a single proton exchange membrane (PEM) fuel cell:

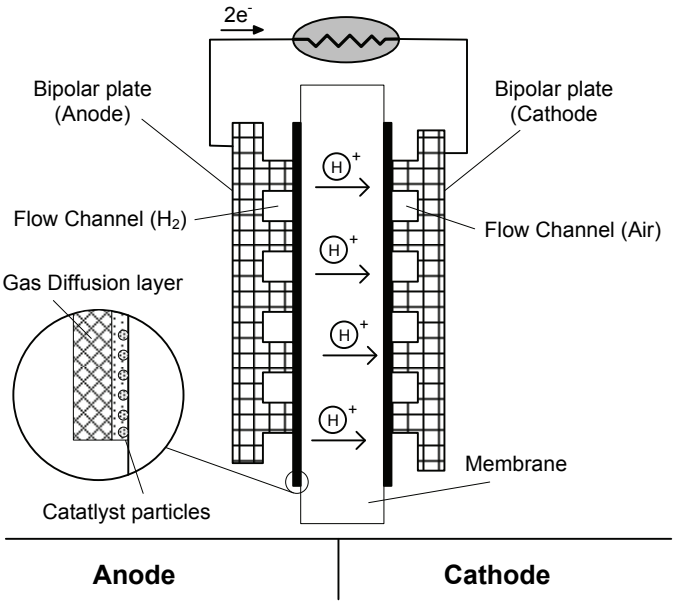

Figur 1: Schematics of a single PEM fuel cell.

An electrolyte separates the anode and the cathode side, allowing only protons (H^+) to pass. Hence the electrons released from the catalyst layer on the anode side are forced through the external circuit hence driving the load. On the cathode side they recombine with oxygen (usually supplied in the form of air) and protons, which have passed through the membrane, producing only water.

The cell voltage would theoretically be 1.48 V if the water was formed in condensed form at 25°C. Since this is usually not the case the theoretically limiting voltage is app. 1.25 V depending on the operational temperature of the cell. Usually 10-100 cells are connected in series to produce a fuel cell *stack* with a higher voltage but at the same current, as the single cell. Today typical maximum current densities (operated on air and not pure oxygen) are in the range from 0.5-2 A/cm^2.

Typical realistic operating cell voltages are between 0.5 and 1V per cell, due to chemical activation, concentration and ohmic losses. These irreversibilities are highly non-linear. Not only do the losses differ from stack to stack but also from cell to cell inside the stack due to manifold design, temperature and specie distributions and production differences.

1.1.3 The road from natural gas to the fuel cell

Since PEM fuel cells cannot operate directly on higher hydrocarbons, such as the content of natural gas, the fuel needs to be split into hydrogen and some by-products. Ideally this can be exemplified by the endothermic *steam reforming* reaction of methane:

$$CH_4 + x_2 H_2O \rightarrow x_2 H_2 + x_3 CO + x_4 CO_2$$

In real systems additional components exist in the gas leaving the reformer including sulphur containing molecules. To clean up the gas, additional steps such as water gas shift and sulphur traps are added prior to or after the reformer it self. All these reactors are commonly termed a *fuel processor* and will be discussed in more detail in section 2.2.

1.1.4 Fuel cell based μCHP

Fig 1 shows a basic fuel cell CHP system for a domestic household. From left the natural gas enters the house, being converted into a hydrogen rich mixture in the fuel processor, from

where it enters the fuel cell. The fuel cell produces electricity, which is fed to the DC/AC inverter providing the power directly to the household or exporting it to the grid. In the case when the fuel cell does not produce sufficient power to meet the household demand, electricity is imported from the grid. As a by-product from the electricity production the fuel cell produces heat, which is fed to the hot water storage. It acts like a thermal buffer enabling a timely offset between power and heat consumption.

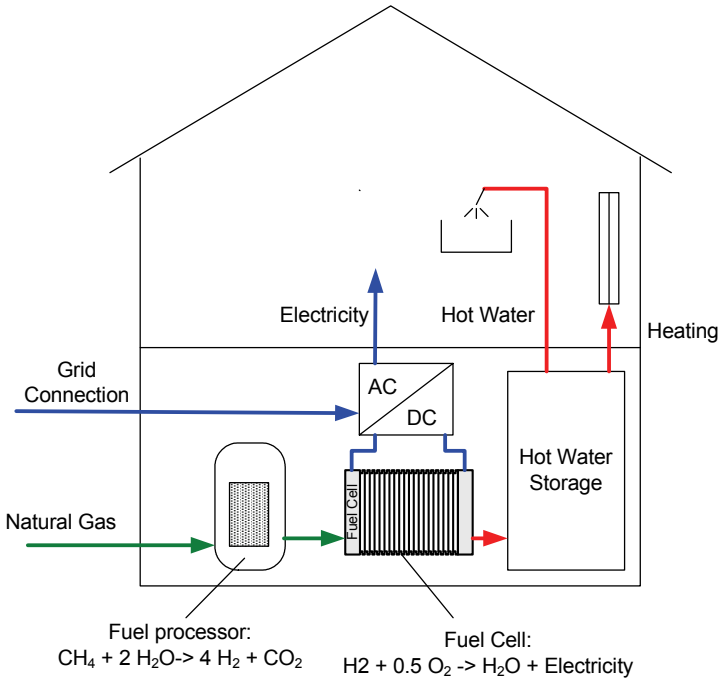

Fig 1: Fuel cell based CHP system for domestic household

If the system is operated with no grid connection at all, it is termed island operation, indicating that all electricity consumption of the household must be supplied by the fuel cell system. The simplicity of such a system is obvious as only one external connection (natural gas) needs to be provided for the house but on the other hand it puts large constraints on the systems reliability and the advantages of possible grid stabilization are not present.

1.1.5 Market and technology perspectives

The overall vision of micro CHP is that electricity is produced as a by-product from the heat production already taking place in several households using traditional gas furnaces. This is in contrast to the heat and power produced in central CHP plants which suffer from transmission losses to the household. In theory, if produced where the consumption is, the overall efficiency can be close to 100%. Since heat and hot water is not consumed simultaneously the electricity can be decoupled from the heat production using a thermal buffer. This would typically be a hot water tank.

Additionally, these small power plants, if there are enough of them, can help stabilize the grid by supplying peak power production to the grid, saving one or more peak power plants. This will in turn allow additional renewable energy sources to be installed.

RWE (a large German energy supplier) estimated in a presentation at the conference Grove Fuel Cell 2005, that there are more than 3.5 million potential units in Europe based on the number of natural gas furnaces they could replace. However, not all of these will be converted to micro CHP and they suggested that 10% would be a more realistic number counting in total 400.000 annual units. Of these figures the German market alone accounts

for 40-60.000 annual units. This makes a fairly large market of an estimated value of 800 M€ based on 2kWe units at sales price of 1,000 €/kW net system power.

From a national point of view, Denmark currently has 300.000 households with natural gas furnaces installed. ***Fig 2*** shows the extensive web of natural gas pipelines currently installed in Denmark. Denmark has currently (2005) a net-export of natural gas.

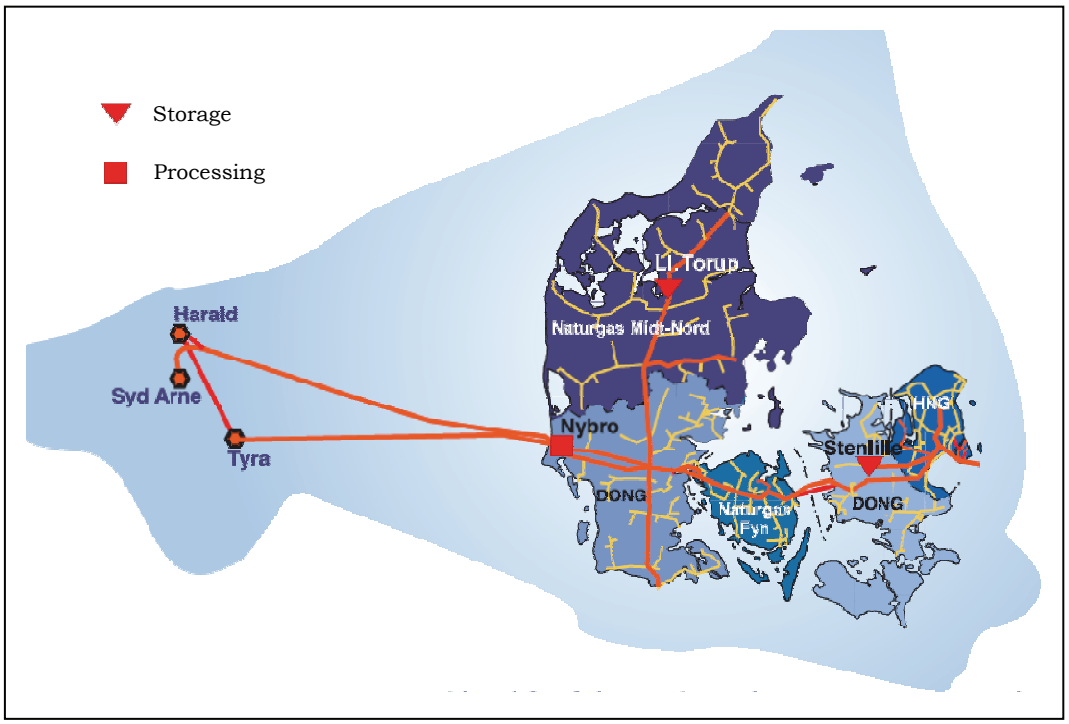

Fig 2: Natural gas pipelines in Denmark.

2 Scope of Project

2.1 Background analysis for µCHP

2.1.1 The Danish electricity grid

In the previous chapter the macro perspectives of the fuel cell based µCHP technology were discussed. In this section the focus will shift towards the impact the technology could have on the national electricity grid in Denmark. However, it is believed that the content will have general relevance to other countries as well.

Referring to Energinet.dk (October, 2006), Denmark has a capacity of 7,269MW of central power plants, 2,217 MW on decentral power plants and 3,133 MW from Wind power. This makes the electrical infrastructure in Denmark one of the most challenging in the world. Most of the central and de-central power production facilities are co-producing units which largely constraints the control system. Additionally, windmills have been installed to such an extent that production from wind energy is larger than the power consumption in some periods during the year. Fig 3 shows an example of such a situation.

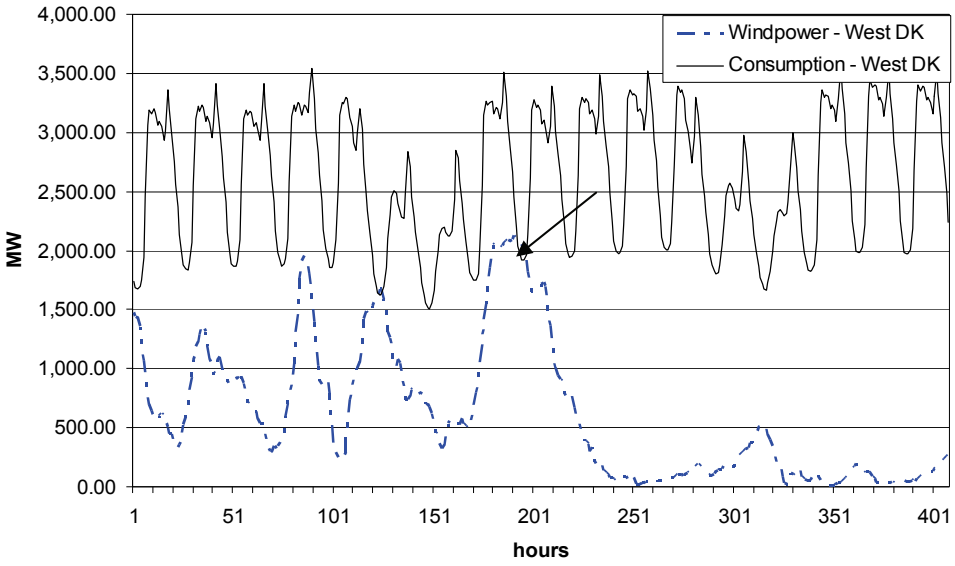

Fig 3: The wind production and power consumption from early November and 2 weeks ahead.

In order to maintain grid stability, significant amounts of electricity is imported/exported across the borders. In extreme cases the spot price on electricity falls to zero and even below.

Table 1 shows a list of the major power producing plants and units in Denmark. The numbers shown are estimates based on litterature studies performed by Énergistyrelsen, Elsam and Energinet.dk (formerly Eltra). Most of the central power plants in Denmark use coal as the primary fuel and a great effort has been put in optimizing these. The total peak

efficiency (heat and power) of these are up to 93%$_{LHV}$ and 52%$_{LHV}$ peak when producing electricity (Avedoere 2) only. These figures are at the optimal conditions and can not be obtained simultaneously. The plants can be turned down to app. 20% of fuel load, but they suffer from a maximum load change of 4%/min. This is often not sufficient to accommodate the disturbances produced by other producers (and consumers) on the market.

Single cycle gas turbines can produce at a similar efficiency but are limited to 20-47% maximum efficiency depending on size. They are typically used at central and de-central natural gas fired plants. However, they are able to respond fairly quickly with load gradients of 10-20 MW/min for the large scale plants (app. 10-20%/min). The maximum turn down is 40-60% of peak power due to the current legislation concerning NOx emissions. They are rather in-expensive to build with 400-530€/kW in specific investment for the larger units, and the maintenance costs are also fairly low. Some of these units also provide peak power production during high consumption hours.

Combined cycle plants are extremely efficient electricity producers but the total efficiency is a bit below the other types, due to high air-to-fuel ratios used. The investment is also fairly low but maintenance costs are a bit higher. The remaining figures are similar to those of the single cycle type.

Wind turbines actually present a low initial investment taking into account that the fuel cost is non-existent. The maintenance costs are however fairly high. The obvious drawback is naturally the non-predictive behavior.

Micro combined heat & power systems based on gas turbines are also included. From the analysis performed they should be regarded as units producing electricity as a by-product, taking into account the electrical efficiency of only 20%. The investment is also fairly high with app. 1000€/kW in initial investment. The overall efficiency is low compared to existing gas furnaces which has demonstrated figures beyond 90%.

	Specific Investment	O&M total	Fixed O&M	Variable O&M	Total eff. (peak)	Electrical eff. (peak)
	M€/MW	**€/MWh**	**k€/MW/yr**	**€/MWh**	**%**	**%**
Advanced pulverized coal power plant	1.1		16	1.8	93	52
Gas turbines single cycle						
Large, 40-125 MW	0.44-0.53		6.7-8	2.0-3.0	92	42-47
Medium, 5-40 MW	0.57-0.86		8	2.5-4	92	36-46
Mini, 0.1 - 5 MW	0.8-1.7	1			80-90	32-42
Micro, 0.003 - 0.010	0.8-1.4	8.0-12.0			65-80	20
Gas turbines combinedsingle cycle						
Large, 100-400	0.4-0.7		11.0-14.0	1.5	90	58-62

Small, 10-100	0.57-0.83		10	2.5-3.5	90	47-55
Wind turbines						
On land	0.62-0.75	8				
Offshore	1.0-1.3	4.0-6.0				
Micro combined heat and power systems						
Gas turbine, 3-10 kW	0.8-1.4	1.0-3.0			65-80	20
Gas engine, 1-20 kW						

Table 1: Major power producing technologies. Expected figures for 2010-2015 [2].

2.1.2 Consumer energy prices

Energy prices for the Danish consumers have been taxed increasingly over the last couple of decades. Table 2 shows an example of the composition of the total electricity price as it looks for the private users in the northern part of Denmark. It is evident that the electricity price in itself only contributes with about 25% of the price, while the rest is mainly taxes and VAT. It should also be noted that the grid payment also contributes with more than 25% of the electricity price itself.

Description	**Price**	**Unit**
Electricity price	52.4	€/MWh
Grid payment	15.2	€/MWh
Public contribution	8	€/MWh
Electricity tax	71.47	€/MWh
CO_2 tax	12	€/MWh
Distribution tax	5.33	€/MWh
VAT	41.11	€/MWh
Total price	205.51	€/MWh

Table 2: Consumer electricity price [3]

Table 3 shows the composition of the consumer gas price based on numbers from DONG Energy. The numbers from the source are converted into kWh instead of m^3. According to DONG the lower heating value (LHV) of natural gas is 11.05 kWh/Nm^3. Additionally an exchange rate of 7.5 DKK/€ is used. In comparison the gas price itself is only marginally cheaper than the electricity price. However, the taxes are much lower which makes it economically viable to use natural gas for heating instead of electricity.

Description	**Price**	**Unit**

Gas price	48.0	€/MWh
Natural gas tax	24.6	€/MWh
CO_2 tax	2.4	€/MWh
Transport	11.7	€/MWh
Vat	21.7	€/MWh
Total price	108.4	€/MWh

Table 3: Consumer gas price [4]

If the natural gas is used to produce the electricity consumed, a margin close to 50% would be obtained. It is questionable, however, if politicians would allow that in a larger scale when tens of thousands of units are producing electricity in this way. However, it could provide an incitement for the first few hundreds or thousands households to begin using micro CHP.

2.1.3 Market energy price structure

If the micro CHP is going to be introduced in larger scale, one has to look at it from a macroscopic point of view. Fig 4 shows the market electricity price in western Denmark. It is clear that the market price is below the average price discussed on the previous section of 52 €/MWh. The higher price is due to the subsidies paid to the environmentally friendly technologies such as decentral combined heat and power facilities and wind mills, although prices tend to increase slightly through 2005.

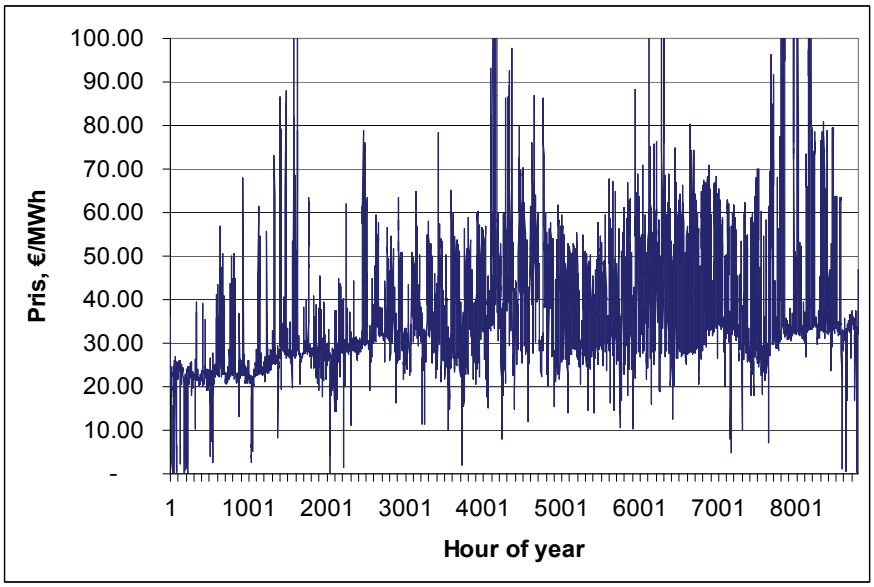

Fig 4: Electricity price DK-vest, year (Data set from energinet.dk, Oct. 2006).

From the above private consumer prices it would be impossible to compete with the spot price for electricity based on natural gas as a fuel. However, commercial customers can obtain natural gas corresponding to the prices shown in Table 4.

Description	**Price**	**Unit**

Gas price	31.6	€/MWh
Energy tax	24.6	€/MWh
CO_2 tax	2.4	€/MWh
Transport	11.7	€/MWh
Total price (excl. transport)	58.6	€/MWh

Table 4: Gas price for industrial consumers [6]

Moreover individual prices are set for larger customers.

Political support for decentralized CHP production is already present for two primary reasons. First of all, decentralized CHP plants will enable a larger fraction of the consumers utilizing the heat from power production, and hence decreasing CO_2 emissions. Secondly grid losses associated with heat distribution are in the order of 20% according to [7]. Moreover, the electrical grid loss could be as high as 19% in peak hours and 9% at low load as shown in Table 5. It has not been possible to validate these numbers against other literature.

Voltage Level	**Low load**	**High Load**	**Peak Load**
150+400 kV	2.8%	4.2%	4.7%
60 kV	2.1%	3.2%	3.6%
10 kV	1.4%	2.7%	3.5%
0,4 kV	2.8%	5.1%	6.8%
Total	**9.1%**	**15.2%**	**18.6%**

Table 5: Marginal electrical grid loss [8]

Moreover, as the electricity consumption is still increasing steadily grid expansion is performed continuously. Estimated cost according to the same source for reduced expansion expenses are shown in Table 6. These numbers are of course mainly suited for comparison when considering new parcel areas. If these numbers can be trusted, the specific investment is of the same order of magnitude as constructing the central single (or combined) cycle gas turbine it self. Another comparison could be made to the expected fuel cell cost beyond 2010, which is believed to be in the range of 3-400€/kW. Hence the saved investment in the grid could actually pay the cost of the fuel cell.

Voltage Level	**Kr/kW[1]**	**kr/kW[2]**	**€/kW[2]**
150 kV	1577	1810	241
60 kV	526	604	81
10 kV	297	341	45
0,4 kV	297	341	45
Total	**2697**	**3096**	**413**

Table 6: Savings due to reduced grid expansion. 1) Price index February 2000. 2) Price index August 2006 [8]

The above figures are used to set a price that reflects the benefit it has to produce heat and power locally. Table 7 summarizes these numbers. At high and peak load there is a quite large margin to the natural gas price in itself. However, at low load the margin is actually negative with the list price obtained from DONG indicating that transmission of the natural gas to the micro CHP system should be almost zero.

	Low load	**High Load**	**Peak Load**
A1/A2-tariff (60/10 kV and 50/10 kV)	28	58	76
B1/B2-tariff (10/0.4 kV)	28	61	81
C-tarif (0.4 kV-net)	29	65	88

Table 7: Time-of-day tariff (€/MWh) [9]

Table 8 shows the standard tariff periods. Note that weekends and holidays are all off peak throughout the day. It is also clear that peak load is in the morning and around noon and high load more or less the rest of the daytime.

Normal working days	**Low load**	**High load**	**Peak load**
Winter (October - March)	21.00– 06.00	06.00 – 08.00	08.00 – 12.00
		12.00 – 17.00	17.00 – 19.00
		19.00 – 21.00	
Summer (April - September)	21.00– 06.00	06.00 – 08.00	08.00 – 12.00
		12.00 – 21.00	

Table 8: Standard tariff periods [9]

It would make most sense to only produce electricity for the grid during daytime (high- and peak-load) and only cover the households own electricity demand the remaining time. One could even imagine that grid electricity is used (power, heat or both) during low load situations and completely shut down the system. This could make sense during summer nights and weekends where the heating demand is low and it may prolong the lifetime of the system components as they currently tend to degrade in a per-operating-hour manner (at least for some fuel cell types).

In the long run authorities will probably require the electricity production to be metered, whereas in the short term this is probably not the case. It is also not evident that the customers can pay (or receive) money for the net annual production as i.e. solar cells can in Denmark. Hence in the short term, the most economical control strategy will most likely be to operate the system in a close to island mode, where the transient power demand is almost completely satisfied by the fuel cell with the exception of minor power peaks.

Concluding, the majority of electricity is (and probably will be) produced by plants utilizing cheap fuel such as coal or renewables. Nuclear power could also be an option but since it is generally unpopular in the Danish population it will not be taken into further considerations here.

2.1.4 Choice of fuel for CHP applications

While oil production begins to peak there will still be fairly high volumes of natural gas reserves left. Fig 5 shows the annual consumption and estimated reserves. It can be concluded that based on the current consumption there is 64 years worth of reserves or more than 100 years from the estimated total reserves. Some of these however will be located in more remote areas difficult to access and as it can also be seen, they are by no means dispersed equally around the world.

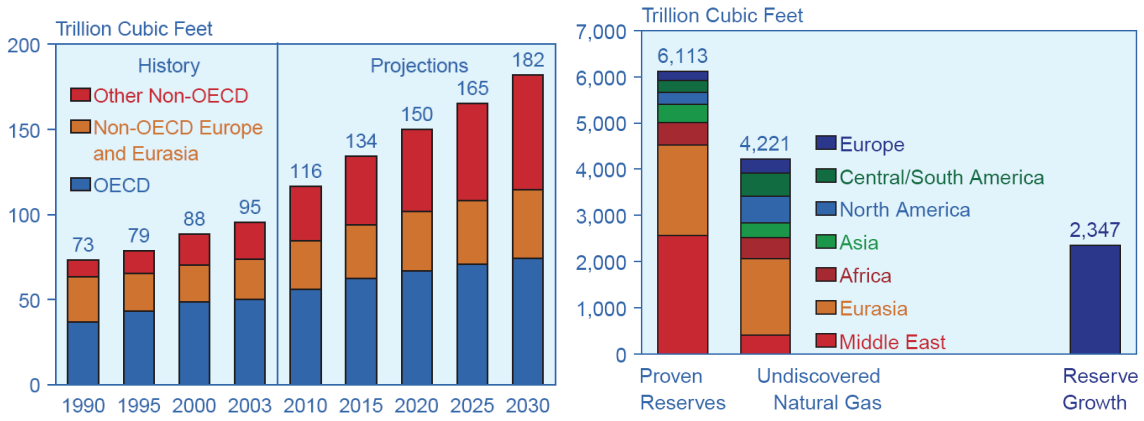

Fig 5: Left; current world natural gas consumption. Right; current estimated reserves. [EIA, 2006, http://www.eia.doe.gov/oiaf/ieo/pdf/nat_gas.pdf, sep. 2006]'

It is believed that a range of different new fuels will become available in the future. This could include biofuels (for instance ethanol, RME, compressed biogas or biodiesel) but the discussion about methanol as the energy carrier is increasing. The main advantage of methanol is that it can be produced from almost any organic source including natural gas (by reforming and afterwards a synthesis of H_2, CO and CO_2), coal or even biofuels using various enzymes or fermentation. Moreover, for fuel cell applications, it is a very convenient fuel especially because it is so easily reformed back to a synthesis gas usable directly in fuels at temperatures below 300°C. In terms of well-to-wheel it may even be more efficient transporting natural gas as methanol and it would presumably make the delivery more secure when regional stability is considered.

Summarizing natural gas may be the fuel of today and many years to come for micro CHP, but a range of other fuels may play an increasing role.

2.1.5 Input data from 25 single house heat and power consumption

In order to validate the feasibility of the system, it is very important to have a set of realistic input data. The remaining part of the analysis in this thesis will be based on datasets from 25 single family Danish houses from 1991. These include measurements every 15 minutes of a year of hot water, central heating and power consumption.

Fig 6 shows the total consumption of heat plus hot water and electric power respectively. It is seen that the total heat and hot water consumption for the houses varies from 4,800 to 20,000 kWh and the total electric power consumption from 2,850 kWh to 1,162 kWh.

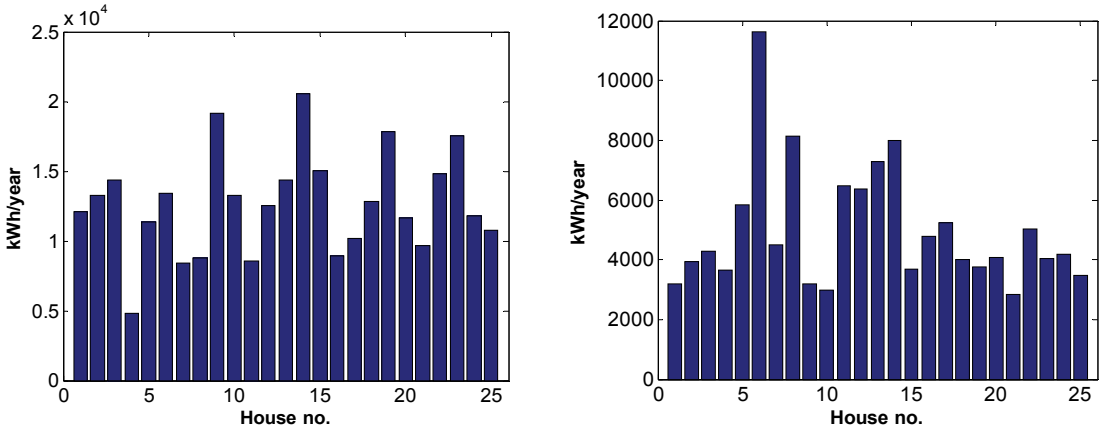

Fig 6: Left; total central heat and hot water consumption. Right; total power consumption.

Fig 7 shows the annual distribution of the consumption data, where the 25 datasets are averaged. It is seen that the hot water and power consumption is fairly constant throughout the year whereas the central heating demand varies, not surprisingly, from app. 2.5kW in winter time to practically zero during the summer months. This means that the heat-to-power ratio is app. 4-1 in the winter time and 1-1 during summer.

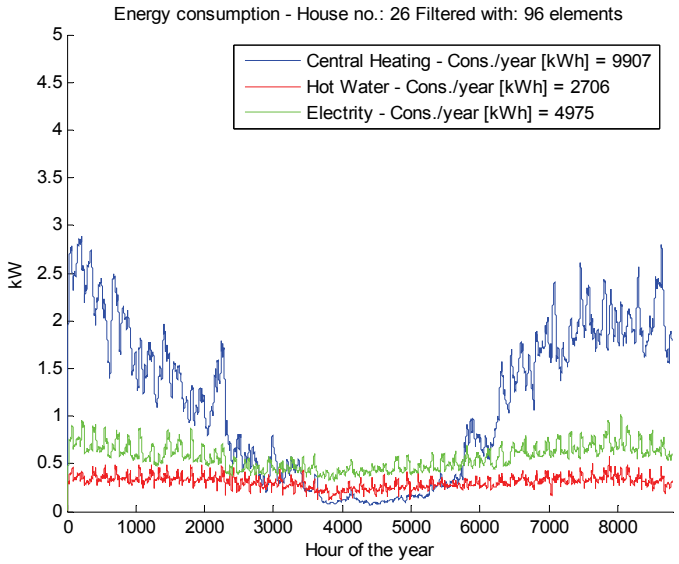

Fig 7: Average distribution of heat and power demand through out the year starting January 1st 1991. The dataset is additionally filtered with a running average (96 data points corresponding to one day).

Fig 8 shows the energy consumption distribution of house 6 (unfiltered). It is clear that this is a completely different pattern than the average scenario. The heat- to power ratio is no more than 2-1 in this case and in summer time (not shown in this figure) it is app. ½-1.

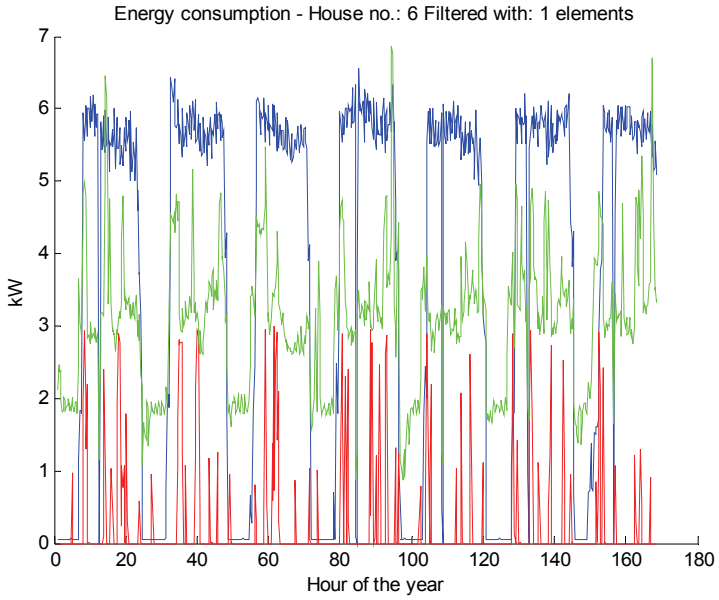

Fig 8: Distribution of heat and power consumption in house 6 during the first week of January 1991.

Hence the system has to be robust not only to large differences in consumption pattern between the different households but also to variations throughout the year. The heat-to-power ratio must be able to vary from around 1-1 during the summer months to 1-4 during winter for the average dataset, which will be even higher for specific households in the dataset. This would indeed be challenging. Hence it is most likely that the system is connected to the grid and not operating in island mode, as to cover peak consumption.

2.1.6 System performance specifications

From the preceding analysis it can be concluded which issues must be addressed when designing the CHP system. Table 9 summarizes these.

Description	**Demand**	**Added value**
Have a total efficiency equal to or higher than conventional gas furnaces	X	
Have an electrical efficiency comparable to that of central power plants (taking transmission losses into account)	X	
Have a fast transient response to have a load following characteristic in relation to the power consumption of the local household		X
Variable heat-to-power ratio		X
UPS capability		X
Provide peak power production capability for the market		X
Large turn-down ratio		X

Fuel flexibility	X

Table 9: Desired features of the fuel cell system

The demands for the system are the issues that must be fulfilled in order for the technology to be feasible. Added value features could be the decision making factor for customers switching to a new technology, as economical concerns are not necessarily the only driving force.

The total efficiency should be equal to or better than what can be achieved with conventional gas fired furnaces, as these units will be operating in heat producing mode in longer periods.

The electrical efficiency must be higher than what can be provided by central or de-central power plants in order to have a larger market potential. If it is not, the marginal production cost will not be lower and it would not make sense to implement these systems from a larger economical or political perspective. However, from the previous section it should be noted that the transmission losses from the central plants are by no means negligible. Additionally, the systems should always be able to supply the household with heat, so the total efficiency should not be lower than what the natural gas fired furnaces could provide. Target electrical efficiencies should be as high as 40-50%.

If the units are going to participate in future grid stabilization (which larger players on the market claim) they should be able to have a fast transient response, almost instantly to provide power in the case of sudden changes due to wind power, power plant black-outs etc. This however, might be a demand as the continuing development of renewable energy sources will tend to destabilize the grid.

The heating demand of households should always be accommodated. If the electricity production should be independent (i.e. in case of island mode or controllable grid export) a variable heat-to-power ratio is needed. This, however, might be questioned if the heating demand could be supplied by electricity during hours of low spot market prices.

UPS (Uninterruptible Power Supply) capability of the system might be an underestimated value for the customer. However, this would be an important feature if the frequency of black-outs and instability of the grid continuous to rise. This might be challenging as it will require changes in the current Danish legislation. Additionally, it may only be for some specified circuits in the local household powering light, computers, TV etc. to prevent overloading of the system during peak household consumption.

As the preceding sections also showed, the national tariff price structure gives rise to significant revenues if peak power production can be provided to the grid. This will significantly influence the payback time of the system.

The system should have a large turn-down ratio without sacrificing the high efficiency. Ultimately it could even be completely turned off to use cheap grid electricity also for heating. This could i.e. be in periods with very high wind power production.

Fuel flexibility could be a major concern when looking 10-25 years into the future referring to the previous discussion, even though it might not be so relevant at the present time. Other fuels, like methanol, will probably be available within the major commercialization period of micro CHP systems. However, the scope of this analysis will be limited to natural gas.

2.2 Technology

From the previous discussion it has been decided which key features the CHP system should have. The fuel cell related technologies to be used in order to fulfill the demands are described in this section. Fig 9 shows a basic fuel cell system with fuel processor connected with the typical inlet-outlet fluid flows. From left a mixture of natural gas and water enters the system in order for the reforming reaction to take place. Since this process is endothermic (it consumes energy) air needs to be supplied to release heat by oxidation of a kind of fuel (typically either natural gas or the combustible parts of the depleted anode gasses). From the fuel processor, the output gas stream (reformate gas) is fed into the fuel cell. After passing through the fuel cell the anode of gas leaves the fuel cell

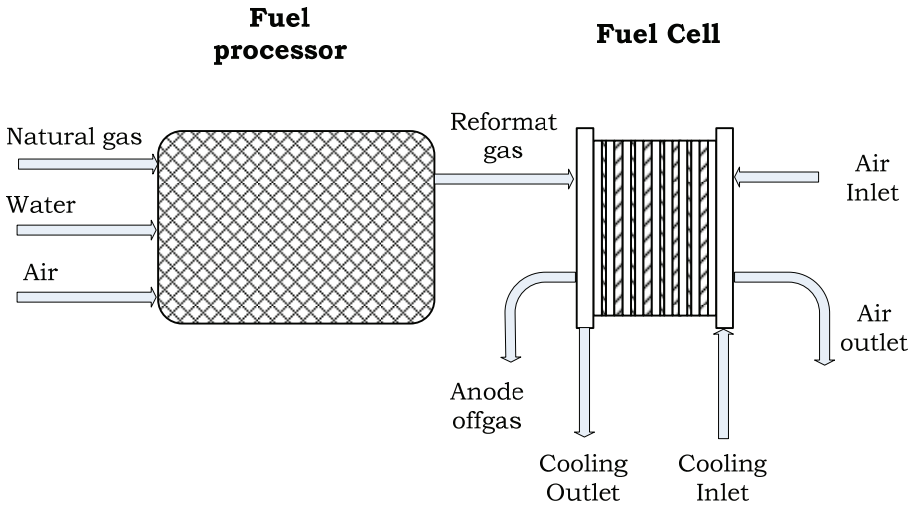

Fig 9: Basic layout of fuel cell system

On the right hand side air is supplied to the fuel cell providing the necessary oxygen for the process. In the bottom right a liquid or gas is entering providing cooling for the system. The excess heat removed by the fluids can cool the system.

2.2.1 Fuel cell types and issues

In the previous chapter a brief introduction to the fuel cell it self was given. In this section the different categories of fuel cells will be discussed.

In low temperature fuel cells that use a polymer membrane as electrolyte (PEMFC), protons are released on the anode side and transported through the membrane to the cathode. The most common in this polymer class is Nafion® produced by Dupont. This type has been widely spread during the last decade to almost every application. Due to the low operating temperature (20-80°C) it is very compatible with many polymers and metals used for constructing the stack such as gaskets and separator plates which are typically made by a polymer/graphite mixture. However in general, this type of fuel cell is very sensitive to pollutants such as carbon monoxide (<50ppm) and sulphur (in the range of ppb´s). Additionally the membrane needs to be humidified to obtain a high efficiency and to secure a long lifetime. Currently a number of MEA developers have shown degradation rates as low as few mV/1000 hours at 0.2 A/cm^2, permitting large scale commercialization and lifetimes exceeding 30-40.000 hours (see i.e. the fuel cell section of www.gore.com, 2006).

The cost of the membrane itself is expected to be very low, but the cost of the catalyst can add up a significant amount of the fuel cell cost itself. At the time of writing the cost of

platinum (the major cost component in the catalyst) is 1140 $/troy oz [10] which equals 36.7 $/g. To relate it to the fuel cell cost, typical Pt loadings are below 1mg/cm^2. One cm^2 of fuel cell typically outputs 0.2-0.6 W/cm2. Recalculated this yields an app. 60-180 $/kW. Several research groups have however already proved a factor of 10 reduction in Platinum use, so the calculated cost will be only 6-18$/kW. Usually, however, this comes of the cost of a shorter lifetime. Comparing that to expected prices of 1000-2000 $/kW, this will most likely not be the major obstacle.

Another type of polymer based fuel cell is the high temperature PEM fuel cell (HTPEMFC). It has been investigated thoroughly in the late 90´s by a few research groups in Europe and United States. It is most commonly based on the polybenzimidazole polymer which is not proton conductive in itself. However once doped with phosphoric acid, the conductivity is comparable with that of Nafion®. The operating temperature is between 120 and 200°C. Even though the catalyst used consist of many of the same materials as the low temperature PEM fuel cell it has a much higher tolerance towards CO (1-5%) and sulphur. Additionally, the membrane need not be humidified and so dry air can be used to feed the fuel cell. Degradation rates of the P1000 MEA of app. 5 mV/hour@0.2 A/cm^2 has been shown over nearly 25.000 hours. The next generation (P2000) is expected to decrease this number even further. Among the drawbacks is that the fuel cell have to preheated to >100°C prior to operation in order to prevent acid leaching and that the efficiency is slightly lower than low temperature version. Catalyst loadings are similar to those of the low temperature PEM fuel cell. Today the membrane electrode assembly (MEA) is produced mainly by a German company PEMEAS GmbH.

An older and well proven technology is the PAFC, which has a lot of similar properties to the HTPEM fuel cell including operating temperature and CO resistance. However, it suffers from the fact that it has a liquid electrolyte, which limits the achievable power density and complicates the stack design, preventing the large scale commercialization, even though these systems have been proven durable over long periods of time. It seems however that most activities within this technology have been decreasing in the current decade. One of the most well known companies working with PAFC is UTC fuel cell.

Solid Oxide fuel cells use a range of ceramic materials to produce a membrane that conducts O^{2-} ions, which are transported in the opposite direction compared to the PEMFC in the above explanation. This type is currently the most efficient fuel cell type. The high operating temperature of 600-1000°C makes it very resistant to pollutants such as sulphur and carbon monoxide (CO). In fact the latter is actually considered a fuel to this type of fuel cell. In some cases the fuel cell may even operate directly on natural gas (methane) even though a brief pre-reforming step is typically added to break down the higher hydrocarbons.

However, the combination of ceramic materials and high operating temperature make it sensible to thermal stress and mechanical stability, and the materials needed to produce the separation plates tend to be rather expensive compared to low temperature fuel cells. Moreover the slow transient startup needed to prevent mechanical failures makes it challenging to use in applications where startup time is an issue. Maybe most importantly it has yet to be proven that long term stability can be achieved under higher loads, low fuel utilization and lower temperatures (<600C) to make it compatible with less exotic materials such as traditional stainless steel. Haldor Topsoe published a range of degradation data in 2005 [13], showing fairly low degradation rates (2mV/1000 hours) when operated at app. 0.14 A/cm2 (12x12cm^2, 20A), but at higher current densities the degradation rate rise exponentially to tens and hundreds (mV/1000 hours) depending on the operating temperature. The fuel utilization ratio used was not given in the referred publication, but it is well know that this also influence the cell life drastically. At last it has yet to be proven that the SOFC technology can actually be produced at competitive prices (300-500€/kW)

which is the typical ambition for μCHP applications. This is yet again strongly linked to the operating temperature and the obtainable current density.

Molten Carbonate Fuel Cells (MCFC) are very durable and also operate at a fairly high operating temperature. The fuel cell stacks made until now have mainly been produced in larger power scales, ranging from a few hundred kilo watts to mega watts. The most well known company working on this technology is MTU Friedrichshafen. The technology is very flexible in terms of fuel, but the price is still quite high even for large scale units (~1000€/kW, presentation, MTU, ASME fuel cell 2006).

In the current project focus will be given towards the PEM type fuel cells as these offer some of the properties needed for CHP systems such as

- high efficiency
- potentially low cost
- transient operation capabilities

Other candidates might however also be interesting to investigate including especially the SOFC fuel cells due to its very high resistance towards impurities in the fuel stream and high efficiency.

2.2.2 Fuel processing

In the previous section it was concluded that the PEM category of fuel cells should be used for the current project why the following discussion will aim on picking the right type of fuel processor for this fuel cell type.

Fuel processors have been undergoing an extensive development in recent years, and many new companies have been established. Also the catalysts used for speeding up the desired chemical reactions have been receiving a lot of attention, thereby increasing performance and lowering cost of the units. This development, however, is still lacking behind the fuel cell development by a number of years.

Reforming

The steam reforming process was briefly described in section 1.1.3. Fig 10 shows a typical integration of such a unit and a fuel cell. Natural gas and water is injected from the right, and after reforming, the reformate gas is fed to the fuel cell. Since the fuel cell has to operate at an anode stoichiometric ratio well above 1 (typically at least 1.2) the remaining hydrogen can be combusted and heat exchanged with the endothermic reforming process. Typical reforming temperatures are in the range from 650-800°C in the case of natural gas. The remaining energy can be utilized for heating various reactants or supply heat to the central heating system.

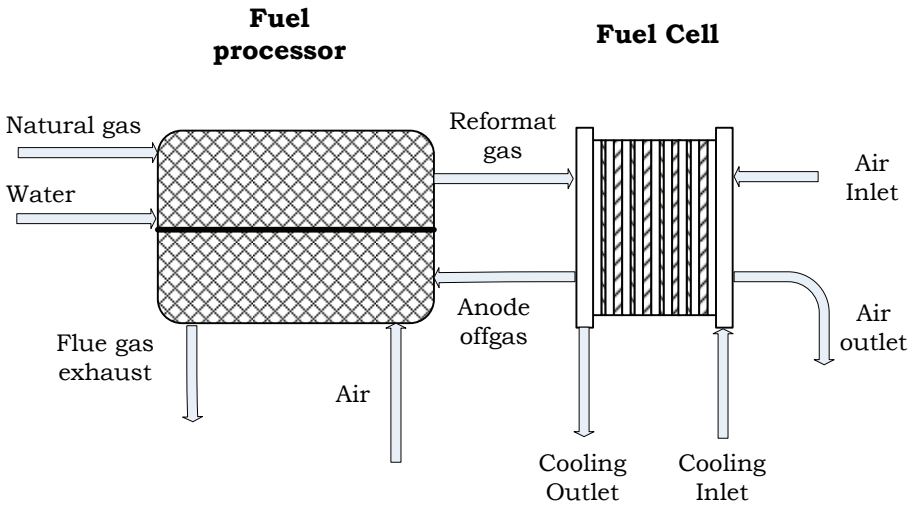

Fig 10: A simplified steam reforming based fuel processor followed by a fuel cell.

Another reforming method is *partial oxidation* (POX) where only oxygen (air) is let into the fuel stream simply oxidizing the fuel leaving relatively high amounts of CO, N_2 and CO_2 besides H_2. The main reaction is shown below.

$$x_1\ CH_4 + x_2\ O_2 \rightarrow x_3\ H_2 + x_4\ CO_2 + x_5\ CO$$

This process can become extremely compact because it operates at fairly high temperatures (1000-1200°C) where reaction kinetics are very fast quickly converging towards chemical equilibrium. A close relative is the Catalytic Partial Oxidation (CPO) where the operating temperature (900-1100°C) is a bit lower due to a catalyst having equally- or even faster kinetics.

A combination of the steam- and partial oxidation reformer is referred to as the *auto thermal* (ATR) reforming process, where oxygen (air) is supplied combusting a part of the fuel to maintain the right temperature of the steam reforming process. The operating temperature is equal to the steam reforming process (700-800°C) to maintain a relatively low CO content. A typical system configuration could look like that of Fig 9. This process exists both in a catalytic and non-catalytic version.

Other reforming methods include cracking and plasma reforming. These are not discussed in further detail since the application in CHP is not considered feasible.

While the steam reforming reaction needs heat exchanging to provide heat for the endothermic process, the reformer in itself tend to be larger in terms of volume than the other 3 reforming methods discussed. However the gas quality is higher as no nitrogen is present in the fuel stream increasing the fuel cell performance. Maybe more importantly, the anode off gas, which still contains fairly high amounts of H_2, can be used to provide the heat for the steam reforming process. This will in most cases increase the overall electrical system efficiency by 15-30%.

POX and CPO reformers are not considered a good choice for PEM fuel cells, as they produce very large amounts of CO. Since PEM fuel cells see carbon monoxide as a pollutant this would require a larger gas purification step.

Sulfur removal

Sometimes additional process steps are needed. One of them is sulphur removal depending on the type of fuel and fuel cell used. Danish natural gas typically contains 6-15 mg/m^3 sulphur [11] partly from the natural gas itself (H_2S) and some from THT which is a sulphur

containing aromatic substance added to give natural gas its characteristic odor. This corresponds to 7-18 ppm sulphur containing gas molecules. The type of sulphur removal depends on the reforming catalyst used. Some can tolerate in the range from tens to hundreds of PPM. The advantage is that not only is the reformer tolerant to larger amounts of sulphur but it also decomposes the sulphur molecules into H_2S which is easily trapped at very little volume at high temperatures after the reformer or even passed through the remaining reactors if they can tolerate it.

CO reduction

To be compatible with PEM fuel cells additional CO cleaning steps are needed. Leaving the steam reformer, the gas contains app. 5-15% CO depending on operating temperature and steam-to-carbon-ratio. To be utilized in high temperature PEM fuel cells the CO level has to be brought down to app. 0.2-5% depending on the fuel cell operating temperature and stoichiometric ratio. Water gas shift reactors are used for this exothermic reaction, which uses water to convert carbon monoxide into carbon dioxide leaving additional hydrogen and carbon dioxide on the product side:

$$CO + H_2O \rightarrow H_2 + CO_2$$

Depending on the space velocity (and the catalyst used) and operational temperature the outlet composition will typically be close to chemical equilibrium. Fig 11 shows the theoretical calculated chemical equilibrium for the water gas shift reaction for different steam to carbon ratios (based on methane reforming, H_2O:CH_4). The CO concentration is however very differently defined in literature. The left figure shows the actual CO concentration in the gas stream. This is however not suitable to use when relating it to fuel cells, as the losses associated with CO adsorption on the catalyst is related the ratio between the bonding species. For PEM fuel cells mainly carbon monoxide and hydrogen will influence the adsorption/desorption kinetics taking place on the surface of the fuel cell catalyst. CO_2 acts mostly as an inert gas. Fig 11, right shows the CO/H_2 ratio based on the equilibrium composition. Hence species such as H_2O, CO_2 and (if present) N_2 are considered inert.

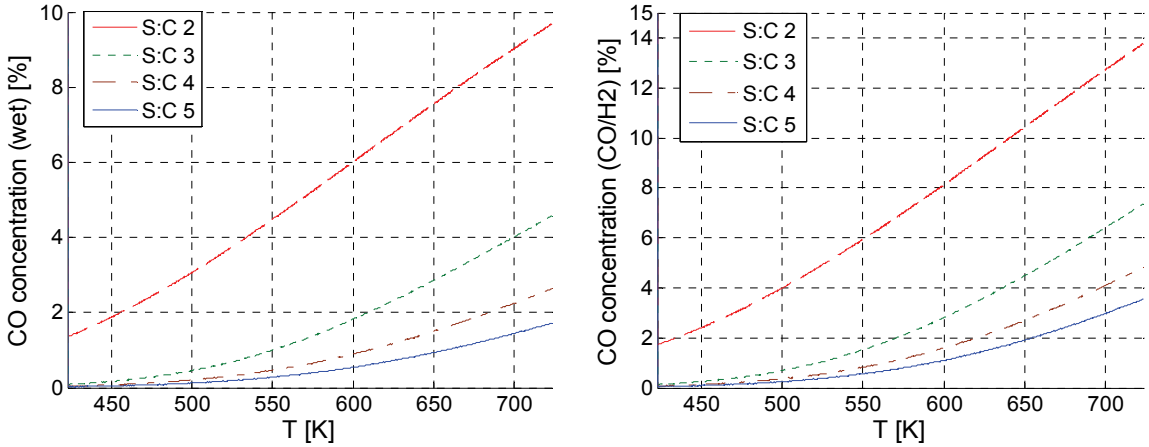

Fig 11: Calculated chemical equilibrium composition. Left; CO concentration (Wet). Right, CO concentration (per hydrogen basis).

Typical high temperature shift reactors operate from 350-450°C while low temperature versions operate down to app. 200°C. Depending on space velocity as well as type and amount of catalyst used, close to equilibrium conditions can be obtained [39]. Typically both high and low temperature shift reactors are needed. The higher temperature favors faster

kinetics while the lower makes it possible to bring the CO concentrations down in the order of 0.1-0.5%.

Gas ultra purification

While PAFC and HTPEM fuel cells can operate directly using only the shift reactor, low temperature PEM fuel cells need additional cleaning steps as they tolerate only 10-50 ppm CO. Several types of clean up steps have been used.

One is the *palladium membrane* used by i.e. Idatech. It provides a very pure H_2 supply completely preventing most of the problems occurring with systems operating on reformate gas. The main drawback is the high cost of the material and the relatively high pressure loss associated with membrane separation, which are the main reasons why many have omitted this option.

Another method is the *pressure swing absorption* technology which has proven to be a cost effective solution in larger systems although some fuel processor producers (such as HyGear) have implemented it on sub 50kWe systems as well. The main obstacle is the system complexity. It similarly produces almost 100% pure hydrogen.

The probably most commonly used method, for smaller systems, is preferential oxidation (PrOx). Oxygen (air) is simply injected into the reformate stream after the shift, preferentially oxidizing the CO over a selective catalyst. However, some hydrogen is also consumed (about the same amount as the CO content). This leaves a reformate stream with a fairly high amount of dilutants such as CO_2, N_2 and H_2O contributing to concentration losses on the anode side. Water, however, is needed anyhow to humidify the low temperature membrane.

Another method is the selective methanation process:

$$CO+3\ H2 \rightarrow CH4 + H2O$$

It is an attractive solution to the carbon monoxide problem as it can be performed passively. Additionally, the methane produced can be used in the burner after passing it through the fuel cell (in contrast to the PrOx where hydrogen and CO is irreversibly combusted). However, a relatively large amount of hydrogen is consumed in the process compared to preferential oxidation. Depending upon catalyst selectivity 3-4 times more hydrogen is consumed than in the preferential oxidation process.

2.2.3 Conclusion

For the current project it has been decided to analyze the behavior of PEM fuel cells for CHP systems. The analysis performed in the previous sections indicated that the technology is mature and it contains some of the characteristics needed as discussed in section 2.1.6. The main advantage includes the current cost and availability but also the transient capabilities (and even frequent start/stops) tend to favor this technology. On the contrary issues such as fuel processing system complexity pulls in the other direction.

The total reformer electrical efficiency will be of major importance. The system efficiency offered by the steam reformer is potentially better as the anode off gas can be utilized for process integration (and not only heat). Other issues, including hydrogen quality, also points towards the steam reformer as the reformate gas stream is not diluted by nitrogen as the other types. Since PEM fuel cells are going to be used, some or all gas clean-up steps are needed.

2.3 Problem statement

From the previous discussion an overall project definition is to be made.

The objective is to design a simple, flexible and robust fuel cell system for stand-alone stationary heat and power generation in local households. Hydrogen is produced from natural gas using a reforming system and hence no additional fuels will be investigated in the current project.

Conventional oil-fired boilers should be substituted by this system. System efficiency should be as high as possible and competitive with similar technologies such as piston engines, micro gas turbines and Stirling engines. The system should (if possible) be able to adjust heat and power production to meet both power and heating demands of the household.

Main focus in the project is to model and design the integrated fuel cell and steam reforming based system to meet requirements given by heat and power demand (i.e. power conditioning, grid and heat supply system). The system is illustrated on Fig 12. The reforming subsystem contains all related system components including gas purification system etc. To further delimit the project a Proton Exchange Membrane Fuel Cell (PEMFC) should be used, though other types of fuel cells should be briefly discussed.

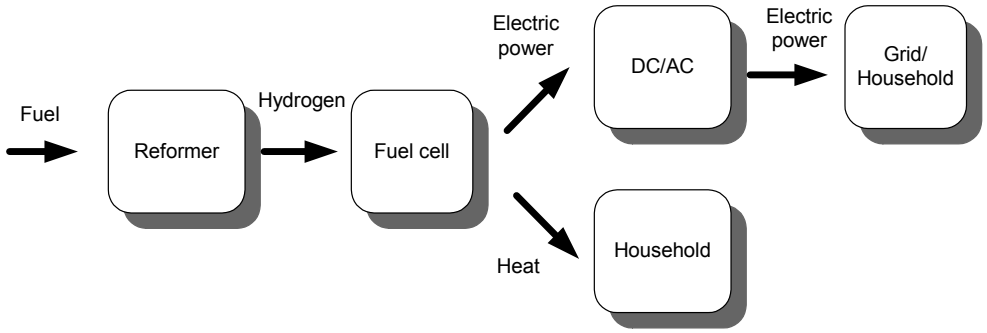

Fig 12: The system produces power to the grid and heat to the household. The main system components are shown.

Three overall control strategies should be investigated concerning the way household heat and power consumption is accommodated:

- *Near future alternative control strategy:* Heat following only, meaning that surplus (or minus) electricity is balanced by the grid.
- *Near to medium term control strategy:* The power is produced on an hour-to-hour basis to fulfill both the household heat and power demand. This would enable a faster commercialization as no special legislation is needed (i.e. net-year power production as for solar cells). The household heat consumption should always be accommodated and hence the heat-to-power ratio has to be variable.
- *Future control strategy:* From the preceding analysis, it is believed that if tens of thousands of systems will be installed in the households, the consumers will be taxed for the electricity produced as they do when they buy from the grid. Hence in order to obtain additional revenues to cover the expenses it should be sought that the system is net-producing electricity to the grid during high- and peak-load hours of the day, while operating at very low load during low load hours (night, weekend)

The model should be able to reflect the practical possibilities of the fuel cell technology for μCHP. The output should be measurable in terms of component sizing and overall over economical figures. The latter could include the margin between having a traditional gas fired furnace and fuel cell based micro CHP system. This will give some indications how large a capital cost that can be accepted. The analysis should be based on the average household consumption of the 25 households presented in section 2.1.5.

2.4 Method

In order to fulfill the goals of the problem statement, a method is provided in the following section. Ideally a complete system should be designed and implemented as a laboratory test rig. Laboratory test facilities of system components should be analyzed to provide input to the modeling. The modeling should then provide the background for extrapolating the test results to a new design and system integration based on modeling.

2.4.1 Modeling

"Starting backwards" the model should be able to describe, with a reasonable accuracy, the system dynamics and steady state operating characteristics. On the other hand the model should be fast enough such that a whole year can be simulated within a few hours to be able to analyze the effect of changing model inputs. These are conflicting goals and it has to be carefully selected at which level of detail the model has to be made.

The models should have reasonable steady state solution to the system, but for control purposes the important factor is the dynamic response where transfer functions and state space formulations are frequently used. To improve simulation accuracy nonlinear dynamical models are to be developed.

The models developed in this project will be made in the Matlab©Simulink environment. It is based on the block diagram formulation principle, and has many built-in blocks, both linear and non-linear in an intuitive interface.

2.4.2 Experimental

To provide reasonable accuracy for the system models, experimental characterization of the system components should be performed. A fuel cell and reformer test rig should be developed with associated control and data acquisition system. The rig should be able test as well transient as static performance of the system components and should be able to simulate the interaction between the fuel cell and the reformer system.

3 Literature overview

Review of the modeling work on the individual technologies is presented in the relevant papers. In this section focus will be on where the current work on a fuel cell based CHP system can be placed.

Commercial progress

Currently a lot of work is put into developing and deploying micro CHP systems. One of the largest players over time was Sulzer Hexis Ag, which terminated its activities in 2005. In 2006 a new enterprise (Hexis Ltd.) still developing on the new generation of the SOFC based system. Currently, the company claims to be able to obtain an electrical efficiency of 25-30% (www.hexis.com, October 2006). The old Sulzer Hexis deployed 110 systems in local households from 2001.

Another company currently deploying systems all over the world is Plug Power. They have collaboration with a range of companies including the European company Vaillant, currently one of the largest manufacturers of household natural gas fired boilers in the world. Plug power claims to have obtained electrical efficiencies up to 31.5%$_{HHV}$ [13]. Work on HTPEM systems has also been ongoing for the last couple of years, and it seems as if they are taking a complete shift towards this technology in μCHP.

Another American company, Idatech, has also been deploying a number of systems in the resent years some of them partnering with the German energy company, RWE. Idatech delivers reformers, fuel cells and fully integrated systems.

A number of Japanese companies have also been deploying a number of systems for field tests in recent years. This includes in particular Osaka gas which has both SOFC and LTPEM activities ongoing.

Nationally most of the activities have been focused on hydrogen fuelled PEM fuel cell systems for demonstrations projects. Intense development is however ongoing on commercializing the long term SOFC research work carried out by the national research institute Risoe together with Topsoe Fuel cell.

Currently a large CHP program is under development which is divided into 3 stages. The first is under completion with one LTPEM and one SOFC system to be evaluated. The next phases are being planned and the ambition is two have 100 systems into operation by 2010.

3.1 Scientific progress

3.1.1 System- and CHP modeling

There have been very little published on system modeling of fuel cell systems. Especially dynamic models which have a sufficient steady state accuracy combined with dynamic terms suitable for simulation of months and years have been absent.

Recently J. Golbert [16] and Pukrushpan et al. [17] made progress in the development of advanced control for fuel cell systems. They applied the models developed by Amphlett et al. [18] which were based on empirical data measured on the Ballard Mark V.

There has been some activity on modeling the impact of micro CHP on a grid perspective by amongst others [25][26][27]. Additionally, a range of different test results have been presented including [28]. However they do not include dynamic models on the micro system level making it difficult to use any of these for this project.

DONG (formerly ELSAM) published a report [12] discussing integration of fuel cell based micro CHP systems in the Danish electricity grid. On of the major conclusions was that efficiencies comparable to those of central natural gas fired power plants should be obtained if fuel cells should get a significant share of the power production in Denmark. Moreover due to the high marginal cost of the fuel (natural gas) they found it most likely that fuel cells will only deliver power to the grid during high and peak load hours of the year.

3.1.2 Fuel cell modeling

On the earliest comprehensive models of PEM fuel cells was developed by Bernardi & Verbrugge in 1992 [20]. The model included water transport in as well the membrane as in the catalyst layer and the kinetics was modeled using the Butler-Volmer equation. The model could predict experimental data at lower densities but failed to describe the mass transfer limitations at higher current densities.

Springer et al. is probably one of the most cited within PEM fuel cell modeling at all providing all the experimental conductivity measurements. They later on presented some both empericical and analytic modeling in [21]. This model also included diffusion processes in the catalyst layer making the model able to predict concentration losses at high current densities. The model, however, did not include the formation of water in liquid phase and gas diffusion limitations caused by that which however was done by Marr & Li [22] in 1998. Nguyen et al. [19] also proposed an along the channel model in 1996 which has been used widely since.

Several researchers have investigated the influence of carbon monoxide. Janssen, G. J. M. [23] did some modeling on the CO2 reduction to CO and the influence on fuel cell performance. It was found that CO2 had a significant influence on anode polarization losses when relatively small amounts of CO were introduced and at low current densities.

Zhigang Qi et al. [24] performed dynamic and static tests on single cell MEA's with varying catalyst loadings. Influence of CO on cathode and anode potentials were investigated. It was proved that CO coverage not only affected the anode potential but also the cathode.

In terms of HTPEM the use of PBI (the material of the membrane) for fuel cell applications was first published by Wainright [29] followed by a number of papers ([30], [31]). Some of the same authors published data regarding the oxygen reduction reaction in [32] and recently they published data on CO coverage in [33]. Other research groups also published data regarding development of PBI based MEA's such as the group of Bjerrum et al. [34][35][36].

Most of the papers presented by these groups focused on membrane and catalyst development not suitable for system modeling.

One of the few authors that did modeling of HTPEM fuel cells is D. Cheddie who published a model of a PBI membrane taking into account the operating temperature while the cathode and anode stoichiometric ratios was unknown [37][38]. Most of these publications however are analytical, focused on electrochemical and diffusion aspects in the membrane and catalyst layer. This limits the usability in terms of system modeling due to the solving time. Additionally the reference tests where based on MEA's the research group made themselves, and not the commercially available types from i.e. PEMEAS GmbH, further limiting the general applicability.

4 Experimental

In this chapter the experimental characterization of the CHP system components will be described. Detailed investigation of both low- and high temperature PEM fuel cells will be performed. Additionally, measurements from a commercial steam reformer will be presented. Most of the content will be given in the form of papers submitted to various journals and conferences.

4.1 Laboratory tests facilities developed

In the following chapter, three papers will be presented concerning the experimental part of the project. The first presents a novel fuel cell test facility and a series of tests performed on a commercial low temperature PEM fuel cell stack from IRD fuel cells A/S. This includes tests in relation to anode/cathode humidity, stoichiometry, CO and CO_2 content in the reformat gas. An interesting observation regarding regeneration of the fuel cell after exposure to CO is also made. Fig 13 shows the test facility.

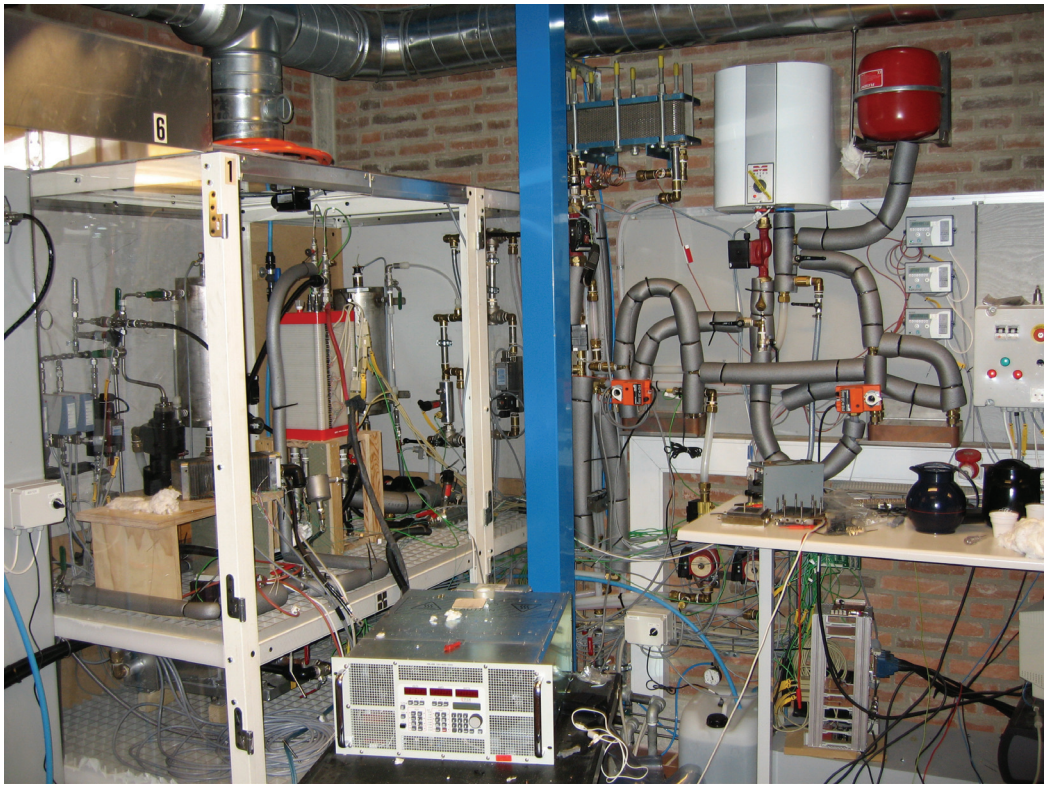

Fig 13: The PEM fuel cell stack test facility.

Next, a paper concerning the performance of high temperature PEM fuel cells follows. An extensive series of systematic tests are presented not previously shown in literature. The analysis includes the influence of CO and CO_2 on the anode side, a wide variation of operating temperature and variation of the cathode stoichiometry from 2-5.

A short description of a natural gas fuelled reforming system designed for the project is also given. Unfortunately this system was not finished in time to provide any test results to the project.

At last another steam reforming system will be presented which was made alongside the other system. In this case a series of measurements where made on both the reformer and the water gas shift reactor. These were based on ethanol which can, to some extent, be regarded as sulphur free natural gas, as the ethanol decomposes rather quickly to methane.

Detailed experimental characterization of a reformat fuelled PEM stack

Anders Korsgaard[a,1], Mads Pagh Nielsen[b], and Søren Knudsen Kær[c]

[A] *Ph.D. Student at Institute of Energy Technology, Thermal Energy Systems, Aalborg University (AAU, IET),*
[B] *Assistant Professor at Institute of Energy Technology, Thermal Energy Systems, Aalborg University (AAU, IET),*
[c] *Associate Professor at Institute of Energy Technology, FACE, Aalborg University (AAU, IET).*

Abstract

Increasing attention is given to fuel cells for micro combined heat and power systems for local households. Currently, mainly three different types of fuel cells are commercially competitive: SOFC, low- and high-temperature PEM fuel cells. In the present paper the Low Temperature PEM technology is in focus.

To be able to design highly efficient micro CHP systems, it is critical to have a reliable performance map of not only the stack performance in the nominal operating point but also at system part load. Issues like parasitic power consumption of the balance of plant components, dynamic performance and process input variations need to be carefully accounted for. Such data will additionally provide valuable input for system modeling and optimization.

The paper presents an advanced experimental test facility capable of performing static as well as dynamic tests on fuel cell stacks with electric power output from 1-3-kW. All process inputs for the stack can be altered to provide realistic performance analyses, corresponding to those encountered in field applications. These include cathode/anode dew point control, cathode flow rate, cooling water temperature control as well as synthesis gas mixing (CO, CO_2, N_2, Air and H_2). The control system includes 12 thermocouple inputs, up to 60 cell voltages, more than 10 flow measurements and 10 pressure measurements, all at sample rates up to 1 kHz. The system design is thoroughly explained to provide valuable information for system integrators.

Additionally, the paper contains a comprehensive set of test results based on a commercial reformate PEM stack A series of different synthesis gas compositions were applied to the stack including 5 and 10 ppm CO content, 20% CO2 and air bleeding. During these tests, the dynamic response of the cell voltage was monitored. The time response of the recovery process was measured while loading and unloading the stack and continuously feeding pure hydrogen.
Also the influences of parameters such as cathode stoichiometry, inlet dew point temperatures of the cathode and anode gas streams were investigated.

Keywords: Fuel Cells; Control; Dynamic; Test bench; Test facility; PEM; Humidification, Labview, Real time.

1. Introduction

PEM fuel cells are electrochemical devices, which efficiently convert energy in hydrogen directly into electricity without combustion and with no moving parts. The process is the opposite of electrolysis and can be compared with the process in a battery. The basic reaction is shown in equation:

$$2H_2 + O_2 \rightarrow 2H_2O \quad (1)$$

Through this reaction, 4 electrons are released. The following figure illustrates the principle of a single fuel cell:

[1] Corresponding author, e-mail: ark@iet.aau.dk, Tel.: +45 96 35 92 53

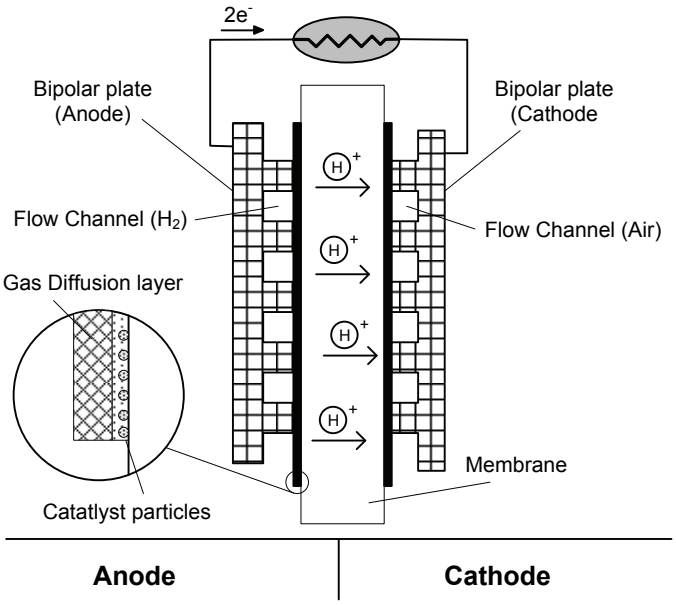

Figure 1: Schematics of a single fuel cell.

An electrolyte separates the anode and the cathode side, allowing only protons (H^+) to pass. Hence the electrons freed from the catalyst layer on the anode side are forced through the external circuit, driving the load. On the cathode side they recombine with oxygen (usually supplied in the form of air) and protons, which has passed through the membrane, producing only water.

The cell voltage would theoretically be 1.48 V if the water was formed in condensed form at 25 °C. Since this is usually not the case the limiting voltage is approximately 1.25 Volt. Usually 10-100 cells are connected in series to produce a higher voltage but at the same current, as the single cell. Today typical current densities are in the range of 1-2 A/cm^2.

Typical operating cell voltages are between 0.5 and 1 V/cell, due to chemical activation-, concentration- and ohmic losses. These irreversibilities are highly non-linear. Not only do the losses differ from stack to stack but also from cell to cell inside the stack due to manifold design, temperature- and specie distribution and production differences. For this reason it is important to test the individual stacks and provide a robust control system before the stacks are put into practical applications. Important considerations must also be made whether or not to include for instance anode humidification, though it clearly complicates the system.

Recently [1, 2 & 3] made progress in the development of advanced controls for fuel cell systems. Dynamical models have been derived by empirical data in [4] of the Ballard Mark V, but issues such as degree of humidification and CO-poisoning have not been published to date on a stack or system level. T.V. Nguyen et al. [5] also proposed an along the channel model in 1996 which has been used widely since.

Janssen, G. J. M. [7] did some modeling on the CO_2 reduction to CO and the influence on fuel cell performance. It was found that CO_2 had a significant influence on anode polarization losses when relatively small amounts of CO were introduced and at low current densities.

Zhigang Qi et al. [8] performed dynamic and static tests on single cell MEA's with varying catalyst loadings. Influence of CO on cathode and anode potentials were investigated. It was proved that CO coverage not only affected the anode potential but also the cathode.

Bhatia, K. K. et al. [9] did various tests of the transient response to CO in the anode feed gas.

This presents a novel test system design that is able to validate the proposed models and controls. Especially issues such as robustness of controls towards liquid water formation/drying of membrane and CO-poisoning need to be investigated before a reformer is connected to the system.

Secondly, test results from the test facility are presented based on a commercial reformate low temperature PEM fuel cell stack.

2. Experimental Setup

2.1. Overview

In general the most important tests to be made on the fuel cell stack characterization facility are:

- Humidification on anode and cathode side

- Anode/-cathode stoichiometry
- Reformate gas composition, including secondary gas compositions of carbon monoxide, carbon dioxide and air bleed
- Variation in fuel cell stack temperature
- Pressure losses in the system

Pressurization of the system is possible to some degree, but it is not considered as an important issue for non-automotive systems.

Fig.1 shows a process instrumentation diagram (PID) of the test facility. From top the air-, distilled water- and synthesis gas- flow system are shown separated by the colors shown in the bottom right. In general component numbers are reflected by the fluid system they are located in: (Axx, Wxx & Hxx) respectively. Electrical control valves are named separately (Vxx).

The cathode air flow is supplied by an oil less air compressor or by an air blower (A02). Usually the first is used together with a mass flow controller (MFC, I25) while the latter is used for system tests with "real" system components and hence the MFC can be bypassed. From the MFC the air is directed through at 3-way valve which either directs the humidifier or is simply bypassed. This is done to test the dynamic response of humidification. This is relevant knowledge in systems where active control of humidification is available. An example of such a test is shown in the result section of this paper.

From the humidifier the air is passed to the fuel cell stack and at the exit thereof condensed to obtain a water balance measurement.

The distilled water system is shown in the center of the drawing. The hot water tank (W02) provides the necessary heat for the vaporization of water in the humidifiers and preheating of the fuel cell. The pump (W06c) circulates the water to the 3-way shunt valves (V40a and V40b), which directs a part of the flow through the heat exchangers (W10), heating the closed loop water systems for the humidifiers (A08 & A09). Water for the humidifiers is continuously supplied by the expansion tanks (A10 & H12).

The part of the water not directed to the shunt valves, flows back to the tank. If valves (W04b & W04d) are closed, the water is forced through the fuel cell stack enabling fast preheating. The system around the circulation pump (W16) cool the fuel cell stack using the heat exchanger (W18), which is connected to a cooling tower. The exit water temperature from the stack can be controlled using a passive control valve as indicated in the drawing.

The synthesis gas mixing is provided by 4 MFC's delivering hydrogen (V16), CO (V20), CO_2 (V22) and air (V23). The CO is not mixed directly into the stream, but is provided through a high precision pre-mixed bottle of hydrogen and 100 ppm CO. As for the cathode system, the humidifier (H09) can be bypassed using the 3-way valve (H08). The fuel cell stack can be operated in a straight through configuration or re-circulated passively using the ejector pump (H30). At the exit a proportional valve (V15) is located to adjust the pressure of the system. Purging is provided using (V34) which is normally left open.

2.2. General design considerations and component selection

Reactant gas supply and mixing

The delivery of reactant gases to the process are to be varied within a large interval. I.e. if the fuel cell stack should be tested in a range from 1/10 of peak- to peak power and the stoichiometry should be varied from 1.5-5, a device with a turn down ratio of more than 1:30, is required. It is even more critical when the synthesis gas stream is considered where power range and stoichiometry should be varied but also the secondary gases. If it is required to test concentrations of CO from 5-100 ppm this would put a demand of the MFC's of 1:600. Devices with such specifications are very difficult to acquire so in general it is chosen to limit the test capability at lower currents and put a minimum flow saturation in the software in order to provide sufficient reactant flow at all times. This is done for all MFC's even though the secondary concentrations of CO, CO_2 and air in the synthesis gas flow may be higher than desired at low loads.

Since the turn down ratio of the MFC's is extremely important for the tests this was given a high priority in the selection process. Flow controllers from Burkert were chosen having a turn down ratio ranging from 1:50 to 1:500 except for the cathode air- and CO_2 mass flow controller which had 1:25.

Humidification

As noticed from the PID the air/synthesis gas is heated and humidified by PermaPure membrane humidifiers in a closed loop water system. In general the PermaPure humidifiers chosen will always provide a relative humidity close to 100% but at varying temperatures the humidity depends on the air flow. The fuel cell stack, on the other hand, responds to the amount of water in the reactant stream relative to the stack temperature rather than the relative humidity and tempera-

ture of the inlet flow. This is the reason why only the temperatures at the inlet of the anode and cathode gas streams are measured and controlled.

Pressure measurements

Pressure transducers are placed throughout the system to be able characterize system components.

Temperature measurements

The flow inlet and outlet temperatures from the fuel cell stack are measured in the center of the flow leaving the end-plate of the stack such that no heat losses in the external piping will influence the measurement. Radiative aspects are not considered for the low temperatures encountered here.

Cell voltage measurements

For low temperature PEM fuel cells cell voltage measurement (CVM) is required in most cases in order to detect cell flooding, which cause decreased cell voltage and ultimately permanently damages the cells. Whenever a cell voltage below 0.5 V is detected a procedure for auto purge is implemented to flush flooded cells. If a cell voltage reaches 0.3V the load is disconnected.

Electronic load

The fuel cell stack is loaded with a 4kW electronic load from DTI. It is controlled remotely from the control system using a simple analog control signal. Typically the stack current is applied though also voltage, power and resistance can be controlled. The actual current is supplied as an output from the load module.

Piping

During the initial tests large problems arose with flooding on the anode side. For various reasons the stainless steel pipes were very long (~2m). This caused wall condensation of humidified hydrogen and periodically liquid water was pulsed in to the stack causing cell flooding. After shortening the pipes (½m) the problem was solved. This clearly illustrates the need for having short and thick pipes between the humidifier and the fuel cell. The cathode at all times had a short (0,3m) and large pipe (25mm) to the inlet of the stack, and hence no problems occurred here.

2.3. Control and data acquisition system

The control system is build up on a real time computer running the Pharlab® operating system, which is compatible with Labview® Realtime module. Programming is carried out using traditional Labview® blocks. The real time execution combined with the fast programming of the Labview environment makes it a very efficient and flexible system. In situations where code execution needs to be very fast, selected routines can be implemented in standard C programming language, which both the Pharlab® and Labview® systems are based on.
Controls and data acquisition routines are carried at sample rates of 100 Hz. However selected routines can be carried out individually at interrupt speeds up to 10 kHz allowing i.e. impedance spectroscopy carried out on 60 cells simultaneously.
96 single ended analog inputs are possible, though 60 of these are used for CVM. These are implemented as differential measurements in hardware. Moreover 14 high precision thermocouple measurements are performed with build-in zero point compensation. The hardware used includes:

- 1 pcs. PCI-6257 from national instruments
- 2 pcs. PCI-6229 from national instruments
- 1 pcs. PCI-4351 from national instruments
- 1 pcs. Dell GX-270

Most of the analog input and outputs are carried out as 4-20mA signals limiting the noise sensitivity.

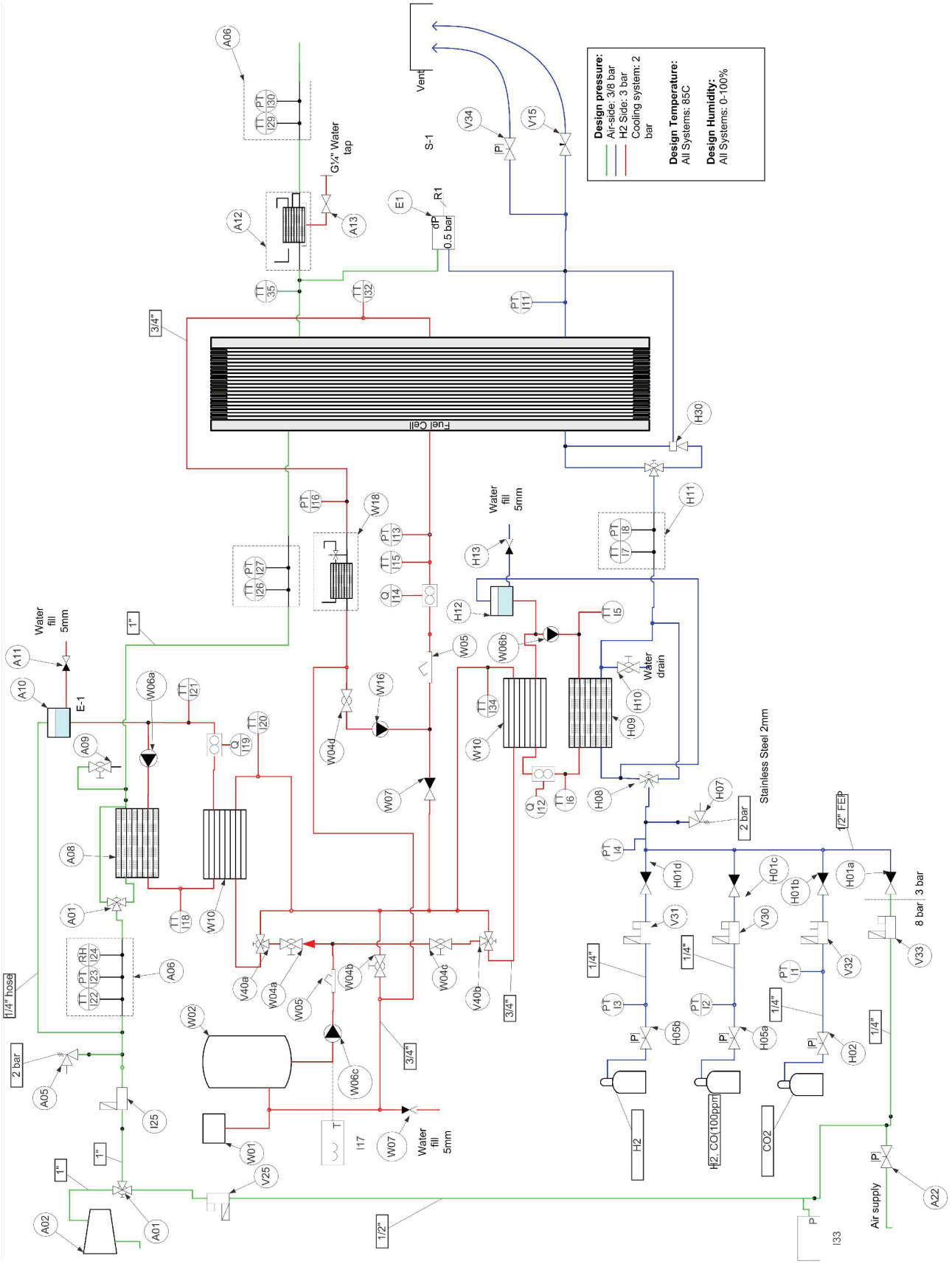

Fig. 1: PI diagram of test facility.

3. Results

The tests performed are based on a commercially available 2.5 kW (nominal) low temperature PEM reformate stack with a Pt-Ru catalyst. The MEA's in the stack have active MEA area of 154 cm^2 and the stack in total consists of 50 cells. The tests reflect some of the most important aspects that must be investigated prior to the operation of a complete system including fuel cell, reformer and balance of plant. Focus is put on the stack response to variations in cathode stoichiometry, humidity of anode and cathode and composition of the reformate gas leaving the reformer entering the fuel cell stack anode manifold.

To maintain an acceptable lifetime, humidification of the inlet reactants must be high. The manufacturer, IRD Fuel Cells, suggests that for a stack operating temperature of 70°C the inlet dew point should be 6/0°C below, cathode/anode respectively. However stack temperature is not easily defined since variations throughout the stack are evident. I.e. temperature differences between anode, coolant and cathode outlet where observed to be 69/71/72°C at 40A (~1400W). These numbers are more or less the same at both lower and higher stack loading. It was decided to use the cooling water temperature as reference since this value is somewhat in between the anode and cathode temperature.

The stack was positioned vertically, allowing possible liquid water in the manifold to be removed by gravity. However occasional cathode flooding occurred; especially in the cells near the end plate and thus periodical purging was required. The pressure loss in the cathode manifolding and bipolar plates were however very small (only a few thousand Pascal's at 1400W). This resulted in low parasitic power consumption for driving the air compressor. This clearly illustrates the tradeoffs which most be addressed in stack designs of high humidity PEM fuel cells as low pressure loss and high stability are contradictory demands.

It was generally difficult to reproduce the datasets mainly due to liquid water accumulation and temperature variations at the endplates. Typically the cell voltage varied between 36.2 and 36.8 volts at the nominal test point of 40A. Hence one cannot compare the steady state voltages between the different sets of measurements precisely. However the tests should be good enough to give a qualitative answer to the influences of the different test conditions. Also occasional purging of the cathode were found to be necessary. This was typically done every 3rd minute.

3.1. Variation of Cathode Stoichiometry

Fig. 2 shows a polarization curve at two typical cathode stoichiometries up to a maximum power of 2.8 kW. As seen the higher stoichiometry improves performance in terms of cell voltage. However it also seems to affect the cell stability, where cell flooding is likely to occur at lower flow rates. It was not possible to perform tests at higher stoichiometries due to limitations in the power input for the hot water tank and hence insufficient heat for the vaporization of water in the humidifiers. This however reflects limitations also encountered in real world systems, where the volume of the humidifiers and condensers would have to be very large to support operation at high stoichiometries.

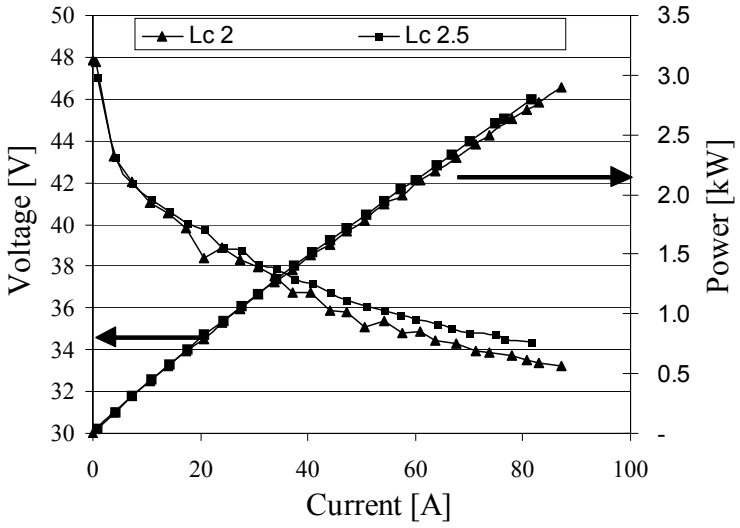

Fig. 2: Polarization curve of the stack at conditions: Dew point C/A=64/69°C, λ_a=1.2 and T_{fc}=70°C.

3.2. Dynamic response to change in humidity

Various tests were performed on changes in humidity. A lot of work has been carried out including the conductivity regressions developed by Springer et al [6]. The objective is not to redo these experiments on stack level, but rather

investigate the dynamic and practical effects this will impose with respect to stack operation. As discussed previously it is well known that low humidity at the inlet causes shortening of lifetime. But occasionally humidification might fail or be reduced due to components malfunctioning.
Fig. 3 left, shows the voltage response to a step input in humidity. At time zero the cathode humidification was changed instantaneously from a dew point temperature of 64°C to dry air with a temperature of 25°C by turning the three way valve (A01). Apparently there exists some kind of time delay where performance is not influenced. But after 2-3 min. the voltage slowly starts to decrease. After a little more than 6 minutes some of the cells show signs of flooding behavior and the stack is purged for 10 seconds. It is quite interesting that the stack still seems to flood even though dry air is injected.
After purging, an increase in stack voltage of about 1V is observed but the performance is still decreasing. After around 9 minutes the stack voltage drops again due to flooding of the ultimate cell closest to the endplate. The experiment was terminated at this point to prevent permanent damage of the stack.
Fig. 3 right, shows selected cell voltages. It is clear that it is the cells near the exit of the stack that cause the flooding behavior. However the performance, once purged, is much better in these cells clearly indicating higher humidity. This is most likely due to a lower temperature in these cells. Unexpectedly, the instability actually seems to increase (or at least does not decrease) with lower humidity. One reason for this may be that the mass flow, and thereby the pressure loss, into the stack is higher under humidified conditions enabling better liquid water transport.

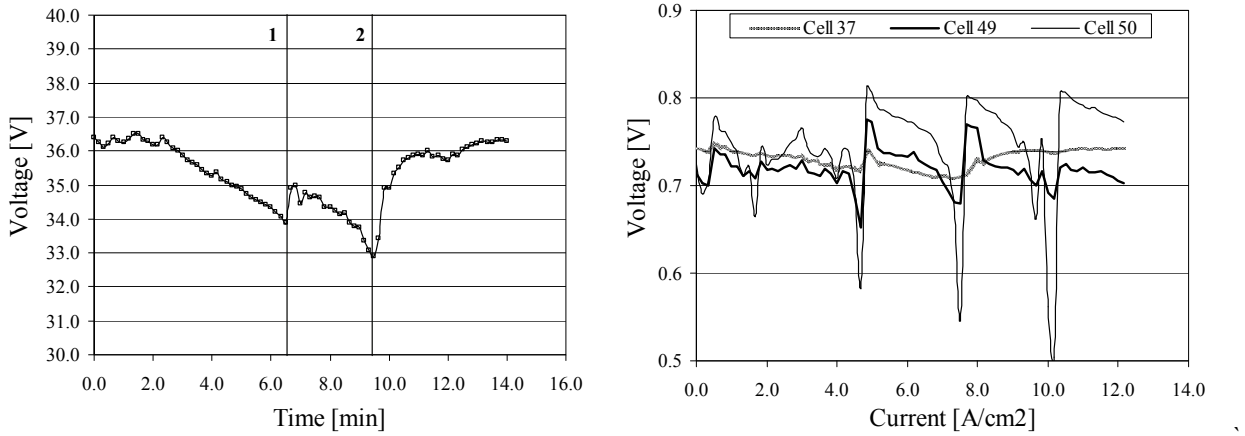

Fig. 3: Stack response to step input in humidification (left; stack voltage, right; selected cell voltages). Initial conditions: Dew point C/A=64/69°C, λ_c=2.5, λ_a=1.2, i=40A and T_{fc}=70°C.

Experiments on varying anode humidity were also performed, but it was found not to influence the performance significantly and have thus not been included in the present publication.

3.3. Dynamic and static response to CO_2 in the anode gas stream

The fuel cell stack is intended for use with micro combined heat and power (μCHP). Carbon dioxide represents approximately 20% of the dry gas volume flow when reforming natural gas (assuming most of the inlet fuel is CH_4) and hence this will be the background of the test. Fig. 4 left, shows the response to CO_2 during a period of 1½ min. After 10 seconds CO_2 is mixed into the gas stream and an instant voltage drop of approx. 0.3V. During the following minute the voltage slowly to decreases. Fig. 4 right, shows the following 35 min. operation and a slow decay in voltage is observed..The stack voltage reaches a steady state after approximately 25-30 min. after an additional 0.5V decrement. Hence the stack does not only see this as an inert dilutant but CO_2 actually participates in the kinetics, most likely through the reverse water gas shift to CO, which covers some of the free catalyst sites.
Fig. 5 shows the steady state polarization curve for pure hydrogen and 20% CO_2 in hydrogen. The tests were made prior to the long term operation, so the CO adsorption had not completed at this test. From the above discussion the CO_2-curve can be offset downwards additional 0.5-0.6V (40A relative) to obtain the steady state operation.
The results are comparable to the results from [7].

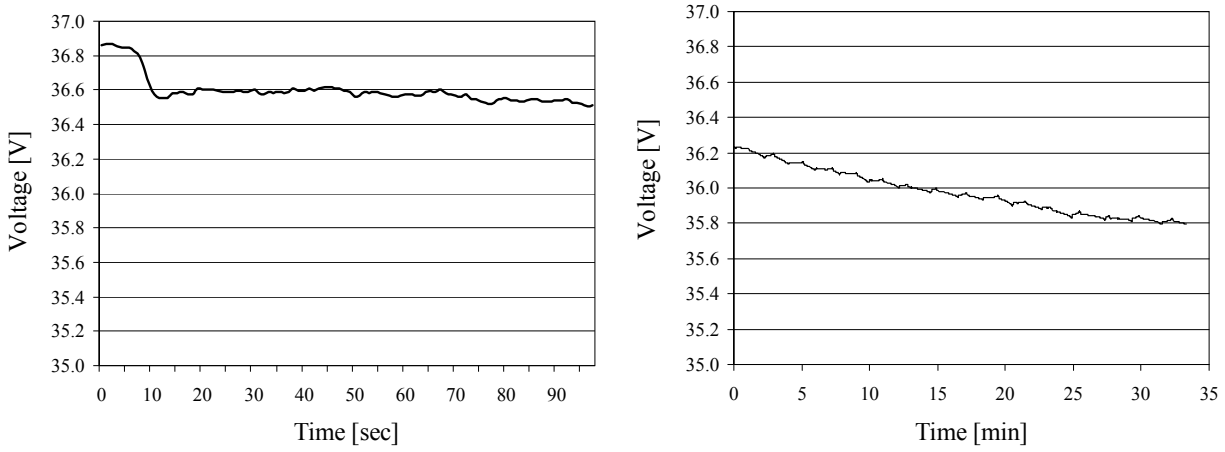

Fig. 4: Left; shows the initial drop under a step in CO2 concentration. Right; shows the slow transient. Conditions: Dew point C/A=64/69°C, λ_c=2.5, λ_a=1.2, i=40A and T_{fc}=70°C.

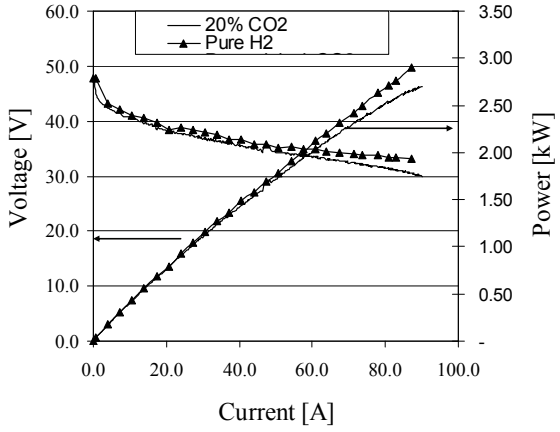

Fig. 5: The steady state polarization curve. Conditions: Dew point C/A=64/69°C, λ_c=2, λ_a=1.2, i=40A and T_{fc}=70°C.

3.4. Dynamic response to CO in the anode gas stream

Generally, the settling time of the cell voltage when exposed to a step input in CO concentration were found to very long, typically in the range of a few hours. Since flooding occurred often, purging of the cathode would have been done every 2-5 min. Nevertheless, sometimes this was not possible to do before the cell voltage of reached 0.3V, and this caused the control system to switch off the load to protect the fuel cell stack. This is the reason why the load breaks out in the following experiments. All the voltage measurements are applied a running average with a window size of 1 min. However these breakouts also provide valuable information about the stack behavior as described later in this section.
Also, as these experiments are very time consuming, there was not enough hydrogen to produce one set of experiments as no hot swap hydrogen supply is currently available. Hence steady state behavior will have to be analyzed in single cell measurements or whenever hydrogen for long term operation is available.
Fig. 6 left shows the decreasing stack voltage when exposed to 5 ppm carbon monoxide at a stoichiometric ratio of 1.2 on the anode. After 165 min. the load is cut out due to a low cell voltage. After 190 min the CO supply is stopped and the regeneration curve is shown. At 210 minutes the hydrogen bottle was unfortunately empty, not allowing the complete regeneration to take place. It is seen that the fuel cell stack recovers much faster than during the CO-adsorption phase. Fig. 6 right shows the cell voltage distribution initially and after 190 min. at the minimum. Initially the first part of the stack has a bit lower performance than the end but after the CO adsorption has taken place the opposite is the case. This indicates that there are some problems with flow distribution between the individual cells. One could suggest

that the first cells, both on the anode and cathode, receive a higher flow than the cells in end. On the cathode side it seems that the end cells have a higher probability of flooding but in general have a higher performance than the first cells. In contrary, on the anode side, where the last cells receive less flow, the CO content will be much higher near the exit of the flow channel, hence limiting the performance.

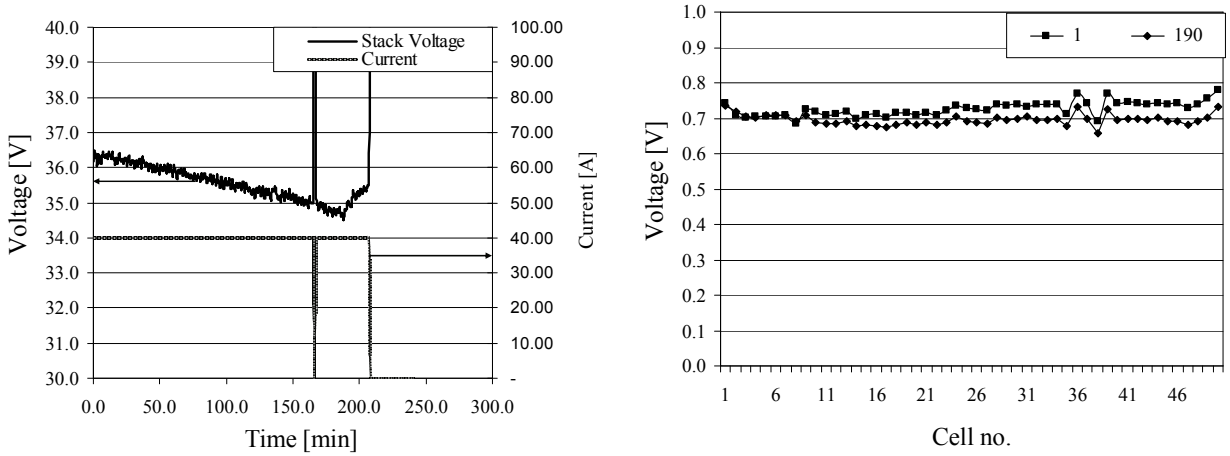

Fig. 6: Left; shows the transient voltage drop when exposed to 5 ppm CO in the anode stream. Right; shows the cell voltage distribution at different times. Conditions: Dew point C/A=64/69°C, λ_c=2, λ_a=1.2, i=40A and T_{fc}=70°C.

Fig. 7 right shows the voltage decay when exposed to 10 ppm CO at a stoichiometric ratio of 1.2. Since the time axis of Fig. 6 and Fig. 7 are the same it is clear the slope of the 10 ppm (~0.027 V/min) is much steeper than the 5 ppm (~0.007 V/min) case. After approx. 85 min. a voltage cutout occurs due to cathode flooding. The load is not re-enabled until 15 min. later while a minimum flow of H_2+CO is still flowing into the fuel cell. It is noted that the decay in cell voltage seems to continue even though the load is disconnected.

After 137 min. the hydrogen and CO supply is suddenly stopped, while the load is still on for 5 sec. until the cell voltage reached 0.3V and the security system shut off the load module. A minimum cathode flow of 20 L/min. continued during this interval. The cell voltage distribution, 5 sec after the fuel interruption, is shown in Fig. 7 right. When the load is re-enabled after a few minutes, the voltage has nearly re-gained the original state. At a first glance this may seem surprising but it can be physically explained. While the current continued to use the remaining hydrogen in the fuel cell stack and connecting pipelines, a high concentration of CO and water was left in the stack. This caused the reactions of electro oxidation of CO and water gas shift to become more dominant recovering a lot the catalyst sites. This method could maybe be used in a more systematic way to periodically regain the performance. However, the influence on catalyst degradation is not known and should therefore be investigated more thoroughly in a single cell test stand, before any conclusions can be drawn.

After the voltage recovery the experiment was continued and it seemed to follow the same slope of voltage decay as before the recovery. Also the recovery seems to happen even faster than for the 5 ppm case, which was also expected. The experiment with 10 ppm shows the same tendencies in regards to the non-even flow distribution among the cells as in the 5 ppm case, which is shown in Fig. 7 right.

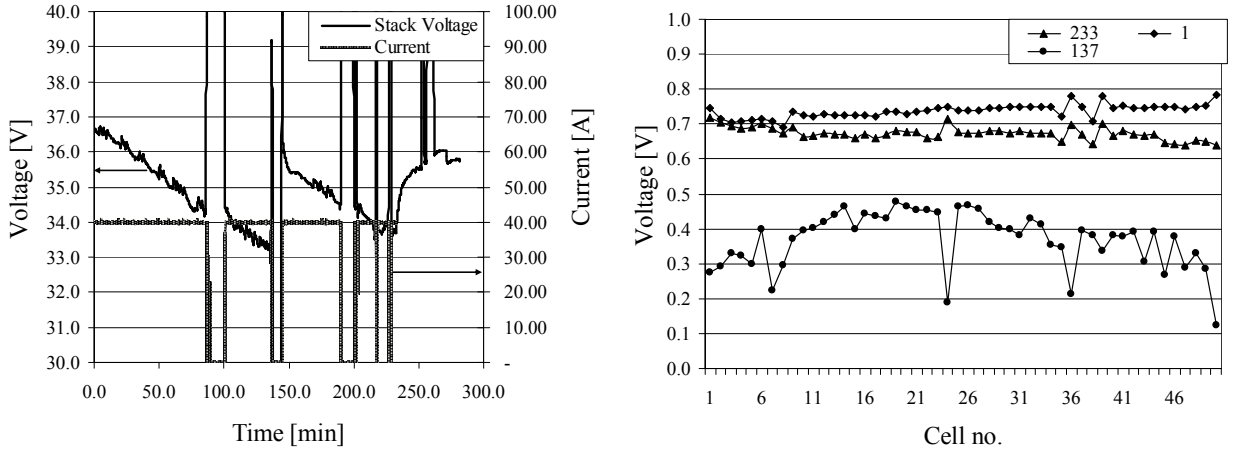

Fig. 7: Left; shows the transient voltage drop when exposed to 10 ppm CO in the anode stream. Right; shows the cell voltage distribution at different times. Conditions: Dew point C/A=64/69°C, λ_c=2, λ_a=1.2, i=40A and T_{fc}=70°C.

Tests based on 20 and 50 ppm CO concentrations were also performed but they have not been included in the present publication.

4. Conclusion

An advanced fuel cell test facility was designed for advanced dynamic testing and characterization of fuel cell stacks in the 1-3 kW range. The test facility is able to vary all process inputs to the stack including humidity, temperature as well as various gas compositions in the anode stream.

A series of tests were performed with varying operating conditions including cathode stoichiometry, humidity and anode gas composition. In general the stack had a good performance with low parasitic losses for driving the anode and cathode streams. However, issues regarding flooding of the cathode flow channels, particularly in the last cells of the stack, and uneven flow distribution were apparent. One of the major conclusions is that CO_2, besides acting as a dilutant on the anode side, also participates in the kinetics and decreases the voltage of the tested stack with 0.3/0.6V respectively. Also fuel supply interruption for a few seconds seemed to regain a lot of the lost performance after introducing CO. However this procedure needs to be tested in terms of permanent degradation of the fuel cell.

5. Acknowledgement

IRD fuel cells A/S is appreciated for their practical inputs to stack operation. A special thanks is given to Danfoss, Grundfos, Burkert and Junair who all supplied components for the system.

6. References

References

[1] S. Caux, J. Lachaize, M. Fadel, P. Shott, L. Nicod, *Modelling and control of a Fuel Cell System and Storage Elements in transport applications*. Journal of Process Control, volume 15, issue 4, 2005;pp 481-491.

[2] Joshua Golbert, Daniel R. Lewin, *Model-based control of fuel cells: Regulatory control*. Journal of Power Sources, Volume 135, Pages 135-151.

[3] J.T. Pukrushpan, A.G. Stefanopoulou, H. Peng, *Modeling and Control for PEM Fuel Cell Stack System,*. Proceedings of the American Control Conference, Anchorage, Alaska, May 8–10, 2002..

[4] J.C. Amphlett, R.F. Mann, B.A. Peppley, P.R. Roberge, A. Rodrigues, *A model predicting transient responses of proton exchange membrane fuel cells,*. J. Power Sources 61 (1996) 183–188.

[5] J.S. Yi, T.V. Nguyen, *An along-the-channel model for proton exchange membrane fuel cells.* J. Electrochem. Soc. 145 (4) (1998) 1149–1159.

[6] Springer T.E., Zawodzinski T.A., Gottesfeld S, 1991, *Polymer electrolyte fuel cell model*, Journal of the Electrochemical Society, Vol 138 pp2334-2342

[7] Janssen, G. J. M. 2004, *Modelling study of CO2 poisoning on PEMFC anodes*, Journal of Power Sources Vol.136 Issue.1, pp. 45-54.

[8] Qi, Z., He, C., & Kaufman, A. 2002, *Effect of CO in the anode fuel on the performance of PEM fuel cell cathode*, Journal of Power Sources Vol.111 Issue.2, pp. 239-247.
[8] Bhatia, K. K. & Wang, C.-Y. 2004, *Transient carbon monoxide poisoning of a polymer electrolyte fuel cell operating on diluted hydrogen feed*, Electrochimica Acta Vol.49 Issue.14, pp. 2333-2341.

Available online at www.sciencedirect.com
ScienceDirect
Journal of Power Sources 162 (2006) 239–245
JOURNAL OF POWER SOURCES
www.elsevier.com/locate/jpowsour

Experimental characterization and modeling of commercial polybenzimidazole-based MEA performance

Anders R. Korsgaard [a,*], Rasmus Refshauge [b], Mads P. Nielsen [a], Mads Bang [a], Søren K. Kær [a]

[a] *Institute of Energy Technology, Aalborg University, DK-9220 Aalborg, Denmark*
[b] *DK-8600 Silkeborg, Denmark*

Received 30 January 2006; received in revised form 15 June 2006; accepted 16 June 2006
Available online 30 August 2006

Abstract

High temperature polymer fuel cells based on polybenzimidazole membranes (PBI) operated at 100–200 °C are currently receiving much attention in relation to fuel cell reforming systems due to two main reasons. At first they have proven to have excellent resistance to high CO concentrations, which decreases the number of system components in the fuel processing system. The preferential oxidation reactors can be left out and in addition a water condenser is not required. These system simplifications additionally decrease the parasitic losses associated with the components.

However, insufficient data are currently published to enable good system design and modeling. In this paper the influence of operation on synthesis gas and the variation of the cathode stoichiometry are investigated based on a generic commercial membrane electrode assembly (MEA). The CO content in the anode gas was varied from 0 to 5%, with CO_2 contents ranging from 25 to 20% at temperatures ranging from 160 to 200 °C. The influence of the cathode stoichiometry was investigated in the interval of 2–5 at temperatures from 120 to 180 °C with pure hydrogen on the anode.

A novel semi empirical model of the fuel cell voltage versus current density, cathode stoichiometry and temperature was derived. It shows excellent agreement with the experimental data. The simplicity and accuracy of the model makes it ideal for system modeling, control design and real-time applications.

Keywords: Fuel cell; PEM; PBI; Intermediate temperature; Modeling; HTPEM

1. Introduction

High temperature polymer fuel cells are receiving increasing attention for several reasons. First of all, the high operating temperature allows a simple fuel processing system. This is due to the fact that CO-desorption is favored at higher temperatures resulting in decreased CO-coverage of the electrochemically active Pt sites. Moreover, better heat integration with the reforming system is possible as no water condensing system is necessary between the reformer and the fuel cell. The membrane electrode assembly (MEA) does not need any external humidification allowing simpler system design leaving out expensive and bulky humidifiers. Additionally, the pressure loss in the fuel cell stack itself can be reduced because no liquid water has to be forced out of the cell. This in turn decreases the parasitic energy need for driving the air blower.

Great efforts have been put into developing polymer-based fuel cells. Main focus has been on developing fuel cell systems based on the PFSA type membranes where sulfur groups have been inserted into the electrolyte to facilitate proton conduction.

Currently a lot of work have been made on this type of fuel cell. Among others Verbrugge and Verbrugge [1] derived a detailed model based on experimental data. Later Amphlett et al. did a coupled mechanistic and empirical model [2]. Lee et al. presented the influence of CO poisoning on the anode overpotential in [3].

A close relative to the PBI type membrane is the phosphoric acid fuel cell (PAFC) which has been known for the last couple of decades. Data were published regarding the influence of CO concentration in [4].

The use of PBI for fuel cell applications was first published by Wainright et al. [5] followed by a number of papers [6,7].

* Corresponding author. Tel.: +45 96359253; fax: +45 98151411.
E-mail address: ark@iet.aau.dk (A.R. Korsgaard).

0378-7753/$ – see front matter © 2006 Published by Elsevier B.V.
doi:10.1016/j.jpowsour.2006.06.099

Nomenclature

a_x, b_x	Regression constants
F	Faraday constant
I	Cell current
I_0	Exchange current density
R	Universal gas constant
R_{xx}	Resistance
T	Cell temperature
U_0	Open circuit potential

Greek letters

α_c	Transfer coefficient
λ	Cathode stoichiometric ratio

Some of the same authors published data regarding the oxygen reduction reaction in [8] and recently they published data on CO-coverage in [9].

Other research groups also published data regarding development of PBI based MEAs such as the group of Bjerrum and coworkers [10,15,16].

Recently, [11,12] published a model of a PBI membrane but it only included one operating temperature and the stoichiometric ratio was unknown.

If systems and models are to be useable for system design and optimization purposes, detailed documented data are required, but only little has been published. Furthermore, it is necessary to formulate simple yet precise and sufficiently detailed mathematical models based on such experimental experience.

In this paper focus is on the performance of the generic polybenzimidazole (PBI) type MEA from a commercially available source.

Additionally, the data are fitted to a semi empirical model based on pure hydrogen tests including the influence of variations in temperature and cathode stoichiometry, which are the most significant parameters to evaluate system performance.

2. Experimental

The MEAs provided have an active cell area of 45.16 cm^2. The electrode consists of woven graphite fibers and has a thickness of 400 μm. A micro porous layer is coated on the back. The catalyst layer, besides carbon and ionomer, has a platinum loading of 0.7 mg cm^{-2} on the cathode and 1 mg cm^{-2} on the anode. It has a total thickness of 50–100 μm. The membrane itself is 100 μm thick with more than 90 wt.% phosphoric acid in a PBI matrix.

Fig. 1 illustrates the experimental setup, which is based upon a standard test cell. The stainless steel plates contain electrical heating elements in order to control the cell temperature. These are controlled from a computer. The flow plates are made of pure graphite. The flow plates contain three parallel flow serpentine channels on the cathode and two on the anode. The width of each channel is 1.5 mm and the wall thickness is 1 mm.

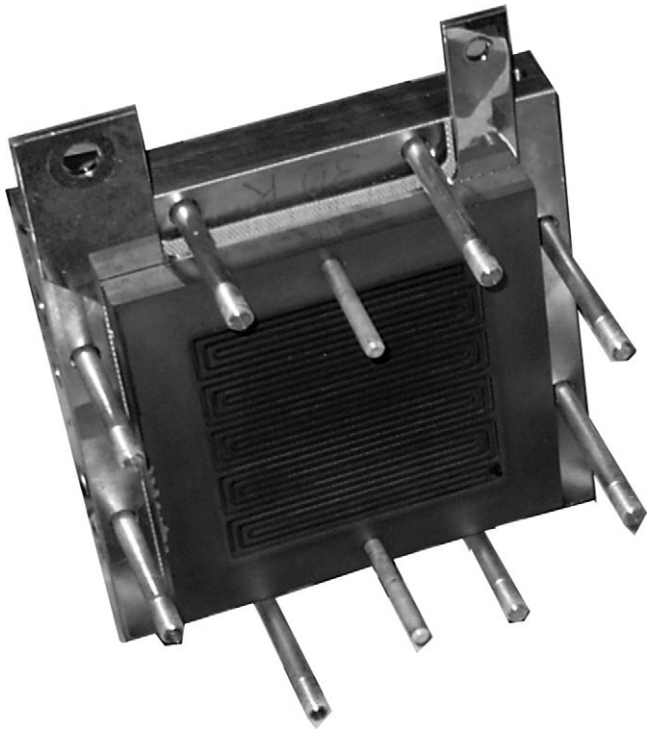

Fig. 1. Picture of test cell.

Fig. 2 shows a schematic representation of the test cell system. Mass flow controllers (of the brand Burkert) were used to control all inlet gases to provide the desired mixture. A water separator was added at the outlet of the test cell. All tests were performed at atmospheric pressure.

A Labview® control and data acquisition system was developed to automatically measure polarization curves. To ensure steady-state conditions, the current was increased by a rate of 30 s A^{-1} until the maximum current of 46 A was reached using a DTI load module (RBL 488). One data sampling was performed each second corresponding to approximately 1500 samples per dataset. The dataset was filtered with a three-point moving average algorithm.

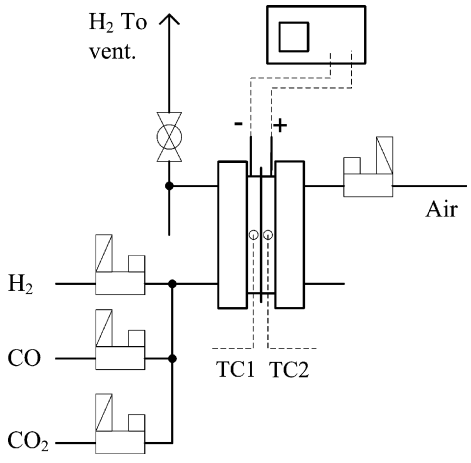

Fig. 2. Schematic of the test setup.

The largest potential measurement error comes from the mass flow controllers (1.8% FS). This will however not affect the measurements since stoichiometric variations in that order will not be readable on the cell voltage. The voltage and current measurements have a relative error less than 0.1%. Hence it is anticipated that differences in the manufacturing process will be the dominating uncertainty in the tests. At small air flows the uncertainty is however much greater, and this can produce measurement errors at low current densities and stoichiometric flows.

To break-in the MEAs they were loaded for 100 h with pure H_2/air with a stoichiometric ratio of 2.5/2.5 at 0.2 A cm^{-2} according to the manufacturer's specifications. During the break-in the performance of the MEA is improved in the order of 20 mV.

The pure hydrogen tests were performed at a stoichiometric ratio of 2.5.

The stoichiometric on the cathode was 2.5 unless otherwise specified.

All synthesis gas tests were performed at high stoichiometric ratios on the anode for two different reasons. First of all the used mass flow controllers for mixing the gases did not have a satisfactory precision at very low flow rates. Moreover, the stoichiometry used in reformer systems will vary greatly with the type of fuel processing technique used, i.e. steam reformer based systems will typically run at higher stoichiometric ratios, while the anode off gas should provide sufficient heat for the burner, than auto thermal or partial oxidation based systems.

The MEA used for the CO tests were replaced in the tests with pure H_2 to prevent any permanent degradation during tests with high CO content at low temperature, influencing the measurements. Additionally, the tests on synthesis gas were performed starting with the higher temperatures for the same reason.

The synthesis gas used was similar to that of a reformed ethanol gas, which has medium carbon content between that of natural gas and diesel.

$$C_2H_5OH + x_3H_2O \rightarrow (2 - x_1)CO_2 + x_2H_2 + x_1CO \quad (1)$$

x_1, x_2 and x_3 express the relative composition of the species in the reactants and products. As can be seen a fixed amount of CO and CO_2 of 25% was maintained while the remaining part is hydrogen. No water was added in these experiments. The CO content was varied according to the following:

- 5% CO, 75% H_2, 20% CO_2;
- 2% CO, 75% H_2, 23% CO_2;
- 1% CO, 75% H_2, 24% CO_2;
- 0.1% CO, 75% H_2, 24.9% CO_2;
- 25% CO_2, 75% H_2;
- 100% H_2.

Tests were also performed at 10% CO but permanent degradation seemed to occur at temperatures below 180 °C.

Tests at 200 °C also permanently degraded the MEA due to the current choice of electrode. Measurement data at this temperature are only provided for the simulated synthesis gas tests.

3. Theory

3.1. Overall model structure

In the present work, a semi empirical model was developed to express the overpotentials in the fuel cell. The expression is extremely simple and has been validated against all the measurement data available.

The cathode activation overpotential is dominant and is based on the Tafel equation. The anode overpotential will be neglected as it is usually very small for pure hydrogen operation as also shown in [1]. Additionally ohmic and concentration losses related to the stoichiometric ratio is expected to exist in the cell. Thus, the overall cell voltage can be written as shown in Eq. (1).

$$U_{cell} = U_0 - \eta_{act} - \eta_{ohmic} - \eta_{diff} \quad (2)$$

This corresponds to the following expression where all the terms are expanded:

$$U_{cell} = \frac{U_0 - RT}{4\alpha_c F} \ln\left(\frac{i + i_0}{i_0}\right) - \frac{R_{ohmic} i - R_{conc} i}{\lambda - 1} \quad (3)$$

The first term, U_0, represents the open circuit voltage and should not be confused with the equilibrium voltage that is sometimes used. The second term is the Tafel equation where i_0 is included in the nominator. This should have a very low impact on the cell voltage but it is incorporated for numerical reasons. The third term is related to ohmic losses, but will also reflect some concentration losses at higher loads.

The last term is a novel approach of including the effect of cathode stoichiometry on performance. As seen this term will approach zero as the stoichiometry goes towards infinity but as it goes towards unity, this term will dominate the result. This is assumed to be in good agreement with the physical behavior of the fuel cell.

3.2. Derivation of regressions

The concentration term in Eq. (3) is physically justified while as λ goes towards 1 this term will completely dominate the cell voltage reduction. The expression, however, is not valid for stoichiometric ratios below 1. As the stoichiometric ratio becomes very high, the influence of this term becomes negligible. The variable R_{conc} is related to the diffusion resistance of the electrode and catalyst layer. It is related to the diffusion coefficient (binary diffusion of O_2 in N_2) and protonic conductivity of the catalyst layer. At higher temperatures this resistance will decrease limiting the influence of this term. A linear regression for the concentration resistance was used as shown in Eq. (4):

$$R_{conc} = a_2 T + b_2 \quad (4)$$

The exchange current density is typically expressed as an exponential function in the form shown in Eq. (5), while Arrhenius type behavior would be expected as the author of [14] suggested.

$$i_0 = a_3 \exp(-b_3 T) \quad (5)$$

The cathode transfer coefficient is assumed to depend on the temperature following a linear relation as [14] and other authors also suggested.

$$a_c = a_0 T + b_0 \quad (6)$$

Note that the actual value of α_c will be lower than the one given by Eq. (6) but this is incorporated open circuit potential.

The protonic conductivity has been given by the manufacturer and has a linear behavior versus temperature ranging from $0.18\,S\,cm^{-1}$ at 100 °C to $0.19\,S\,cm^{-1}$ at 150 °C. The thickness of the membrane is approximately 100 μm. However, not only the membrane contributes to the ohmic losses as the catalyst layer itself is 50–100 μm with a conductivity less than the membrane. At low current densities the reaction takes place relatively close to the membrane but at higher current densities the reaction moves towards the gas diffusion layer as oxygen diffusion limitations begin to dominate. A detailed discussion of this subject is included in the work of Bang et al. [13].

The reaction displacement will result in increasing ohmic losses. It is assumed that the dominating losses will be in the ionomer, consisting of PBI material with the same temperature dependency as the membrane itself. Hence, if the conductivity of the membrane versus temperature can be expressed as a linear regression so can the total ohmic loss:

$$R_{ohmic} = a_1 T + b_1 \quad (7)$$

3.3. Parameter fitting

With the pure hydrogen test data a least square optimization algorithm was used to fit the parameters at each temperature from 120 to 180 °C. Four degrees of freedom were chosen with α, i_0, R_{ohmic} and R_{diff} as the parameters. Then a physical evaluation was done regarding the values of each of the parameters. Afterwards regressions were made stepwise in the following order:

- Linear regression of the diffusion resistance term (R_{diff});
- linear regression of the ohmic resistance (R_{ohmic});
- exponential regression of the exchange current density (i_0);
- linear regression of the charge transfer coefficient (α).

4. Results

4.1. Variation of cathode stoichiometric ratio versus temperature

Fig. 3 shows the tests performed with pure H_2 and air. The stoichiometric ratio was held constant at 2.5 on the anode at all times. It is seen that the performance is significantly improved from 120 to 180 °C. This is due to the better conductivity at higher temperatures. However, at 120 °C it is possible to operate the fuel cell with acceptable performance.

The stoichiometric ratio seems to cause a similar voltage offset at all temperatures even though the overpotential is slightly higher at lower temperatures. This could be due to the fact that

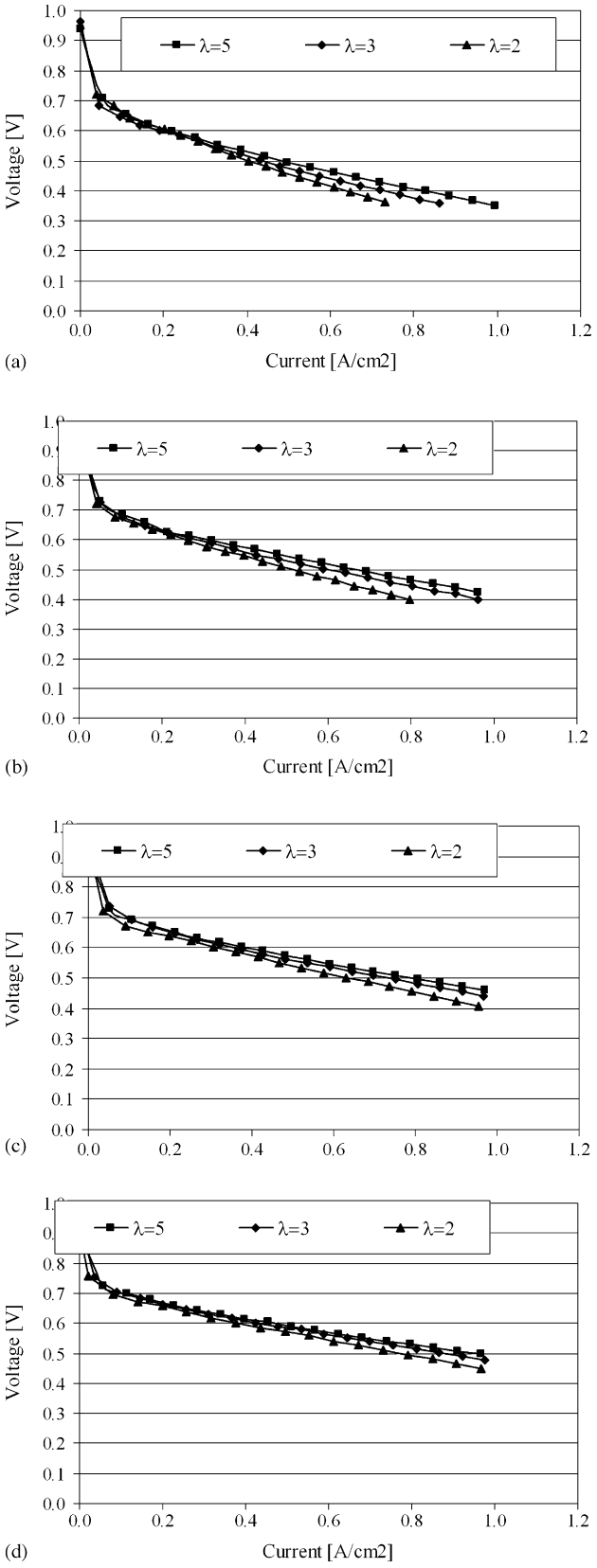

Fig. 3. Test results for pure H_2 and air at temperatures (a) 120 °C, (b) 140 °C, (c) 160 °C and (d) 180 °C.

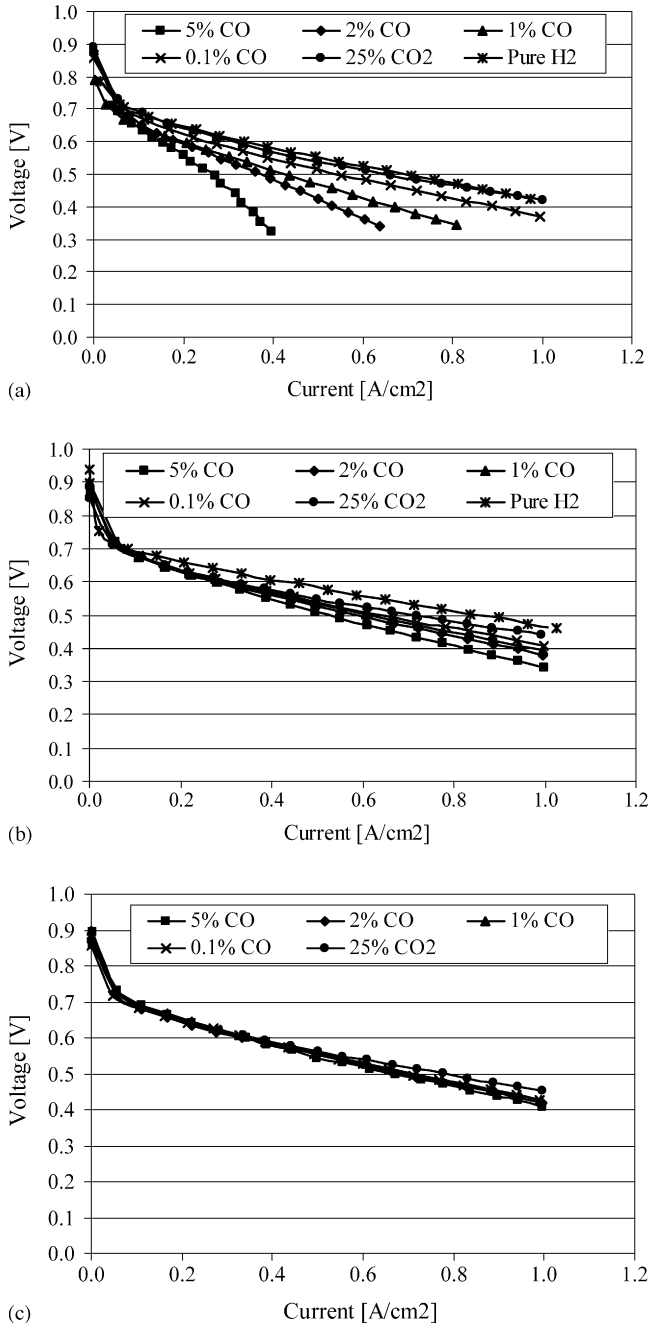

Fig. 4. Test results for synthesis mixture compared to pure H_2 curves for temperatures (a) 160 °C, (b) 180 °C and (c) 200 °C.

the oxygen diffusion coefficient in air increases with temperature and thereby decreasing the cathode overpotential.

4.2. Synthesis gas influence anode overpotentials

Fig. 4 shows the tests performed on synthesis gas at 160, 180 and 200 °C.

At 160 °C and 5% CO, the cell performance is significantly affected but at 2% CO the operation seemed stable though a performance decrease is clear. By lowering the CO concentration to 1% and below, cell performance is considerably improved.

The carbon monoxide impact is also reduced at 180 °C and the fuel cell is stable at all operating conditions, even though performance is still significantly reduced. At 200 °C only limited performance degradation was observed when varying the CO content. The presence of CO_2 had only negligible effect on the performance.

4.3. Model fit of pure hydrogen tests versus temperature and cathode stoichiometry

Fig. 5 shows the modeling results for the pure hydrogen tests. Results for stoichiometric ratios 2, 3 and 5 are shown. In each of the plots, four temperature curves are shown with both experimental and model results. The lowest cell potential corresponds

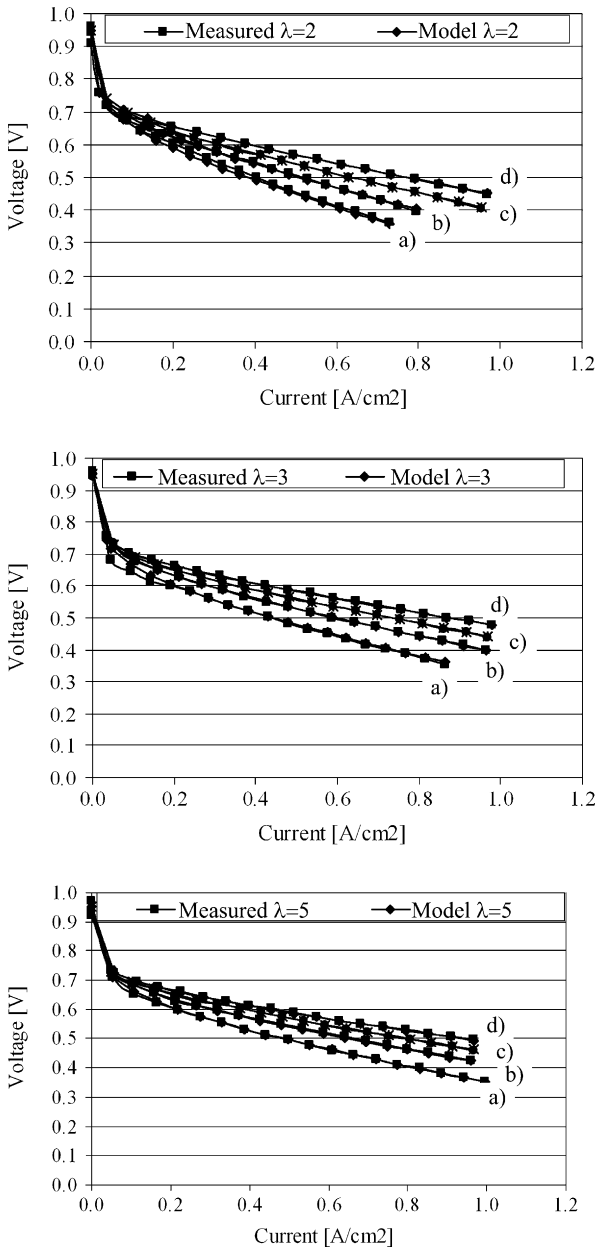

Fig. 5. Modeling results for pure hydrogen vs. specific current, stoichiometric ratio and temperatures from (a) 120 °C, (b) 140 °C, (c) 160 °C and (d) 180 °C.

Table 1
Numerical values used in model

Membrane	
Membrane thickness, t_{memb}	0.1×10^{-3} m
Values used for regressions	
Charge transfer constant, a_0	2.712×10^{-3} K^{-1}
Charge transfer constant, b_0	−0.9049
Ohmic loss constant, a_1	−0.0006488 Ω K^{-1}
Ohmic loss constant, b_1	0.4410 Ω
Diffusion limitation constant, a_2	−0.001106 Ω K^{-1}
Diffusion limitation constant, b_2	0.5569 Ω
Limiting current constant, a_3	33.3×10^3 A
Limiting current constant, b_3	−0.04506
Open circuit voltage, U_0	0.95 V
Other values	
Universal gas constant, R	8.3143 J mol^{-1} K^{-1}
Faradays constant, F	96485 C mol^{-1}

to the lowest cell temperature and upwards. As it is seen, a very good agreement between model and experiments was achieved. The overall average error was only 5 mV. The errors in the low ranges of the current density can be explained by the turn down ratio of the mass flow controller. It is within its nominal operating range at currents larger than 0.1 A cm^{-2}. Table 1 shows the values of the parameters derived during the fitting procedure.

5. Discussion

5.1. Experimental results

It is seen that the CO surface coverage is highly temperature dependent. This was however also expected as the kinetics favor CO-desorption at higher temperatures. The reason for the minor CO_2 performance degradation is not entirely understood. Possibly, the water–gas-shift reaction plays a role. The presence of water at both the anode and cathode compartments was observed during the experiments. The experiments performed show good agreement with the results of [15,16]. As explained the experiments with synthesis gas were made at high anode stoichiometric ratios. Hence the results cannot directly related to.

Future tests with an inert gas such as nitrogen will reveal the ad-/de-sorption kinetics dominating the performance.

It is also shown that increasing operating temperature and stoichiometric ratio significantly enhances the performance. However, these parameters might also limit lifetime of the MEA. Upcoming studies will reveal the relationship between these operating conditions and degradation and MEA failure.

5.2. Modeling results

It was found that the total ohmic losses were approximately three times what the resistance of the membrane itself would predict, which is believed to be realistic. Additionally, the transfer coefficient was found to be in the range from 0.14 at 120 °C to 0.32 at 180 °C. This is in the lower region compared to what is typically published for low temperature PEM MEAs. It should

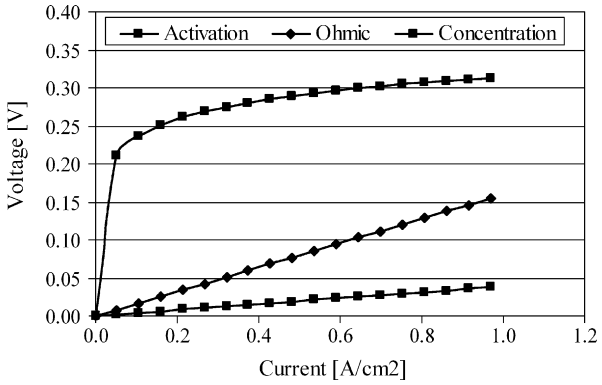

Fig. 6. Distribution of overpotentials vs. current at 160 °C and a cathode stoichiometry of 3.

be stressed however that these values cannot be directly related to the values given in other literature, as the open circuit is used instead of the equilibrium voltage.

The slope of the charge transfer coefficient however, is found to be 0.0028 which is in perfect agreement with the work carried out by Parthasarthy et al. [14]. They measured the slope of the charge transfer coefficient to be 0.0023 for Nafion, and referred to other publications for phosphoric acid fuel cells where the rate is between 0 for 98% H_3PO_4 and 0.0034 for 85% H_3PO_4.

The ohmic resistance is also believed to be of a realistic magnitude compared to the published data for the MEA itself.

A model of the anode kinetics as well as a detailed model of the catalyst layer is being developed.

Fig. 6 shows the loss distribution in terms of activation, ohmic and the concentration losses related to the cathode stoichiometry. Comparing to the work of [12] the ohmic losses contribute much more to the total losses. This could be due to the fact that the catalyst layer protonic loss was not included in their work. The concentration loss also has a significant loss associated while the activation losses are lower. This however, is caused by the use of the open circuit voltage in Eq. (3) instead of the equilibrium voltage as previously discussed.

6. Conclusions

Tests were performed on commercial intermediate temperature MEAs based on the polybenzimidazole membrane. The influence on cell performance of operating parameters such as cathode stoichiometric ratio and operating temperature were investigated.

It was found that it is possible to operate the fuel cell from 160 °C with a CO content of up to 2%. Even higher CO concentrations are possible but operation at these temperatures requires an increase of temperature.

A very simple model of the cell voltage was developed based on pure hydrogen tests, which will be very useful in any system model. It agrees very well with an average error on each point less than 4 mV in the range from 120 to 180 °C and stoichiometric ratios from 2 to 5. A novel method for modeling the influence of cathode stoichiometry was also included with very good results.

In general the model is very suitable for applications such as system modeling, control design or for use in real-time applications.

Acknowledgements

The authors would like to thank a number of companies supporting the work including Dantherm, Danfoss and APC Denmark.

References

[1] D.M. Verbrugge, M.W. Verbrugge, J. Electrochem. Soc. 139 (1992) 2477–2490.
[2] J.C. Amphlett, R.M. Baumert, R.F. Mann, B.A. Peppley, P.R. Roberge, J. Electrochem. Soc. 142 (1995) 1–8.
[3] S.J. Lee, S. Mukerjee, E.A. Ticianelli, J. McBreen, Electrochim. Acta 44 (1999) 3283–3293.
[4] Rak-Hyun Song, Dong Ryul Shin, Int. J. Hydrogen Energy 26 (2001) 1259–1262.
[5] J.S. Wainright, J.-T. Wang, D. Weng, R.F. Savinell, M. Litt, J. Electrochem. Soc. 142 (1995) 121–123.
[6] R.F. Savinell, J.S. Wainright, M. Litt, Electrochem. Soc. (1995) 214–215.
[7] J.T. Wang, R.F. Savinell, J.S. Wainright, M. Litt, H. Yu, Electrochim. Acta 41 (1996) 193–197.
[8] Zhenyu Liu, Jesse S. Wainright, Robert F. Savinell, Chem. Eng. Sci. 59 (2004) 4833–4838.
[9] J.D. Holladay, J.S. Wainright, E.O. Jones, S.R. Gano, J. Power Sources 130 (2004) 111–118.
[10] Qingfeng Li, et al., Solid State Ionics 168 (2004) 177–185.
[11] D. Cheddie, N. Munroe, J. Power Sources 156 (2006) 414–423.
[12] D. Cheddie, N. Munroe, Energy Convers. Manage. 47 (2006) 1490–1504.
[13] M. Bang, M. Odgaard, T.J. Condra1, S.K. Kær, ASME Fuel Cell (2004).
[14] A. Parthasarthy, S. Srinivasan, A.J. Appleby, J. Electrochem. Soc. 139 (1992) 2530–2537.
[15] Q. Li, R. He, J.O. Jensen, N.J. Bjerrum, Fuel Cells 4 (3) (2004) 147–159.
[16] Li Qingfeng, H.A. Hjuler, N.J. Bjerrum, J. Appl. Electrochem. 31 (7) (2001) 773–779.

4.4 Additional measurements on the high temperature PEM fuel cell

Before moving on, some additional tests performed on the high temperature PEM MEA's will be presented.

Most of the tests performed in the paper were made on the single fuel cell test facility shown in Fig 14. To the right two mass flow controllers are providing air and hydrogen to the single cell test block in the center. 4 heating elements are inserted into the block. On each side two blowers are placed to provide fast cool down capability of the test stand.

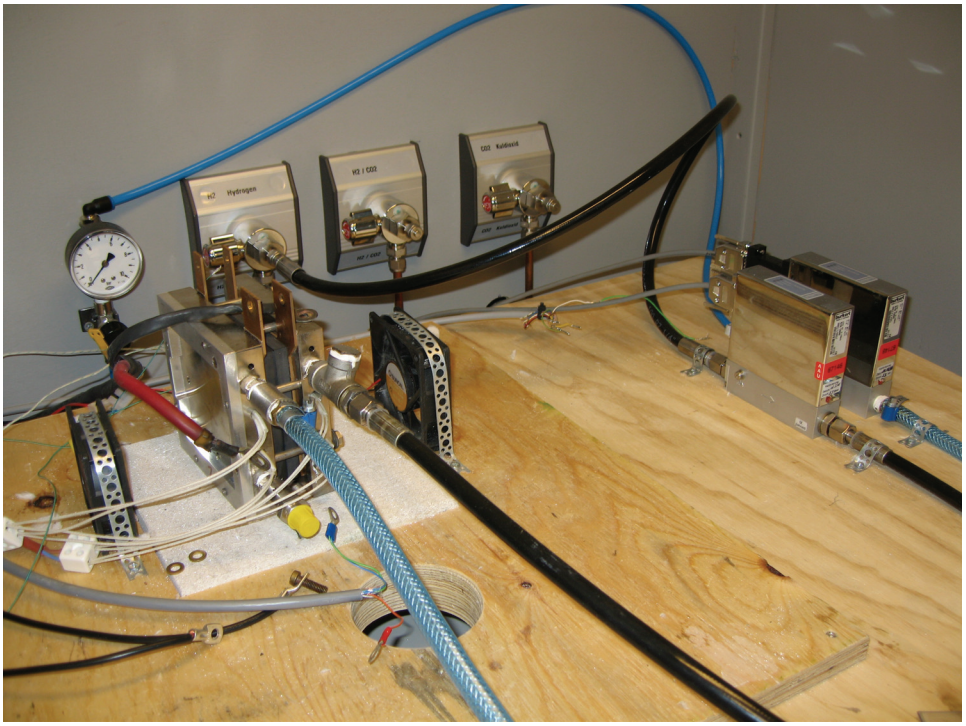

Fig 14: One of the two single cell test facilities

This feature is added to be able to perform quick transient startups and shut downs in order to test the degradation mechanisms regarding thermal cycling. Fig 15 shows one of the tests made. Each cycle lasted app. 2 hours (11 per day). The fuel cell was heated from 30°C to 160°C (~20 min), then loaded at a constant load for 5min (0.5 A/cm^2). The mean value corresponds to a one single cycle value in the figure. Afterwards a polarization curve was made (app. 15 min). Following the unit was flushed (only with air and hydrogen) and then cooled down using the cooling fans to 30°C, where another cycle started.

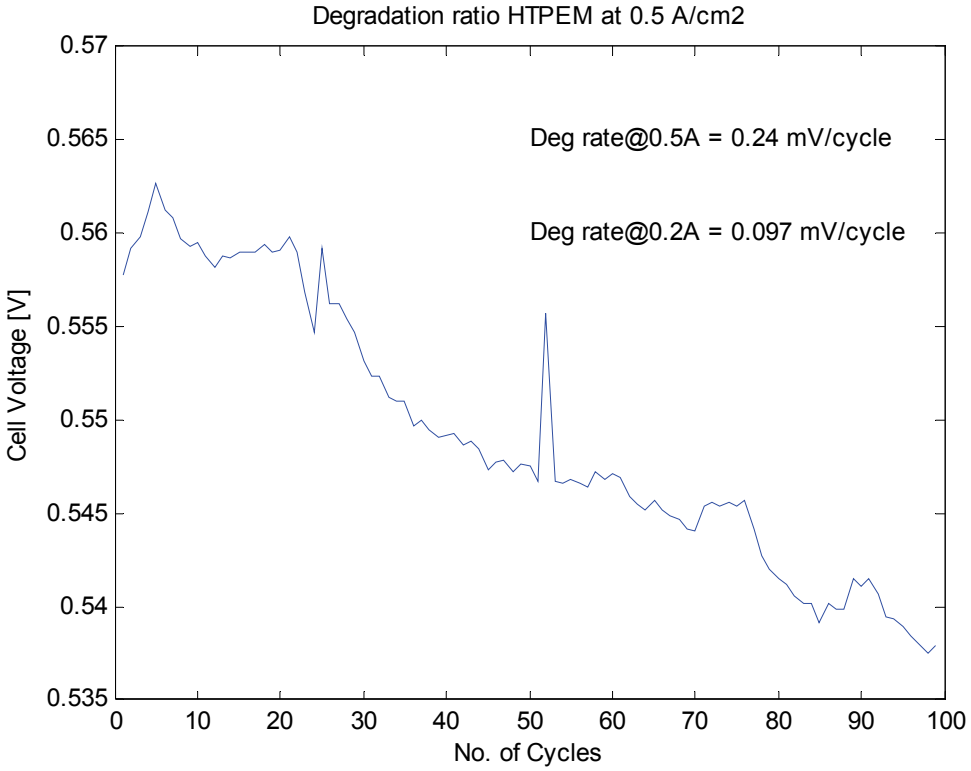

Fig 15: HTPEM resistivity towards thermal cycling (startup/shut down)

The figure shows app. 0.24 mV degradation per cycle at a fairly high load. It should be noted that the losses are resistive, meaning that doubling the current density also doubles the voltage loss (and thereby the power loss). In most CHP applications, however, the fuel cell will only be operated on such high current density during peak hours of operation. It is expected that the cyclic degradation losses will be reduced by on order of a magnitude over the coming years as new generations of MEA's are developed.

Fig 16 shows the dynamic response to changes in CO concentration in the anode supply gas. From the initial 150°C the 1% CO was added at a very high stoichiometry ratio. During heating, the CO mass flow controller was pulsed off periodically. It can be seen that the response is nearly instant in contrast to the low temperature fuel cell, where adsorption/desorption kinetics are much slower. Hence in terms of a CHP system the response can be considered instantaneous and balance of plant components will most likely have time constants that are much slower than this.

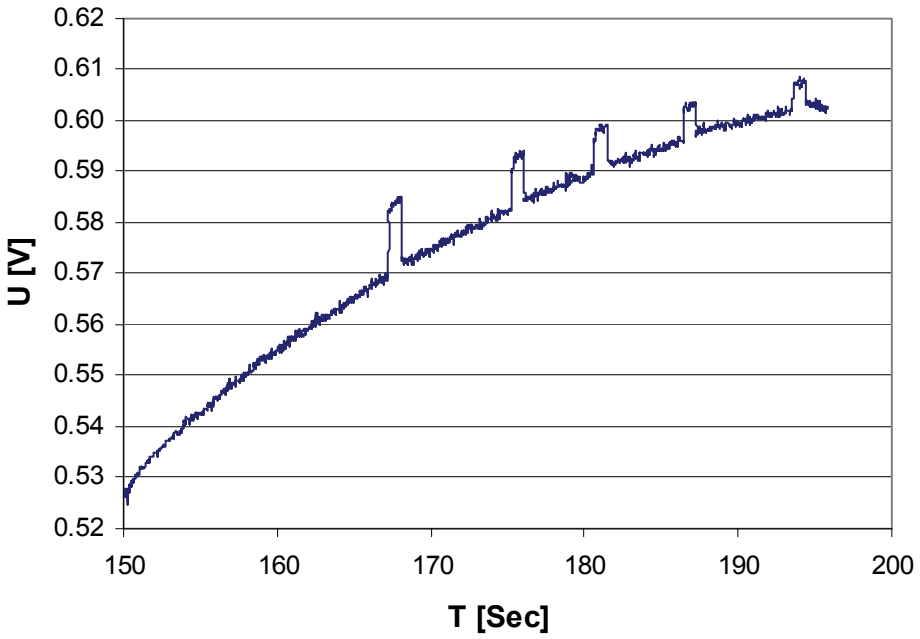

Fig 16: CO influence on performance (i=0.33 A/cm², lambda=2.5, 1000 PPM CO)

4.5 Evaluation of the PEM fuel cell technology for CHP

From the presented papers, an evaluation of the two different technologies is to be made. In general it is believed that both technologies could be viable prospects for micro CHP systems. The low temperature PEM fuel cell stack had a very good performance in terms of cell voltage and had a surprisingly low pressure drop of only a few thousand Pa. However cell monitoring showed that occasional cell flooding occurred and was never permanently resolved. In most cases, however, purging the cathode seemed to solve the problem and it could be suggested that relatively high variations of cell performance in the stack indicated flooding of some of the cells. Next the sensitivity towards CO and CO_2 were fairly high, although it seemed like the performance could be recovered after CO poisoning by some degree of fuel starvation. This might, however, come at a cost of higher degradation rates.

The high temperature PEM fuel cell technology suffered from a bit lower performance than the low temperature version. The issue that it should be heated to above 100°C before loading could also be considered a drawback.

Having said that, the technology seemed very convincing and it was easy to reproduce the results from previous tests, indicating a mature technology. High tolerance towards impurities also votes for this technology as does the relatively high operating temperature, making it easy to integrate with the household heating system. From a system integrators viewpoint the fact that no humidification is needed is also very attractive since water management in general increases system complexity significantly.

Summarizing it has been decided to use the high temperature PEM for the modeling part in the next chapter.

4.6 Natural gas fuel processing system

Fig 17 shows the natural gas reforming system designed for the project. The unit itself was delivered by Hygear, a Dutch company, and includes all chemical reactors including:

- Sulphur removal reactor
- Reformer
- 2 water gas shift reactors
- Preferential oxidation reactor

Fig 17: Picture of the natural gas fuel processor

Fig 18 shows the process instrumentation diagram for the fuel processing system. The internal layout of the reformer is hypothetical as all information about these matters is confidential. From the right, the natural gas (or methane) is supplied through the mass flow controller (V12) and passes through a low temperature desulphurization unit to the evaporator which mixes a certain amount of steam into the stream. It then enters the steam reformer where it mixes with steam from a heat recovery heat exchanger cooling down the reformate exit gas stream. Heat for the process is provided from the ignition burner, which should be started up on hydrogen but can, once heated, operate on fuel cell anode waste gas or methane which is supplied by (V05) or (V11) respectively. Air for the burner is provided by (V13).

From the exit of the reformer the reformate gas can be vented to the exhaust to be able to run the reformer alone or passed to the shift reactor by turning the 3-way valve. After passing through the first exothermic water gas shift step the reformat stream is cooled by (D04) and subsequently enters the second step. From the exit of the water gas shift it passes directly to the first PrOx step (exothermic) and being cooled with (D03) before entering the last PrOx step. At this point the gas should contain less than 10 ppm. A condenser on the exit ensures that the dew point of the gas is equal to or below the fuel cell temperature, preventing condensation in the fuel cell.

As the shift reactors are based on traditional non-precious metal catalysts it is very sensitive to oxygen and if exposed to the temperature will rise resulting in sintering of the catalyst.

On the other hand the reactors need to be heated to a few hundred degrees Celsius to be operational. Hence a nitrogen preheating system is added which is added from the bottle (V20). Once the chamber and pipes are filled the blower ($C0_2$) recirculates the nitrogen through the pre-heater (H02).

In the top left, two three way valves controls whether to pass the reformat stream to the fuel cell, burner or both. It can however also be vented directly to the exhaust.

The system was unfortunately completed just one month before the project was terminated and hence it did not make sense to make a series of test on this unit. However, the process of building and designing the balance of plant did provide a substantial amount of knowledge to the modeling work.

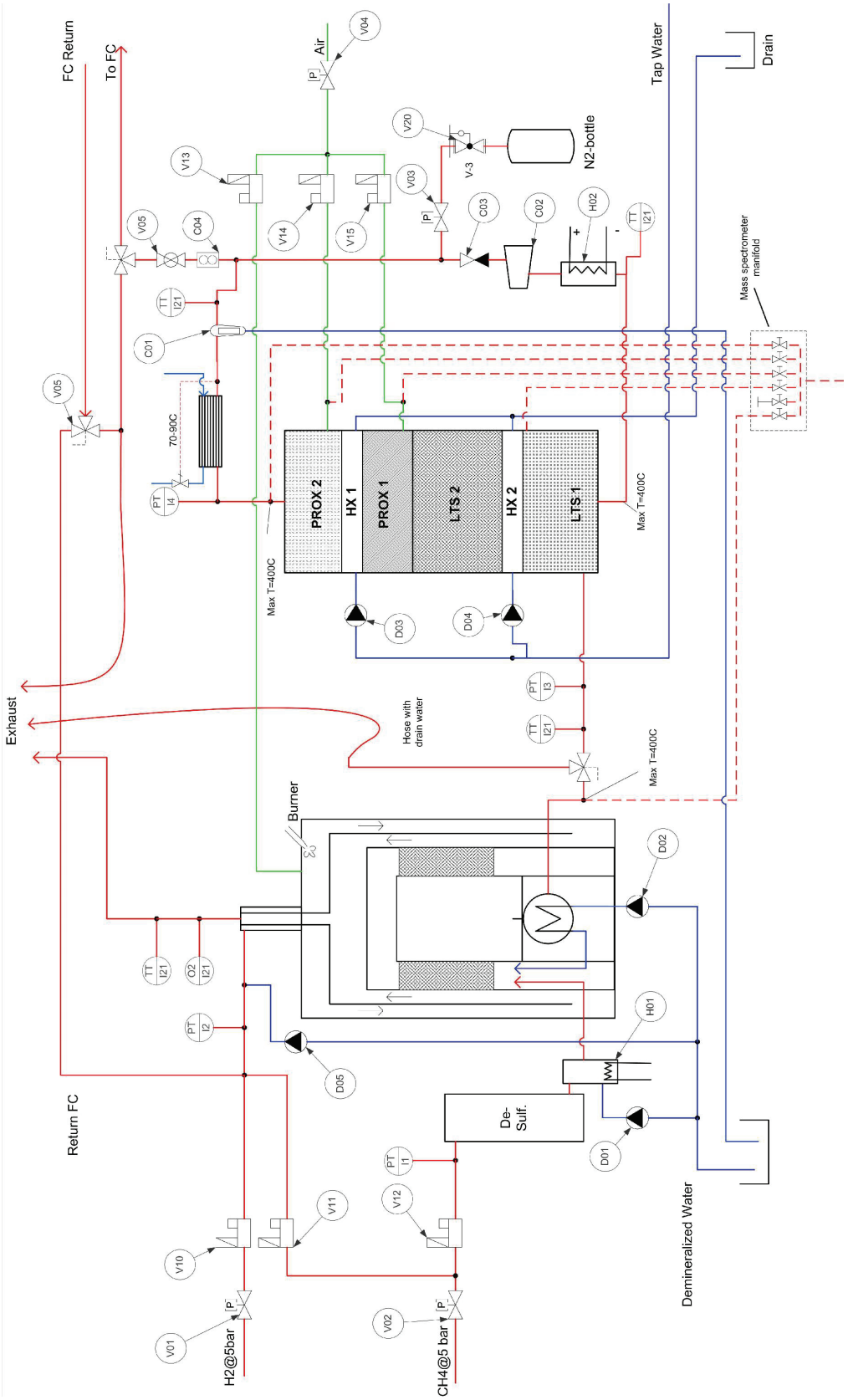

Fig 18: Process instrumentation diagram for Hygear reformer (red lines: fuel/reformat streams, blue lines: water/steam and green: air)

5 Modeling

5.1 Modeling method

In the following chapter a range of different models will be presented. Most of the work is contained in the papers referred to through the text.

A range of models have been developed through the project, where some of them did not fit the purpose of simulating the performance CHP systems on yearly basis. This was mainly due to long simulation times.

One of the models developed were of a steam reforming based fuel processor, where all reactors were described in detail by 1D partial differential equations taking into account heat transfer, kinetics etc. Each reactor was split into more than 50 nodes and integrated over time. the method of lines was used to integrate the partial differential equations. The model provided very good insight into the basic heat exchanging and kinetics of the reactors but was too slow to be used for modeling yearly consumption patterns as desired (Real Time/100). The transient model was based on earlier work presented in [41].

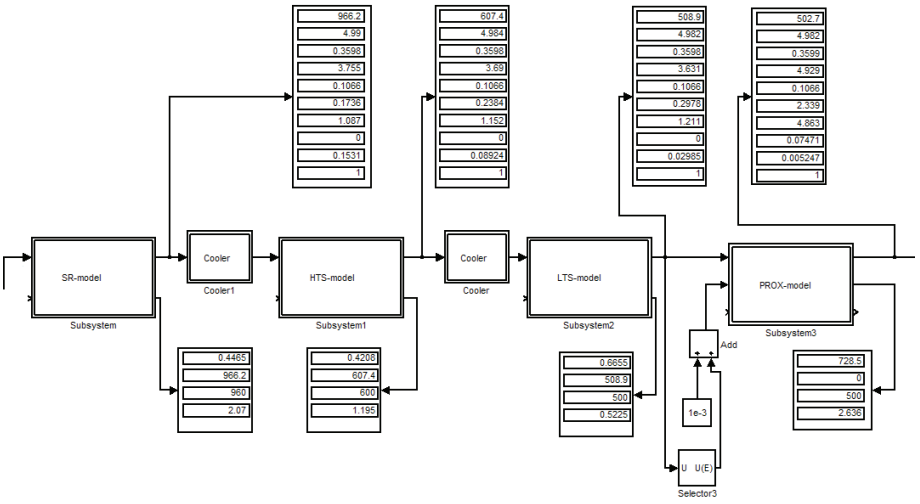

Fig 19: Shows an overview of the Matlab®Simulink model developed of the fuel processor.

The modeling approach was instead used for another project at Aalborg University where an ethanol steam reforming unit was designed and characterized. This is straight forward as ethanol quickly decomposes to methane. A master thesis was written on this subject [40] where a range of systematic tests were performed on a STUR reforming unit from Catator AB, Sweden. Fig 20 shows the system which besides the steam reformer, consists of a water gas shift, a partial oxidation reactor and a catalytic burner.

Fig 20: Catator STUR fuel processing unit.

One of the main conclusions drawn during this work was that the outlet gas composition of the reformer and water gas shift reactors can be estimated as being in chemical equilibrium. The major conclusion of the work is presented in the publication "Experimental characterization of ethanol reformer" which follows this section.

This is immediately followed by a publication based on the experiments of the paper presented in section 4.2. While this paper contained a basic model of the cathode over potential the next publication describes a 1st order chemical model of the ad-/desorption mechanisms of CO on the anode side, considerably lowering the active sites available for hydrogen. The model in general provided very good agreement with the experimental results.

Afterwards a publication concerning modeling of a complete system follows. The model shows excellent performance, effectively simulating as well system transients as well as steady state behavior which both are crucial to make any major conclusions regarding system efficiency and response time.

The last paper deals with evaluation of sublevel control strategies as well as the three control scenarios already outlined in section 2.3. The system as well as the model shows good performance covering most of the demands which were set to the system in the introductory chapters. The paper was published in Journal of Power Sources (August 2006).

Experimental characterization and modelling of an ethanol steam reformer

M. Nielsen, A. Korsgaard, M. Mandø, M. Bovo, S. Kaer, M. Bang
Aalborg University, Aalborg East, Denmark

Abstract

This work describes the characterization of an ethanol reforming system for a high temperature PEM fuel cell system. High temperature PEM fuel cells are well suited for operation on reformate gas due to the superior CO tolerance compared with low temperature PEM. Steam reforming of liquid biofuels (ethanol, bio-diesel etc.) represents sustainable sources of hydrogen for micro Combined Heat and Power (CHP) production as well as Auxiliary Power Units (APUs). The system was experimentally characterized and theoretically modelled using a 1-dimensional system model implemented in MATLAB/Simulink. Detailed aspects of the reforming system were investigated and preliminary results indicate good agreement between modelling and experiments.

Experimental Facility

The experimental test facility was established using a commercial STUR unit (Single-Train Ultraformer Reactor) supplied by the Swedish company Catator AB. The experimental setup includes an advanced LabView based control and data acquisition interface.

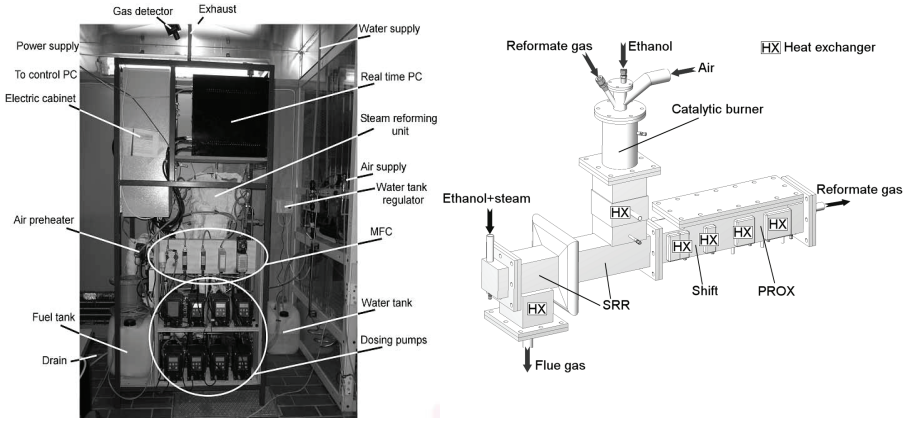

Figure 1: Experimental Facility (test facility is shown to the left – STUR unit to the right).

The STUR unit is composed of four main components, a catalytic burner, a steam reforming reactor (SRR), a water gas shift reactor and a preferential oxidation reactor (PROX - this was not included in the present analysis. The catalyst used in all reactors is based on a novel technique using wire mesh supports which is a patented property of Catator AB. The catalysts in each reactor step, which are noble metal based, are of wire mesh type, where the substrate material was prepared according to Catator´s patented thermal spray technology [Patent Catator AB, EP 0 871 543 B1]. The unit is a prototype able to work with different fuels (e.g. natural gas, gasoline and ethanol). The catalytic burner is supplied with ethanol and ambient air. For start-up, an electrical preheater is used for heating inlet air and hence, the burner catalyst. The burner catalyst facilitates an efficient and clean combustion at relatively low temperature. The heat generated in the burner is used to sustain the endothermic steam reforming reaction in the SRR. To do so the flue gas stream from the catalytic burner and the reformate gas stream are arranged in counter current mode as shown in figure 2.

The heat generated in the burner is also used to vaporize the ethanol/water mixture to be reformed. For this purpose two heat exchangers are included and arranged in series. The first heat exchanger is placed at the exit of the flue gases from the SRR reactor. The second heat exchanger is constructed with externally mounted plates surrounding the combustion chamber. Sensor locations in the experimental STUR unit are shown in figure 2 (left) as well as flow paths (right):

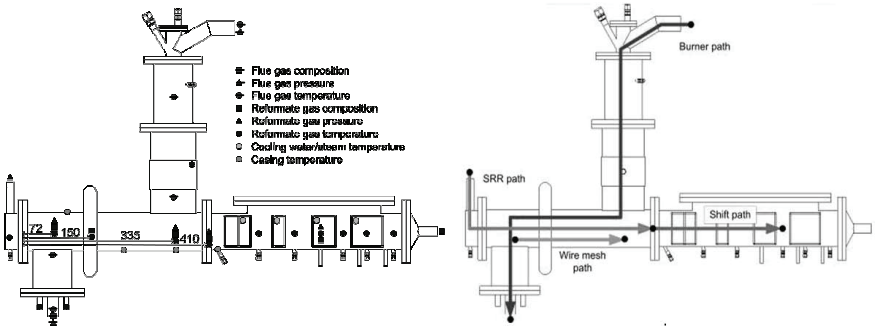

Figure 2: The location of sensors in test facility (left) and flow paths in STUR unit (right).

Detailed temperature, pressure drop and reformate gas composition measurements were collected inside the reformer. A wide range of operating condition was investigated including various steam-to-carbon ratios (SCR), loads and load steps. The gas composition measurements were made with a mass spectrometer.

Theoretical modeling of the STUR unit

The developed transient system model consists of blocks which have inputs and outputs of the temperature, pressure and molar flow rate of the species in the reformate gas. In the figure below is shown an illustration of the 1D model (plug flow is assumed in all reactors):

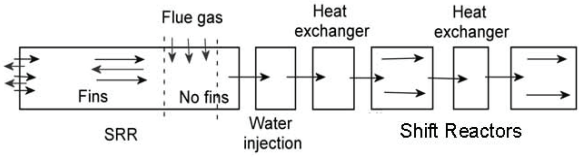

Figure 3: 1D-modeling approach.

The model has been created by setting up partial differential equations describing the mass and energy balances of the different reactors of the fuel processing system. The principle of conservation of mass is implemented in the model using continuity equations for each species:

$$\underbrace{\rho_f\left(\frac{\partial x_j}{\partial t}+u_s\cdot\frac{\partial x_j}{\partial z}\right)}_{accumulation+convection}=\underbrace{\frac{\rho_f\cdot A_{CS}\cdot u_s}{F_{ethanol,in}}\cdot r_j}_{reaction}\quad ,where\ x_j=\frac{F_{j,in}-F_j}{F_{j,in}}$$

where u_s is the superficial velocity [m/s], ρ_f is the fluid density [kg/m^3], A_{CS} is the cross sectional area [m^2], r_j is the conversion rate [kmol/(kg·s)], F is the molar flow rates [kmol/s] and x_j is the conversion variable. The conversion rate r_j is found using kinetic expressions has initially been based upon previous works in the open literature from papers and books. The kinetics used in the steam reforming reactor is based on the work of Therdthianwong et al, (2001) and Froment and Bischoff, (1990). The kinetics used in both the high temperature and the low temperature shift reactors are based on the kinetic scheme developed by Keiski et al, (1996).

The evaluation of energy transfer in the reactors has resulted in a number of equations; one for each temperature modelled as a state variable (walls, solid and gas). In the SRR this gives 4 equations while in the shift 3 equations are used. The energy equation of the reformate gas stream is shown:

$$\underbrace{\rho_g c_{p_g}\left(\frac{\partial T_g}{\partial t}+u_s\frac{\partial T_g}{\partial z}\right)}_{\text{accumulation+convection}}=\underbrace{\sum_i -dH_i r_i}_{\text{reaction}}+\underbrace{k_g\frac{\partial T_g}{\partial z^2}}_{\text{conduction}}+\underbrace{U_{w,g}\frac{P}{A_{CS}}\left(T_w-T_g\right)}_{\text{wall boundary condition}}-\underbrace{U_{g,s}\frac{A_{surf}}{V}\left(T_g-T_s\right)}_{\text{wire mesh boundary condition}}$$

The thermodynamic properties density ρ, specific heat capacity c_p and gas conductivity k_g depend on the composition of the gas and the temperature. They are calculated using polynomial fits of the thermodynamic data. The gaseous phase consisting of H_2, CO, CO_2, N_2 (in the case of autothermal operation adding air at the SRR-inlet), H_2O and CH_4 is due to the low pressure and the high temperature considered as ideal gasses. Similar expressions have been formulated for the energy balance of the flue gas stream, the inner wall and for the wire mesh screens.

The model, comprising of the partial differential equations, was implemented in the MATLAB/Simulink environment. The partial differential equations have been discretized using the method of lines. Each reactor has been divided into a number of elements along their longitudinal axis. For the model of the SRR, 50 elements have been used, while for both the high temperature and the low temperature shift reactor, 20 elements have been used. The number of elements where chosen considering the gradients of the temperatures and conversion variables. S-functions in Simulink were used to reformulate the partial differential equations into a system of ordinary differential equations. These S-functions require the state variables as input in vector form to perform the time integration via the built-in Simulink integrators.

Results

Very good agreement was found between the steady-state experimental data, predictions made with the 1-dimensional system model and chemical equilibrium calculations. Below is a comparison of post-shift compositions (left) and modelled species composition along the length of the SRR (right). In the gas composition profiles, the first 0.4 m represents the steam reforming reactor.

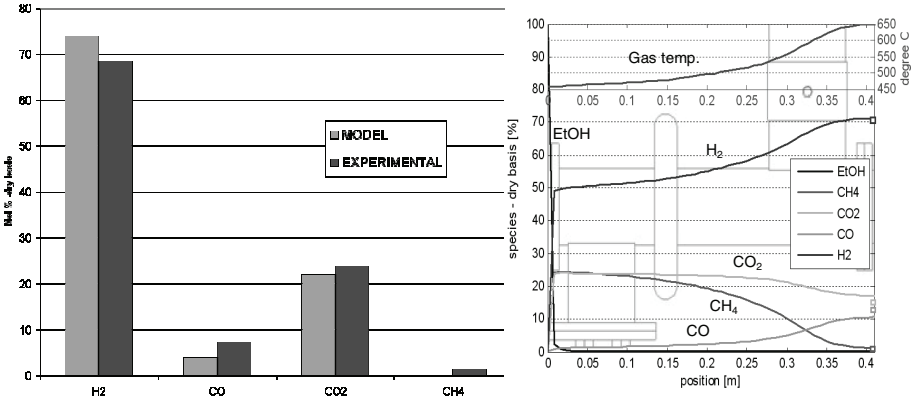

Figure 4: Modelling results. Composition after shift (left) composition through SRR (right)

The thermal efficiency of the unit was measured based upon the following definition:

$$\frac{F_{H_2}\cdot LHV_{H_2}}{\left(F_{EtOH,burner}+F_{EtOH,SRR}\right)\cdot LHV_{EtOH}}\cdot 100\%$$

Experimental efficiencies at different loads and steam to carbon ratios are shown below:

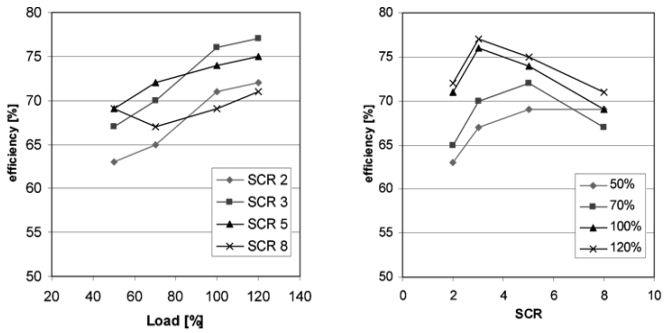

Figure 5: Thermal efficiency of the STUR unit at different loads and SCR's (excl. preheater).

Conclusion

The initial experimental results obtained with the investigated STUR-unit can be summarized as follows:

- Thermal system efficiency was at best 77 % (based on the above definition)
- The efficiency of the unit is highest for SCR's between 3-5 depending on the load
- Start up time to produce FC grade reformate gas at 100 % load is approximately 70 min.
- Total system weight ~150 kg, total system volume ~1.5 m^2
- Effective turn down ratio 1:2
- Hydrogen production at 100 % load: 7.8 kW_{H2} based on LHV (2.6 Nm^3/h)
- CO content after shift reactors < 2 %

Some aspects of the 1D transient modelling are still to be verified but initial results indicate good agreement with experiments. At the current stage, the unit is used to gain fundamental knowledge about the processes hence a large number of mass flow controllers and high precision dosing pumps are used to ensure well defined operating conditions. In the next generation system, these components will be replaced by much cheaper sensors or completely eliminated through advanced model based control principles.

References

A. Therdthianwong, T. Sakulkoakiet and S. Therdthianwong, "Hydrogen Production by Catalytic Ethanol Steam Reforming", ScienceAsia Vol. 27 pp. 193-198, 2001

Gilbert F. Froment and Kenneth B. Bischoff, "Chemical reactor analysis and design", second edition, Wiley, ISBN: 0-471-51044-0, 1990

M. Bovo and M. Mandø, "Characterization of a fuel processing unit" – M.Sc. Thesis, Aalborg University, Institute of Energy Technology, Denmark, 2006

R. L. Keiski, T. Salmi, P. Niemistö, J. Ainassaari and V. J. Pohjola, "Stationary and transient kinetics of the high temperature water-gas shift reaction", Applied Catalysis A: General Vol. 137 pp 349-370, 1996

Parts of the figures 1 and 2 were based on drawings originally created by Catator AB.

Journal publication consideration requested
Proceedings of FUELCELL2006
The 4th International Conference on FUEL CELL SCIENCE, ENGINEERING and TECHNOLOGY
June 19-21, 2006, Irvine, CA

FUELCELL2006-97214

MODELING OF CO INFLUENCE IN PBI ELECTROLYTE PEM FUEL CELLS

[1]Anders Risum Korsgaard/Ph.D. Student [1]Mads Pagh Nielsen / Assistant Professor

[1]Mads Bang/Assistant Professor [1]Søren Knudsen Kær/Associate Professor

[1] Institute of Energy Technology, Aalborg University, DK-9220 Aalborg, Denmark

ABSTRACT

In most PEM fuel cell MEA's Nafion is used as electrolyte material due to its excellent proton conductivity at low temperatures. However, Nafion needs to be fully hydrated in order to conduct protons. This means that the cell temperature cannot surpass the boiling temperature of water and further this poses great challenges regarding water management in the cells. When operating fuel cell stacks on reformate gas, carbon monoxide (CO) content in the gas is unavoidable. The highest tolerable amount of CO is between 50-100 ppm with CO-tolerant catalysts. To achieve such low CO-concentration, extensive gas purification is necessary; typically shift reactors and preferential oxidation. The surface adsorption and desorption is strongly dependent upon the cell temperature. Higher temperature operation favors the CO-desorption and increases cell performance due to faster kinetics.

High temperature polymer electrolyte fuel cells with PBI polymer electrolytes rather than Nafion can be operated at temperatures between 120-200°C. At such conditions, several percent CO in the gas is tolerable depending on the cell temperature. System complexity in the case of reformate operation is greatly reduced increasing the overall system performance since shift reactors and preferential oxidation can be left out.

PBI-based MEA's have proven long durability. The manufacturer PEMEAS have verified lifetimes above 25,000 hours. They are thus serious contenders to Nafion based fuel cell MEA's.

This paper provides a novel experimentally verified model of the CO sorption processes in PEM fuel cells with PBI membranes. The model uses a mechanistic approach to characterize the CO adsorption and desorption kinetics. A simplified model, describing cathode overpotential, was included to model the overall cell potential. Experimental tests were performed with CO-levels ranging from 0.1% to 10% and temperatures from 160-200°C.

Both pure hydrogen as well as a reformate gas models were derived and the modeling results are in excellent agreement with the experiments.

INTRODUCTION

High Temperature Polymer based electrolytes provide a good alternative to the Nafion based fuel cells. Primarily they have a very high CO resistance, due to the possibility of operation at elevated temperatures, making them significantly easier to integrate with fuel processors where one or more of the traditional reaction steps can be left out in the gas purification process. Fueled with pure hydrogen they are also significantly easier to operate as no external humidification is needed, leaving out costly humidification components. Lately stabile long term operation has also been proven making them attractive for applications demanding long lifetime such as combined heat and power plants.

Modeling of CO poisoning in low temperature PEM fuel cells has been performed by several authors.

Springer et al. [1] formulated a mechanistic model describing the effects of CO poisoning and hydrogen dilution due to the presence of carbon dioxide in reformate gas.

Baschuk et al. [2] formulated a similar anode model accounting for operation on reformate gas. The model was found to correlate well with the experimental results published by Lee et al. [3]. The model used by [2] also considered the variation of the temperature and furthermore included the effects of oxygen bleeding.

The use of PBI for fuel cell applications was first published by Wainright [4] followed by [5]. Recently, the same authors published results regarding CO coverage of the catalyst [7], and

did some measurements on the oxygen reduction reaction in [6]. Qingfeng Li et al. [8] developed PBI MEA's and performed extensive studies on the performance of PBI based membranes including the effect of carbon monoxide.

Recently [9] & [10] published models of PBI fuel cell membranes. However these models where only verified at one operating temperature and neither the anode or cathode stoichiometric ratio were known. Furthermore, the effect of CO was not included in the model.

There is thus a need of a detailed and accurate model describing the effect of operation on reformate gas including the effect of cathode stoichiometry and operational temperature.

NOMENCLATURE

a_x , b_x	Regression constants used in cathode model
F	Faraday's constant [C/mol]
i	Cell current [A/cm²]
i_0	Exchange current density [A/cm²]
n	Order of anode kinetic model [-]
p	Pressure [bar]
R	Universal gas constant [J/kmol·K]
R_{xx}	Resistance [ohm·cm²]
T	Cell temperature [K]
U_0	Open circuit potential [V]
y_{xx}	Molar fraction [-]
λ	Cathode stoichiometric ratio [-]
α	Charge transfer coefficient [-]
η	Over potential [V]
θ	Surface coverage [-]
ρ	Density (kg/m3)

EXPERIMENTAL METHODOLOGY

The experimental data were based on performance measurements on commercial MEA delivered by PEMEAS GmbH. These data has previously been published in a paper submitted to Journal of Power Sources entitled "Experimental characterization and modeling of commercial polybenzimidazole-based MEA performance".

The MEA has an active cell area of 45 cm² with a platinum loading which is comparable with similar low temperature PEM membrane assemblies. The catalyst layer is 50-100 µm thick. The GDL is of the woven type and has a thickness of 400 µm. It assists the transport of species to and from the catalyst layers and furthermore act as an acid barrier minimizing loss of phosphoric acid from the acid doped PBI electrolyte. The test cell was provided with air and hydrogen using mass flow controllers.

Pure hydrogen tests were performed at temperatures varying from 120-180°C and cathode stoichiometric ratios of 2, 3 and 5. The anode stoichiometry was held constant at 2.5.

Figure 1 shows measurements performed at 160°C with pure hydrogen:

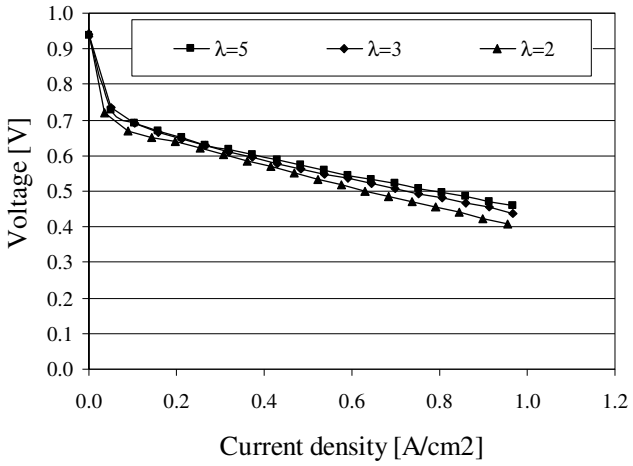

Figure 1: Tests performed at 180°C and λ_a=2.5.

For the synthesis gas tests a fixed total amount of CO+CO_2 of 25%vol was maintained while the remaining part of the gas was hydrogen. No external water was added in these experiments at either the anode or cathode. The CO content was varied according to the following gas compositions:

- 5% CO, 75% H_2, 20% CO_2
- 2% CO, 75% H_2, 23% CO_2
- 1% CO, 75% H2, 24% CO2
- 0.1% CO, 75% H_2, 24.9% CO_2
- 25% CO_2, 75% H_2
- 100% H_2

MODELING OF CATHODE OVERPOTENTIAL

The cathode model was also derived and described in detail in the previously mentioned publication, which is expected to be available in Journal of Power Sources in near future. It is based on the following semi-empirical expression:

$$U_{cell} = U_0 - \frac{RT}{4\alpha F}\ln\left(\frac{i+i_0}{i_0}\right) - R_{ohmic}i - \frac{R_{conc}i}{\lambda - 1} \qquad (1)$$

The constant U_0 is the open circuit voltage. The second term is the Tafel equation and includes the charge transfer coefficient. The third term is related to the ohmic loss in the membrane and catalyst layer. The last term is a novel way of including the cathode stoichiometry's influence on performance. It was found that the above equation gives excellent agreement when fitted to the experimental data.

Additionally, 4 of the variables from equation 1 have been made temperature dependant through suitable regressions.

The charge transfer coefficient is expressed by a linear regression as:

$$\alpha_c = a_0 T + b_0 \quad (2)$$

The authors are not aware of a similar expression presented earlier in literature and may be subject to detailed discussions in future work.

The exchange current density is expressed as an exponential function, which is expectable considering the physical nature of this constant:

$$i_0 = a_3 e^{-b3T} \quad (3)$$

The ohmic losses are defined by a linear relationship as:

$$R_{ohmic} = a_1 T + b_1 \quad (4)$$

Finally, the resistance equivalent to the concentration losses associated to the stoichiometric ratio is given by:

$$R_{conc} = a_2 T + b_2 \quad (5)$$

The above expressions were fitted to the data in the temperature range from 120-180°C and cathode stoichiometries of 2,3 and 5. The constants derived can be found in table 1.

It was concluded in the previous work that the given model fits very well to the experimental results compared to previous publications. The nature of the modeled overpotentials are very similar to those obtained in [1] & [2] but the ohmic resistance is more dominant. This difference could be due to the fact that the PEMEAS membranes might have a thicker cathode catalyst layer with a higher platinum loading as this could explain the lower activation overpotential and higher resistance due to the longer proton path in the cathode catalyst layer. This has however not been verified yet.

MODELING OF ANODE KINETICS

It was assumed that the surface kinetics of the CO-coverage can be described using a model expressing the steady-state reaction rates as function of the surface coverage of the vacant catalyst sites. Springer et al. [1] suggested a set of chemical reaction equations to describe the adsorption, desorption and electro-oxidation of hydrogen and CO on the catalyst surface:

$$CO + M \underset{b_{fc}(\theta_{CO})k_{fc}}{\overset{k_{fc}}{\rightleftharpoons}} (M - CO) \quad (6)$$

$$H_2 + 2M \underset{b_{fh}k_{fh}(\theta_{CO})}{\overset{k_{fh}}{\rightleftharpoons}} 2(M - H) \quad (7)$$

$$(M - H) \xrightarrow{k_{eh}} H^+ + e^- + M \quad (8)$$

$$H_2O + (M - CO) \xrightarrow{k_{ec}} M + CO_2 + 2H^+ + 2e^- \quad (9)$$

In the equations M corresponds to a vacant catalyst site, otherwise H or CO is attached to a site. Equation (6) and (7) account for the competing processes of CO adsorption and dissociative chemisorption of hydrogen. The forward rate constants k_{fh} and k_{fc} are expressed in [A/(cm²·bar)]. The desorption constants b_{fc} and b_{fh} [bar] are the inverse of the equilibrium constants for the processes. As indicated, the authors assumed the forward rate of hydrogen chemisorption and desorption of CO to be dependant on the surface coverage using a Temkin isotherm to obtain a better fit to experimental data. In this work they are assumed constant as the elevated operational temperatures of PBI-membranes makes this dependence much less significant.

The additional rates are assumed constant as well. Equation (8) describes the electrochemical oxidation of the adsorbed hydrogen atoms. The final reaction equation (9) describes the oxidation of CO to CO_2, which normally only reaches significant rates at high current densities [1]. All electro-oxidation rates are given in [A/cm^2]. Here it is assumed that the required oxygen atom is originating from the water present in the anode catalyst layer. During the experiments performed on the single cell test facility in this work, the presence of water in the anode compartment was indeed confirmed, so it is assumed that the CO electro-oxidation could play a role at high current densities in PBI MEA's as well.

From these reaction mechanisms, a set of kinetic equations describing the steady-state balances of the rate of change of hydrogen and CO coverage on the catalyst surface in terms of the rates of adsorption, desorption, and electro-oxidation can be formulated. The assertion of steady-state conditions proves to be quite valid due to the fact that the CO poisoning and recovery processes occur almost instantly at the operational temperatures investigated experimentally. Modeling the fast transients could, however, be relevant when designing the power electronics used to condition the power from fuel cell stacks. However, for most other applications such as control, system design and optimization they are considered unimportant, because the dynamics are found to be very fast with time constant below 1s. The used expressions in this work are identical to those developed by [1] but are here formulated as function of the current density:

$$\rho \frac{d\theta_{H_2}}{dt} = 0 = k_{fh} \cdot y_{H_2} \cdot p \cdot \left[1 - \theta_{H_2} - \theta_{CO}\right]^n - b_{fh} \cdot k_{fh} \cdot {\theta_{H_2}}^n - i \quad (10)$$

$$\rho \frac{d\theta_{CO}}{dt} = 0 = k_{fc} \cdot y_{CO} \cdot p \cdot \left[1 - \theta_{H_2} - \theta_{CO}\right] - b_{fc} \cdot k_{fc} \cdot \theta_{CO} - \frac{i \cdot k_{ec} \cdot \theta_{CO}}{2 \cdot k_{eh} \cdot \theta_{H_2}} \quad (11)$$

In the above equations, θ_{H2} expresses the surface coverage of hydrogen and θ_{CO} is representing the surface coverage of carbon monoxide. y_{H2} and y_{CO} respectively express the molar fractions of hydrogen and carbon monoxide in the catalyst layer. The parameter ρ is the molar area density of catalyst sites times Faraday's constant given in [C/cm^2], which obviously becomes redundant in the steady-state case. The parameter n is chosen to

a value of 2 indicating that the intermediate hydrogen step is second order in catalyst sites.

It is not possible to solve the two expressions analytically so the numerical non-linear equation solver "Engineering Equation Solver" (EES) was used to do this. It should be stressed that it is important to add constraints to the coverage variables prohibiting them from exceeding the interval $\theta \in [0;1]$.

The anode overpotential was related to the current density and the surface coverage of hydrogen assuming Butler-Volmer kinetics with a symmetry factor of α=0.5, which simplifies the Butler-Volmer equation to the following expression as the exponential forward and backward rate terms in this case forms the inverse hyperbolic sinus function:

$$\eta_a = \frac{R \cdot T_{cell}}{\alpha \cdot F} \cdot \sinh^{-1}\left[\frac{i}{2 \cdot k_{eh} \cdot \theta_{H_2}}\right] \quad (12)$$

RESULTS

Combining the cathode and anode models, the overall model was fitted to experimental steady state polarization curve data for CO poisoning at temperatures at 160 and 180°C at CO concentrations of 0 ppm, 1000 ppm, 10000 ppm, 20000 ppm and 50000 ppm (~5%$_{vol}$ CO).

The rate constants were assumed to have temperature dependences following Arrhenius-like correlations such as:

$$\text{Rate constant} = \text{Pre-exp. factor} \times \exp\left(\frac{-Activation\ Energy}{R \cdot T}\right) \quad (13)$$

Using a non-linear optimization algorithm to find the best possible fit to the experimental data, pre-exponential factors and activation energies were found for the various parameters. The table below summarizes the parameters used in both the anode and the cathode model described in the previous sections:

Membrane		
Membrane thickness, t_{memb}	0.1×10^{-3}	m
Values used for cathode model		
Charge transfer constant, a_0	2.761×10^{-3}	K^{-1}
Charge transfer constant, b_0	-0.9453	-
Ohmic loss constant, a_1	-1.667×10^{-4}	$\Omega\ K^{-1}$
Ohmic loss constant, b_1	0.2289	Ω
Diffusion limitation constant, a_2	-8.203×10^{-4}	$\Omega\ K^{-1}$
Diffusion limitation constant, b_2	0.4306	Ω
Limiting current constant, a_3	33.3×10^{3}	A
Limiting current constant, b_3	-0.04368	-
Open circuit voltage, U_0	0.95	V
Pre-exponential factors used for anode model		
CO desorption rate, b_{fc}	8.817e12	bar
H_2 desorption rate, b_{fh}	2.038e6	bar
CO electrooxidation rate, k_{ec}	3.267e18	A cm^{-2}
H_2 electrooxidation rate, k_{eh}	25607	A cm^{-2}
CO adsorption rate, k_{fc}	94.08	A cm^{-2} bar^{-1}
H_2 adsorption rate, k_{fh}	2.743e24	A cm^{-2} bar^{-1}
Activation energy values used for anode model		
CO desorption rate, E_{bfc}	127513	kJ/kmol
H_2 desorption rate, E_{bfh}	47904	kJ/kmol
CO electrooxidation rate, E_{kec}	196829	kJ/kmol
H_2 electrooxidation rate, E_{keh}	34777	kJ/kmol
CO adsorption rate, E_{kfc}	19045	kJ/kmol
H_2 adsorption rate, E_{kfh}	1.899e5	kJ/kmol
Other constants		
Universal gas constant, R	8.3143	J mol^{-1} K^{-1}
Faradays constant, F	96485	C mol^{-1}

Table 1: Numerical values used in the overall model

A parameter variation study was performed to verify that all parameters acted in the physically expected manner. It was found that the model produces consistent results with respect to all parameters. Furthermore, the magnitudes of the surface coverage's are very similar to those estimated by [7]. Additionally, it was concluded that the CO-electrooxidation term can be neglected for approximation purposes as this term only contributes at high current densities (i.e. k_{ec} can be set to 0).

Including the cathode and ohmic loss model described previously, comparisons between modeling and experimental data were performed. The following plots show these comparisons:

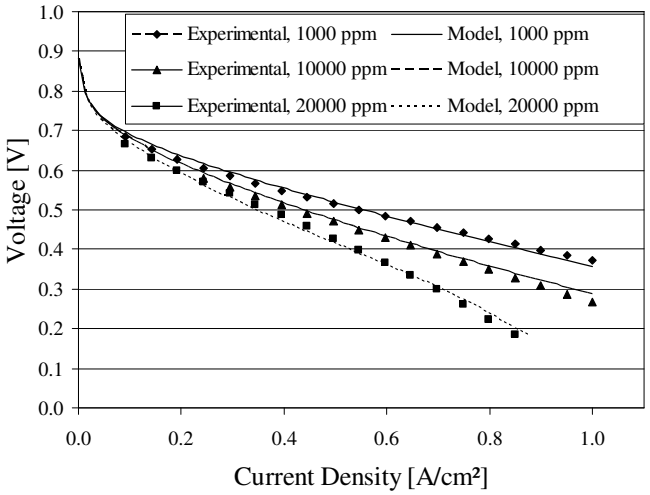

Figure 2: Model vs. experiments at 160°C.

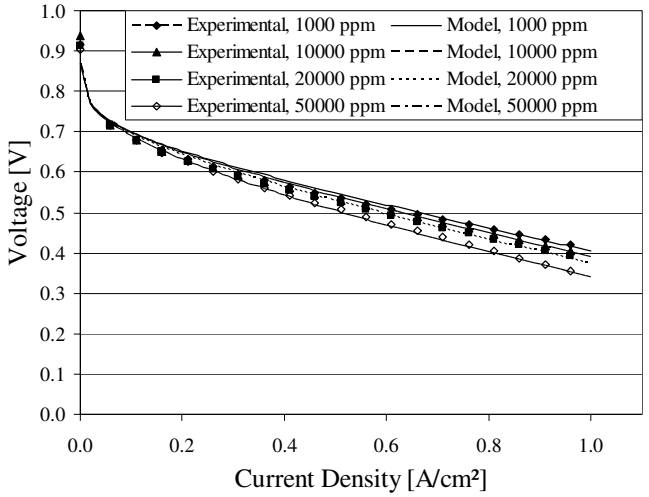

Figure 3: Model vs. experiments at 180°C.

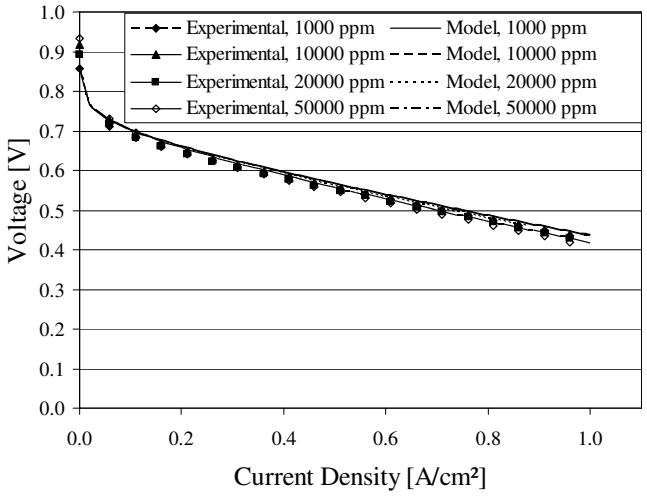

Figure 4: Model vs. experiments at 200°C.

As seen from the plots, the modeling results are in excellent agreement with the experimental data at all the temperatures and CO-concentrations. In spite of the fact that the model was not fitted to the data measured at 200°C, it still produces results within the uncertainties of the experimental data, which indicates that the Arrhenius temperature dependence functions for the kinetic constants are correct.

CONCLUSION

A simple physically based model has been developed through this study. The model was fitted to measurements obtained with commercial state-of-the-art PBI-membranes. Along with the temperature dependent cathode model, it covers all practical operational ranges of PBI-membrane fuel cells integrated with reformers. Its precision and simplicity makes it an excellent tool for design and optimization purposes. It is expected that the model easily can be fitted to other particular PBI-based MEA's. Further studies are however needed to prove this.

REFERENCES

[1] Springer, T. E., Rockward, T., Zawodzinski, T. A., & Gottesfeld, S. 2001, "Model for polymer electrolyte fuel cell operation on reformate feed: effects of CO, H2 dilution, and high fuel utilization", Journal of the Electrochemical Society Vol.148 Issue.1, pp. 11-23.

[2] Baschuk, J. J. & Li, X. 2003, "Modelling CO poisoning and O_2 bleeding in a PEM fuel cell anode", International Journal of Energy Research, vol. Vol.27 Issue.12, pp. 1095-1116.

[3] S.J. Lee, S. Mukerjee, E.A. Ticianelli, J. McBreen, "Electrocatalysis of CO tolerance in hydrogen oxidation reaction in PEM fuel cells", Electrochimica Acta 44 (1999) 3283-3293.

[4] J.S. Wainright, J.-T. Wang , D. Weng, R.F. Savinell, M.Litt, "Acid-doped polybenzimidazoles: A new polymer electrolyte", J. Electrochem. Soc. 142 (1995) 121-123.

[5] J., T. Wang; R. F. Savinell; J.S. Wainright, M. Litt; H. Yu, "A H2/O2 fuel cell using acid doped polybenzimidazole as polymer electrolyte", Electrochimica Acta, 41 (1996) 193-197.

[6] Zhenyu Liu, Jesse S.Wainright, Robert F. Savinell, "High-temperature polymer electrolytes for PEM fuel cells: study of the oxygen reduction reaction (ORR) at a Pt-polymer electrolyte interface" Chemical Engineering Science, 59 (2004) 4833-4838.

[7] J.D. Holladay, J.S. Wainright, E.O. Jones, S.R. Gano, "Power generation using a mesoscale fuel cell integrated with a microscale fuel processor", J. of Power Sources 130 (2004) 111-118.

[8] Qingfeng Li et al., "Water uptake and acid doping of polybenzimidazoles as electrolyte membranes for fuel cells", Solid State Ionics 168 (2004) 177–185.

[9] Denver Cheddie, Norman Munroe, "Parametric model of an intermediate temperature PEMFC", Journal of Power Sources, In Press.

[10] Denver Cheddie , Norman Munroe, "Mathematical model of a PEMFC using a PBI membrane", EnergyConversion and Management, In Press.

Submitted to Journal of Hydrogen Energy, accepted with minor revisions, second revision is being processed.

Part one: A novel model of HTPEM based Micro Combined Heat and Power Fuel Cell System

Anders R. Korsgaard[a], Mads P. Nielsen[a], Søren K. Kær[a]

[a] *Institute of Energy Technology, Aalborg University, DK-9220 Aalborg, Denmark*

Elsevier use only: Received date here; revised date here; accepted date here

Abstract

Fuel cell based CHP systems have received increasing attention during the last decade. This is mainly due to the high efficiencies obtainable on even a small scale system basis. The current paper focuses on the development of a complete model of a system consisting of the HTPEM fuel cell stack based on PBI membranes, steam reforming reactor, burner, heat reservoir and other auxiliary equipment included in a typical reforming based fuel cell system. The model is implemented in the Matlab®Simulink environment enabling both static system integration as well as dynamical control strategies to be evaluated. All results of the submodels correspond well with experimental results obtained. Additionally, a novel system integration of a HTPEM fuel cell and a steam reforming based fuel processing unit is presented. The total energy utilization efficiency of the system modeled is as high as 90-100%$_{LHV}$ depending on the operating point chosen, whereas the electrical efficiency can be up to 45%$_{LHV}$. This is more than 30% better than the best low temperature PEM based systems demonstrated today.

Keywords: Fuel Cell; PEM; PBI; Intermediate Temperature, System, Modeling, HTPEM, CHP.

1. Introduction

Fuel cell based micro Combined Heat and Power (CHP) systems have received increasing attention recently. This is due to a number of reasons. First of all distributed generation minimizes transmission losses. Secondly, a well-developed infrastructure for distributed natural gas is already present in several countries. Therefore the step to produce electricity in domestic households is realistic provided that the technical and financial issues of the CHP units can be resolved.

A range of different technologies for micro CHP exist including conventional internal combustion engines (ICE´s), the stirling engine as well as fuel cell systems. The latter is the focus of this paper. Additionally, within the fuel cell area alone a range of sub categories exist where today mainly (Solid Oxide Fuel Cells) SOFC and Proton Exchange Membrane (PEM) dominate. In the present paper the focus will be on a branch of the PEM type fuel cell which operates at a slightly higher temperature (120-200°C) than the conventional low temperature Nafion-based technology. Low temperature fuel cells used in rela-

tion with reforming systems suffer from the severe shortcoming that CO concentrations down to 5 or 10 ppm is required in order to avoid poisoning due to CO adsorption and coverage of the catalyst layer. The high temperature PEM fuel cells are commonly termed HTPEM (or intermediate temperature PEM) and the higher operational temperature increases the efficiency significantly.

A peak electrical efficiency of 31.5%$_{HHV}$ has been achieved by Osaka Gas [1] and a total thermal system efficiency of 77%$_{HHV}$. Other sources claim that much higher system efficiencies must be obtained as natural gas will be much higher valued in the future as a fuel for balancing the grid. Dong Energy, the largest Danish energy supplier and owner of 50% of the power plants in Denmark, claims that efficiencies comparable to modern combined cycle central power plants must be obtained (45-50%) [2], to be able to get a larger market share in the future energy system. In order to obtain high system efficiencies, system integration must be given careful consideration.

The present paper has a twofold objective. First of all it describes a novel approach of modeling reforming based fuel cell systems for CHP operation. Secondly, it presents a novel system layout which would fulfill the demands suggested by [2].

The use of PBI (the material of the membrane) for fuel cell applications was first published by Wainright [3] followed by a number of other works [4][5]. Some of the same authors published data regarding the oxygen reduction reaction [6] and recently they published data on CO coverage [7].

Other research groups also published data regarding development of PBI based MEA's such as the group of Bjerrum et al. [8][9][10].

A model of a PBI membrane was recently published [11][12]but it only included one operating temperature and the stoichiometric ratio was unknown.

The authors of this paper presented an empirical model of the HTPEM fuel cell [13] [14] which forms the basis of the fuel cell stack model described in this paper.

A wide range of methods of modeling the fuel processors exists. Some of the most well known approaches within modeling of such chemical reactors are presented in the book by Froment & Bishop [15], which is also used in the authors work [16].

There has been some activity on modelling the impact of micro CHP's from a grid perspective [17], [18] and [19]. Additionally, a range of different test results have been presented [20].

There are only very limited references addressing dynamic system models of complete CHP systems relating subcomponents such as the fuel cell stack, reformer and heat storage on the one hand to the household energy consumption on the other hand.

2. Theory

In this section an introduction to the system modeled is given. This is followed by an outline of the Simulink model developed.

2.1. System layout

2.1.1. Fuel Processor

Fig 1 shows the physical system modeled which is based on a natural gas fuel processing unit (a steam reformer), a HTPEM fuel cell stack and a novel water reservoir wherein a fuel cell stack is placed.

The fuel processor consists of a steam reformer, which has the advantage that it can use the chemical energy in the fuel cell off gas for the reforming process. Furthermore, the outlet hydrogen concentration is much higher than systems using auto thermal reforming or partial oxidation reactors, which prolongs the fuel cell lifetime and increases efficiency. Even though HTPEM fuel cells can tolerate significant amounts of CO, a water gas shift (hereafter termed shift) reactor is needed to enhance the fuel cell performance. In this model the shift is modeled as a counter flow combination of high and low temperature shift that will decrease the inlet CO concentration to less than 1%. The exothermic shift reactor is cooled using the exhaust cathode gas, which, at the inlet, once the hot water reservoir is heated up, is never less than approx. 140-150°C. The advantage of this coupling is mainly present in HTPEM based systems as the temperature would drop too low if 80°C air from a low temperature PEM system was used.

From the shift reactor the air passes to the burner (11) now heated to about 300°C. In the catalytic burner it is mixed with the anode off gas (12) raising the temperature to 700-950°C depending on operating conditions. The gas leaving the burner (termed flue gas) passes through the heat exchanger in the reformer providing the energy for the endothermic reforming process. At the exit of the reformer the flue gas temperature should be from 200-500°C. From here the flue gas flow enters the heat exchanger (14), which effectively cools the gas down to the temperature of the heat reservoir by natural convection through (13) and (15).

Hence, if the gas is 500°C entering the heat exchanger significant amount of energy will be released to the thermal buffer (30) whereas if it is only 200°C this will be reduced to near zero. By controlling the cathode air blower 4 different process steps are implicitly controlled:

- Cathode air flow
- Cooling of shift reactor
- Control of reformer temperature
- Amount of heat released to the thermal reservoir

This significantly reduces complexity of the system, but it does on the other hand put some constraints on the control system. A more in depth discussion is provided in the results section and it is also validated that a good interaction between all the process steps can be obtained.

From the heat recovery heat exchanger the flue gas passes through the condenser/evaporator (16) which also evaporates the incoming water/natural gas mixture (21, 20).

Optionally, the flue gas is passed through the last heat exchanger (18) to regain the remaining energy from condensation of the water in the flue gas. This is left out in the model presented for economical reasons due to the low temperature difference and thereby large heat exchanger surface area, which poses a significant cost contribution to the system.

2.1.2. The fuel cell and the heat reservoir

The fuel cell (27) is passively cooled by natural convection of the fluid in the heat reservoir, needing no external actuators or controls always maintaining the fuel cell at its nominal operating temperature. The set point temperature in the reservoir is therefore to be maintained within the bounds of the allowed fuel cell operating temperature. This temperature strongly depends on the quality of the reformate gas stream entering the anode and is so bounded to the exit concentration of CO from the shift.

The hot liquid reservoir consists of a container with a fluid with the following properties:

- The fluid is maintained in the liquid state even at temperatures above 190°C
- High specific heat capacity, maximizing the buffer effect of the system
- High viscosity
- Low price
- Low corrosive behavior

The advantage of placing the fuel cell inside the heat reservoir is that it can be left in standby mode during periods where it is not economically viable to produce electricity. However, it will still remain able to be put into operation instantly provided that the reformer is operational as well. Moreover, no parasitic losses for potentially expensive high temperature pumps are needed. At last, as all the heat generated by the fuel cell is produced inside the heat buffer, near zero heat loss can be obtained in contrast to using pipes, valves and pumps to connect the fuel cell to the reservoir.

2.2. Modeling method

In the following section the CHP system model is presented. First a brief overview of the model is presented followed by the overall approach for energy conservation, heat exchanging etc. This is followed by an in depth explanation of the models of sub components in the system.

The model is developed in the Matlab®Simulink environment and physical properties of the various streams are generally obtained from EES (Engineering Equation Solver).

2.2.1. Overall model layout

Fig 2 shows the front block diagram of the Simulink model corresponding to the system layout of Fig 1. It is divided into blocks each representing a reactor, fuel cell, heat exchanger etc. These are interconnected using the bus-system (thick lines) which is a vector with one temperature of the fluid stream and 7 molar gas flows in the order CO, H_2, CO_2, CH_4, H_2O, N_2 and O_2 hence representing all information about the composition, transport properties and the enthalpy of the gas stream. If liquid water is likely to

occur, the liquid water fraction (X_{water}) is added relating the amount of liquid water to the total flow of water.

The thin lines represent scalar values and vectors of molar flows in some of the sub masks.

In the left end of the figure, the control system block is placed calculating the signals to the balance of plant components such as pumps and valves, based on set points and measurements in the system. To the right of the control block, the system actuators are placed feeding the fluid inputs to the plant. The fuel processor contains a number of sub-reactors including the shift- and steam reforming reactors along with various heat exchangers, condensers etc. In the bottom right, the fuel cell and the heat storage tank are placed.

In the bottom left, the input consumption data is given to the model. For the current paper these are merely constants but in the second part of the publication these will be replaced by measured consumption data from Danish households. The control system will likewise be explained in the second part.

2.2.2. Component layout

Most of the components in the fuel processor are modeled by the same principle. Fig 3 shows the structure of the shift model, which has the same structure as most of the other components containing two heat-exchanging streams. Generally, the top and bottom subsystem calculate the change in energy of the gas streams. They utilize the in- and output temperatures together with the molar flows to output the resulting energy release to the heat exchanger.

The center subsystem contains the heat exchanging model. It calculates the output temperatures of the gas streams from the energy release given each of the gas streams and input temperatures.

2.2.3. Energy conservation

In each reactor or component the enthalpy difference is calculated using the Janaf tables, assuming that all gas components follow ideal gas behavior. The values are made available for the code using lookup tables based on regressions from EES. Hence for a given gas stream entering a reactor:

$$\Delta\overline{h}_{stream} = \overline{h}_{in} - \overline{h}_{out} \quad (1)$$

Equation 1 is only valid if no gas accumulation is present. This is a good assumption since the time frame which is going to be analyzed is hours and days and not seconds (or msec) which the pressure drop dynamics typically are given in.

The energy exchange can be expressed as

$$\dot{Q}_{stream} = \overline{\dot{n}}\,\Delta\overline{h}_{stream} \quad (2)$$

, where the molar flow $\overline{\dot{n}}$ is a vector of molar flows and $\dot{Q}_{stream}$ is the change in energy of the gas stream per second.

2.2.4. Heat exchanging

In many of the blocks heat exchanging between two fluids is taking place. Hence the outlet temperatures need to be calculated for both streams. This is performed using a time integrated solution. It is assumed that the thermal heat capacity of the solid can be represented by the fluid temperature satisfying:

$$T_{out} = \frac{1}{mc_p}\int (\dot{Q}_{conv} + \dot{Q}_{stream})\ dt \qquad (3)$$

, where m is the mass of the part of the reactor that the gas stream passes through and c_p is the heat capacity of the solid. A small dynamic error is made since the temperature of the fluid is used for calculating the thermal inertia instead of the solid temperature i.e. the temperature difference between the solid and the gas is disregarded. This, however, does not influence the steady state equilibrium calculations and it simplifies the model considerably allowing much faster convergence. Table 2 shows the estimated masses of the individual components.

The energy transferred by convection (and conduction through the wall) is calculated as:

$$\dot{Q}_{conv} = UA_{\text{int}}\ \Delta T_{av} \qquad (4)$$

, where UA_{int} is the overall internal heat transfer coefficient multiplied by the heat exchanger area and ΔT_{av} is the average temperature difference which is calculated using the traditional log mean temperature difference method (LMTD) [21] in most cases. However, during transients, crossing temperature profiles may occur. In these cases an arithmetic temperature difference (AMTD) [21], altered slightly by the authors, is used to accommodate the numerical solution, as LTMD is not applicable.

Fig 5 shows the 4 different cases considered in a counter flow heat exchanger. The average temperature difference is shown at each outlet. The case to the left shows the usual situation where a conventional LMTD can be used. The right hand side shows the case where crossing temperature profiles occur during transients. This is especially the case during start-ups. In order to improve numerical stability during sign changes of ΔT_1 a small contribution to the temperature difference at the opposite end of the heat exchanger ($\Delta T_2 / 20$) is added, limiting zero crossing problems. The number 20 cannot be justified theoretically but is found simply by a trial and error approach. The term does not influence the steady-state solution.

Conduction along the reactor path is disregarded even though this might introduce significant errors at low load. The thermal short circuit can be minimized using long thin thickness plate heat exchangers, which is a design task and out of the scope for this publication.

To take into account heat losses, a simple heat loss expression is included and subtracted, using:

$$\dot{Q}_{loss} = UA_{ext}(T_{fluid,av} - T_{amb}) \qquad (5)$$

, where UA_{ext} is the overall all heat transfer coefficient to the surroundings multiplied by the area, T_{amb} is the ambient temperature and $T_{fluid,av}$ is the average temperature of the fluid in the outer shell.

Fig 6 summarizes the above expressions showing the resulting block diagram in the Simulink model exemplified by the shift reactor. Inputs 2 and 4 provide the inlet temperatures of the CH_4/H_2O mixture and the flue gas from the burner respectively. With the initial value of the integrators known, the 4 temperatures are fed to the average temperature calculation block. Depending on the situation (referring to Fig 5), the average temperature found is multiplied by the UA-value and fed to the sum blocks. Here inputs 1 and 3 are added representing the energy change of the fluid

streams given by Eq. 2. The heat loss to the surroundings is subtracted in sum 2 in the flue gas stream.

Using Eq. 3 the outlet temperatures of each of the fluid streams are calculated with integration symbolized by the Laplace operator (1/s).

2.3. Evaporator/Condenser

The fuel and water inlet to the reformer is supplied through the evaporator. Since the water supplied is considered being in liquid form, it is supposed that it is injected into the methane stream using a nozzle or similar. Basically, the component is modeled using the generic heat exchanger model described previously. However, vaporization of the water injected and condensation of the outlet flue gas stream need to be taken into account.

A regression of the saturation pressure of water is implemented based on data from EES.

If the saturation pressure is larger than the partial pressure of water in the gas stream, everything is already in vapor form. In contrast if the partial pressure of water in the gas stream is larger than the saturation pressure only a part corresponding to P_{sat} is in vapor form. This can be expressed as:

$$x_{H2O,gas}=\min (P_{sat}(T), P_{H2O}) / P_{tot} \quad (6)$$

The water exiting the evaporator in gaseous form is expressed as:

$$\dot{n}_{H2O,gas} = x_{H2O,gas}\ \dot{n}_{tot} \quad (7)$$

The liquid water fraction is obtained by:

$$X_{water} = (\dot{n}_{H2O,tot} - \dot{n}_{H2O,gas}) / \dot{n}_{H2O,tot} \quad (8)$$

Having the amount of water evaporated the energy of vaporization is found by multiplying with h_{fg} found from standard data available in EES. Hence the water is assumed evaporated at 25°C and heated using the ideal gas assumptions, of the Janaf tables, following the method of section 2.2.4.

Fig 7 shows the block diagram of the evaporator part. Equation 8 is included in the "H_2O Liquid/gas". Multiplying h_{fg} and the mass of water in gaseous form at the outlet yields the energy required for vaporization of the water injected. The result is added to the enthalpy difference calculation.

The flue gas water condensation part is calculated in a similar way but h_{fg} is naturally multiplied with the amount of condensed liquid water and $T_{evap,in}$ is substituted with the outlet flue gas temperature.

2.4. Recuperator

This component extracts the remaining energy to the heat reservoir by means of natural convection. It could either be placed inside the reservoir or externally as shown in Fig 1. A rough model is made of this component as it is assumed that the outlet temperature of the flue gas stream equals the heat storage temperature. This is justified by the large temperature differences, which are present in the reservoir and the heat exchanger could be connected to a colder region of the reservoir. Hence the enthalpy difference is only calculated for the flue gas side and heat is transferred directly to the heat storage (see Fig 2).

2.5. Reformer model

The reformer is based on the same structure as presented in section 2.2.4 with only one major difference which is the calculation of the outlet composition of the reformate stream. It is assumed that the conversion of methane follows chemical equilibrium, which has also been verified from experiments on a commercial steam reformer. A lookup table was applied to the model based on calculations using the NASA Lewis equilibrium code by Gordon & McBride [22] valid at steam to carbon (SC) from 1-6 and temperatures from 500-1600K. Any carbon deposition is disregarded and at temperatures below 500K the catalyst is considered inactive and hence no conversion takes place.

Fig 8 shows the resulting block diagram for the reforming side.

2.6. Shift

The shift reactor outlet composition is calculated from standard thermo dynamical equilibrium composition, as this is a simple set of equations to solve. They could have been solved explicitly but due to model readability concerns they have been kept in their original form as they are solved quickly and are numerically stable. It is assumed that nearly 100% methane conversion has been taking place in the reformer and that the low temperature shift reactor does not promote either the methanation or the steam reforming reaction.

$$\Delta G_{wgs} = G_{CO2} + G_{H2} - G_{CO} - G_{H2O} \qquad (9)$$

, where Gibbs free energy of each of the species (xx) can be calculated from:

$$G_{xx} = h_{xx}(T_{out}) - T_{out}\, S_{xx}(T_{out}) \qquad (10)$$

T_{out} denotes the outlet temperature of the shift reactor and S the entropy of each of the species.

The equilibrium constant for the water gas shift, assuming ideal gas behavior of all gas components, is calculated as

$$\mathrm{K_{wgs}} = \exp(-\Delta \mathrm{G_{wgs}}/(8.314\,\mathrm{T_{out}})) \qquad (11)$$

Hence K_{wgs} is dependent only on temperature and hence a lookup table has been implemented based on data from EES:

$$\mathrm{K_{WGS}} = \mathrm{f(T_{out})} \qquad (12)$$

For the first order water gas shift reaction the species composition should obey (assuming near 100% methane conversion in the reformer):

$$\mathrm{x_{H2O}\, x_{CO}\, K_{wgs} = x_{H2}\, x_{CO2}} \qquad (13)$$

and

$$\mathrm{x_{CO} + x_{H2O} + x_{CO2} + x_{H2} = 1} \qquad (14)$$

For 100% CO and CH4 conversion the ratio x_{CO2}/x_{H2}=0.25. Hence for the incomplete CO conversion the following relationship is valid.

$$\frac{n_{CO2,in} + n_{CO,in} = n_{CO2,compl}}{n_{H2,in} + n_{CO,in} = n_{H2,compl}} = 0.25 \qquad (15)$$

And as the total molar flow is unchanged it can be rewritten in the form:

$$(\mathrm{x_{CO} + x_{CO2}})/(\mathrm{x_{CO} + x_{H2}}) = 0.25 \qquad (16)$$

To solve equation 13-16 an integral solution is applied similar to that of the heat exchanger in section 2.2.4. The heat exchanger model is similar to the other components.

The model of the shift catalyst is saturated such that the equilibrium composition is equal to that of 220°C when the temperature drops below this point, as the kinetics typically will be very slow below this temperature.

2.7. Burner

The burner is modeled as a continuously stirred reactor with two inputs (air and anode off gas) and one output. The remaining H_2 and CO is completely combusted provided that sufficient oxygen is available. This is considered a good approximation since a catalytic burner is used. Hence the energy balance is calculated as:

$$\dot{Q}_{burner} = h_{air}(T_{air})\dot{n}_{air} + h_{offgas}(T_{offgas})\dot{n}_{offgas} - h_{flue}(T_{out})\dot{n}_{flue} \quad (17)$$

Where flue denotes the outlet gas and $\dot{n}_{flue}$ is calculated from combustion of H2 and CO:

$$x_1H_2 + x_2CO + 0.5(x_1 + x_2)O_2 -> x_1H_2O + x_2CO_2 \quad (18)$$

The problem is solved for the outlet temperature using an integral solution similar to that of the heat exchanger. A heat capacity is added corresponding to that of solid surrounding the burner. Hence

$$T_{out} = \frac{1}{m_{burner}\, c_{p,burner}} \int (\dot{Q}_{burner} - \dot{Q}_{heat,loss})\, dt \quad (19)$$

2.8. HTPEM fuel cell

The fuel cell model used was described in previous publications [13] and [14]. It is based on an extensive set of measurements performed by the authors at temperatures from 120-200°C, cathode stoichiometric ratios from 2-5 and CO concentrations from 0.1-10%.

2.8.1. Cathode model

From the experiments made in [14] it was derived that a very good fit could be obtained with the following equation:

$$U_{cell} = U_0 - \eta_{act} - \eta_{ohmic} - \eta_{diff} \quad (20)$$

The constant U_0 is the open circuit voltage. The second term is the Tafel equation and includes the charge transfer coefficient. The third term is related to the ohmic loss in the membrane and catalyst layer. The last term is a novel way of including the cathode stoichiometry's influence on performance. Rewriting equation 20 yields:

$$U_{cell} = U_0 - \frac{RT}{4\alpha F}\ln\left(\frac{i+i_0}{i_0}\right) - R_{ohmic}i - \frac{R_{conc}i}{\lambda - 1} \quad (21)$$

Where the 4 variables α, i_0, R_{ohmic} *and* R_{conc} are obtained from equation 22 to 25

$$\alpha = a_0T + b_0 \quad (22)$$

$$i_0 = a_3e^{-b3T} \quad (23)$$

$$R_{ohmic} = a_1T + b_1 \quad (24)$$

$$R_{conc} = a_2T + b_2 \quad (25)$$

The constants used can be obtained from Table 1. For further information about the background for the expressions please refer to the cited papers.

2.8.2. Anode model

In addition to the model of the cathode a detailed investigation of the influence of CO and CO_2 on the fuel cell performance were performed in [13]. Four different mechanisms are considered in the model of the CO adsorption/desorption mechanisms in the anode catalyst layer:

$$\mathrm{CO} + \mathrm{M} \leftrightarrow \mathrm{M\text{-}CO} \tag{26}$$

$$H_2 + 2M \leftrightarrow 2(M-H) \tag{27}$$

$$(M-H) \rightarrow H^+ + e^- + M \tag{28}$$

$$H_2O + (M-CO) \rightarrow M + CO_2 + 2H^+ + 2e^- \tag{29}$$

Equation 26 and 27 describes the general adsorption/desorption processes of H_2 and CO. Equation 28 describes the electrochemical oxidation of the adsorped hydrogen atoms and equation 29 the oxidation of CO to CO_2. The latter however only plays a significant role at very high current densities utilizing the water from the steam reforming process. Equation 30 and 31 show the resulting set of kinetic equations expressing the coverage of hydrogen and carbon monoxide at steady-state conditions.

$$\rho\frac{d\theta_{H2}}{dt} = 0 = k_{fh}x_{H2}p(1-\theta_{H2}-\theta_{CO})^n - b_{fh}k_{fh}{\theta_{H2}}^n - i \tag{30}$$

$$\rho\frac{d\theta_{CO}}{dt} = 0 = k_{fc}x_{CO}p(1-\theta_{H2}-\theta_{CO}) - b_{fc}k_{fc}\theta_{CO} - \frac{ik_{ec}\theta_{CO}}{2k_{eh}\theta_{H2}} \tag{31}$$

In the above equations, θ_{H2} expresses the surface coverage of hydrogen and θ_{CO} is representing the surface coverage of carbon monoxide. y_{H2} and y_{CO} respectively express the molar fractions of hydrogen and carbon monoxide in the catalyst layer. The parameter n is chosen to a value of 2 indicating that the intermediate hydrogen step is second order in catalyst sites.

From the above equations the anode over potential is calculated as:

$$\eta_a = \frac{RT_{cell}}{\alpha F}\arcsin h\left(\frac{i}{2k_{eh}\theta_{H2}}\right) \tag{32}$$

, which is subtracted from equation 20 giving the resulting cell voltage under reformat conditions.

The model shows good agreement with the experiments performed in [13].

The anode stoichiometric ratio is calculated inside the fuel cell block and the average CO concentration from inlet to outlet is used as model input. Future studies should include the effect of anode stoichiometry in the expressions

Table 1 shows the constants used for the fuel cell model. The cell voltage is multiplied with the number of cells and the current with active area to provide the stack outputs.

2.8.3. Heat production

The energy conservation equations are formulated as in the previous section such that:

$$\dot{Q}_{heat} = h_{in,c}\dot{n}_{c,in} - h_{out,c}\dot{n}_{c,out} + h_{in,a}\dot{n}_{a,in} - h_{out,a}\dot{n}_{a,out} - P_{el} \tag{33}$$

The electric power is subtracted such that only the part of the change of energy that relates to heat is obtained.

2.9. Heat storage tank

The hot water tank is for the current publication modeled as a constantly stirred tank assuming isothermal conditions. It takes as input the energy input from the recuperator and the fuel cell as well as the hot water and heat consumption of the household. Additionally, heat loss to the surroundings is taken into account.

$$T_{\tan k} = \frac{1}{m_{liq} c_{p,liq}} \int (\dot{Q}_{FC} + \dot{Q}_{rec} - \dot{Q}_{HW} - \dot{Q}_{H} - \dot{Q}_{HL})\, dt$$

Where the heat loss to the surroundings is calculated from:

$$\dot{Q}_{HL} = UA_{\tan k}\ (T_{\tan k} - T_{amb}) \qquad (34)$$

2.10. Heat loss to surroundings

All components (except the fuel cell) have been modeled including some degree of heat loss to the surroundings. The parts of the fuel processor (reformer, shift, evaporator etc.) have been assumed having the same surface area ($0.04m^2$) and a heat conductivity of the insulation of 0.025 W/mK corresponding to the better mineral insulation types available. The thickness of the insulation has been set to 40mm on all fuel processor components.

The hot water tank has been modeled as a circular tank with a volume of 250 L (0.4m in diameter by 2m high) with 100mm insulation on the surface.

The overall heat transfer coefficient has been calculated neglecting all convection and radiation contributions such that:

$$UA_{ext} = k_{ins} \frac{A_{surf}}{t_{ins}} \qquad (35)$$

2.10.1. Balance of Plant (BOP) components

For the present paper the BOP components (fans and pumps) have been considered ideal meaning that the output will follow the reference signal precisely. These can however easily be replaced more detailed models if this is needed.

3. Results

The result section will be limited to steady state analysis of the two scenarios demonstrating the model and system capabilities. The dynamic operation of the system will be presented in another publication where also the control system and overall control strategies are presented.

Fig 9 shows the steady state values of the system during a typical summer day. The heat consumption is very low typically only supplying the household with hot water. Electricity production is 666 watts and about 1.5kW equivalent of methane is supplied to the system on an average basis. This results in a fairly high efficiency of 45% electrical and 88% in total when heat production is included. The efficiency is defined as the amount of energy transferred to the heat reservoir plus the electricity produced divided by the energy equivalent input of methane hence not taking into account the heat loss from the reservoir. This is done to make it comparable to conventional gas furnaces, where the heat storage tank is a separate unit.

The methane, once mixed with water, (S/C=2.5) is fed to the reformer at 174°C. This is a fairly low temperature so it has to be heated to 400-500°C. Hence the first part of the

heat exchanger would presumably not include a catalyst, as the low inlet temperature is always present. The outlet temperature of the reformer is controlled to be 670°C.

After the reformer, the gas stream is cooled by injecting an amount of water corresponding to a steam to carbon ratio of 0.5. As very low CO concentrations are desirable, the shift unit contains both a high and a low temperature water gas shift catalyst. As this is a rather low operating point the outlet temperature drops to well below 200°C before entering the fuel cell.

Cathode air is supplied at 25°C and a stoichiometric ratio of 1.8, which is the minimum which the control system will allow. The air is passed through the shift heat exchanger leaving at 315°C to the burner inlet (λ=3.9) were it is mixed with the anode off gas and combusted, using a catalytic burner, raising the temperature to 707°C. The flue gas leaves the reformer at 238°C and enters the recuperator where it is cooled to 175°C before condensing in the evaporator where it is finally cooled to 58°C. This is not sufficient to obtain water balance in the system as only 70% of the injected water is extracted at this temperature. Hence additional water condensation would be needed either using ambient or cathode air if no net water supply is desired.

Fig 10 shows a typical high load scenario where the 2.5kW heat and 1kW power is needed. It is noted that the total system efficiency at this point is very high (92%$_{LHV}$). The electrical efficiency is naturally low as the heat to power ratio is manipulated intentionally.

In contrast to the low heat production scenario, a large part of the produced energy now comes from the recuperator (1709W). Hence the fuel cell is operated at high stoichiometric ratios to supply air enough to generate the required heat with the burner. The burner temperature is still rather low but the outlet temperature on the flue gas side of the reformer is raised to 478°C providing energy to the recuperator. The outlet temperature from the system is 55°C, but since the water content is only 13%, the condensation temperature needs to be very low to obtain water balance.

A method to limit the water balance problems could be to reduce the steam to carbon ratio at high heat production hours of the year, as the fuel cell stoichiometric ratio is much higher in these situations. Reducing the steam to carbon ratio to 1.5 in the reformer, results in a high outlet concentration of methane (6%@670°C). However as only app. 50% of the hydrogen is used this does not influence the fuel cell performance significantly. This results in a total efficiency of 101%$_{LHV}$, indicating that large benefits can be obtained optimizing the control system for the reformer. Issues such as carbon deposition should however be addressed during low SC operation.

4. Discussion

The proposed model provides a platform for testing a variety of system layout and control methods. A couple of scenarios were presented in the previous section based on the proposed system layout.

Another way of increasing the heat production is to let the fuel cell produce all the heat energy, and thereby increasing the electrical efficiency. This would however demand that the electricity could be sold to the grid at reasonable prices and more importantly that the fuel cell size should be increased by a factor of 2-3. This might become economically feasible but for the present it is believed that keeping the system in a near island production mode is better.

A general observation is that a low anode stoichiometry is a clear identifier for good electrical system efficiency and so is a low flue gas outlet temperature.

While the uncertainties are quite large for the models of the individual reactors the results should not be seen in relation to a specific design of the reactors. What the model will do is to provide an overall guideline for advanced design of the reactors using numerical tools such as Computational Fluid Dynamics (CFD). Once these components are designed an empirical fit can be performed to increase the model accuracy.

The turn-down ratio is vital for the economy of the system. To maintain a good efficiency two reactor design aspects must be addressed. One is the losses through the insulation which are more or less constant at both low and high load. Another is the in plane conductivity of the heat exchangers which will significantly degrade the system performance at low load if not minimized.

Parasitic losses for BOP components have not been included in the models and it is vital that all reactors are optimized for minimal pressure losses. For the current system it should however be possible to go as low as 1-2% as no liquid water has to forced out of the HTPEM stack, which is typically using 10-30% of the output power in conventional fuel cell CHP systems.

5. Conclusions

A novel modeling approach of fuel cell based CHP systems was presented. The model is able to simulate a whole year taking into account fuel processing, heat exchangers fuel cell and heat storage reservoir with a resolution of 1 second in less than 1 hour.

Additionally a novel system layout was presented giving electrical efficiencies up to 45%$_{LHV}$ (LHV, BOP contributions excluded) and total efficiencies from 90-100%$_{LHV}$. The system is extremely simple in comparison to other low temperature PEM fuel cell based systems allowing large-scale commercialization.

The model will provide a new base for the control and optimization of future CHP systems taking into account the most important characteristics of the components of the plant. The structure of the model makes it easy to incorporate more detailed models of the components once more test data become available.

Acknowledgements

The authors would like to acknowledge the financial support from Dantherm Air Handling, American Power Conversion and Danfoss.

Nomenclature

α	Charge Transfer coefficient	-
λ	Cathode stoichiometric ratio	-
ρ	Density	Kg $(m^3)^{-1}$
θ	Surface coverage	-
A	Area	M2
a_x , b_x	Regression constants for cathode fuel cell model (See Table 1)	-
b_{xx} *and* k_{xx}	Pre-exp. Factors for anode fuel cell model (see Table 1)	-
c_p	Specific heat capacity	J kg^{-1} K^{-1}
E_{xxx}	Activation energy	J $mole^{-1}$
F	Faraday constant	C $mole^{-1}$
G	Gibbs free energy	J $mole^{-1}$
h	Enthalpy	J $mole^{-1}$
i	Cell current	A
i_0	Exchange current density	A $(cm^2)^{-1}$
k	Heat conductivity	W m^{-1} K^{-1}
m	Mass	Kg
n	Moles	Mole
P_{tot}	Total pressure	Pa
Pxx	Partial pressure of specie xx	Pa
Q	Heat energy	J
R	Universal gas constant	J $mole^{-1}$ K^{-1}
R_{xx}	Ohmic resistance	Ohm
T	Temperature	K
x	Molar fraction	-
t	Thickness	m
U_0	Open circuit potential	V
UA	Overall heat transfer coefficient	W K^{-1}

References

[1] Masashi and Tanaka, Osaka gas, 23rd World Gas Conference, Amsterdam 2006

[2] Elsam, Furim project report, (2006)

[3] J.S. Wainright, J.-T. Wang , D. Weng, R.F. Savinell, M.Litt, J. Electrochem. Soc. 142 (1995) 121-123.

[4] R.F. Savinell; J.S. Wainright; M. Litt, Electrochem. Soc (1995) 214-215.

[5] J., T. Wang; R. F. Savinell; J.S. Wainright, M. Litt; H. Yu, Electrochimica Acta, 41 (1996) 193-197.

[6] Zhenyu Liu, Jesse S.Wainright, Robert F. Savinell, Chemical Engineering Science, 59 (2004) 4833-4838.

[7] J.D. Holladay, J.S. Wainright, E.O. Jones, S.R. Gano, J. of Power Sources 130 (2004) 111-118.

[8] Qingfeng Li et al., Solid State Ionics 168 (2004) 177–185.

[9] Q. Li, R. He, J.O. Jensen, N.J. Bjerrum, Fuel Cells Volume 4 Issue 3 (2004) 147-159.

[10] Qingfeng, Li; Hjuler, H.A.; Bjerrum, N.J., Journal of Applied Electrochemistry Vol.31 Issue.7 (2001), 773-779

[11] Denver Cheddie, Norman Munroe, Journal of Power Sources, Vol. 160, (2006), 299-304.

[12] Denver Cheddie , Norman Munroe, EnergyConversion and Management, Vol. 47, (2006)1490-1504.

[13] Anders R. Korsgaard et al., Proceedings of ASME fuel cell conference 2006 -97214

[14] Anders R. Korsgaard et al., Experimental characterization and modeling of commercial polybenzimidazole-based MEA performance, Journal of Power Sources (2006)

[15] Froment & Bischoff, Chemical reactor analysis and design, 2. edn, Wiley, (1990)

[16] Mads Pagh Nielsen, Anders Korsgaard and Søren Knudsen Kær, Conference on Simulation and modelling (SIMS), 2004

[17] M.Y. El-Sharkh, M. Tanrioven, A. Rahman, and M.S. Alam, Journal of Power Sources , In Press

[18] A.D. Hawkes, and M.A. Leach, Energy, In Press

[19] Michel De Paepe, Peter D'Herdt and David Mertens, Energy Conversion and Management, Vol. 47, Issues 18-19, (2006), 3435-3446

[20] G. Gigliucci, L. Petruzzi, E. Cerelli, A. Garzisi and A. La Mendola, J. of Power Sources, Vol. 131, Issues 1-2, (2004), 62-68

[21] A.F. Mills, "Heat and Mass Transfer", 2nd edition, Richard D. Irwin INC, 1995, ISBN-10: 0256114439

[22] Glenn Research Center, Sep. 19th 2007, http://www.grc.nasa.gov/WWW/CEAWeb/

Figures

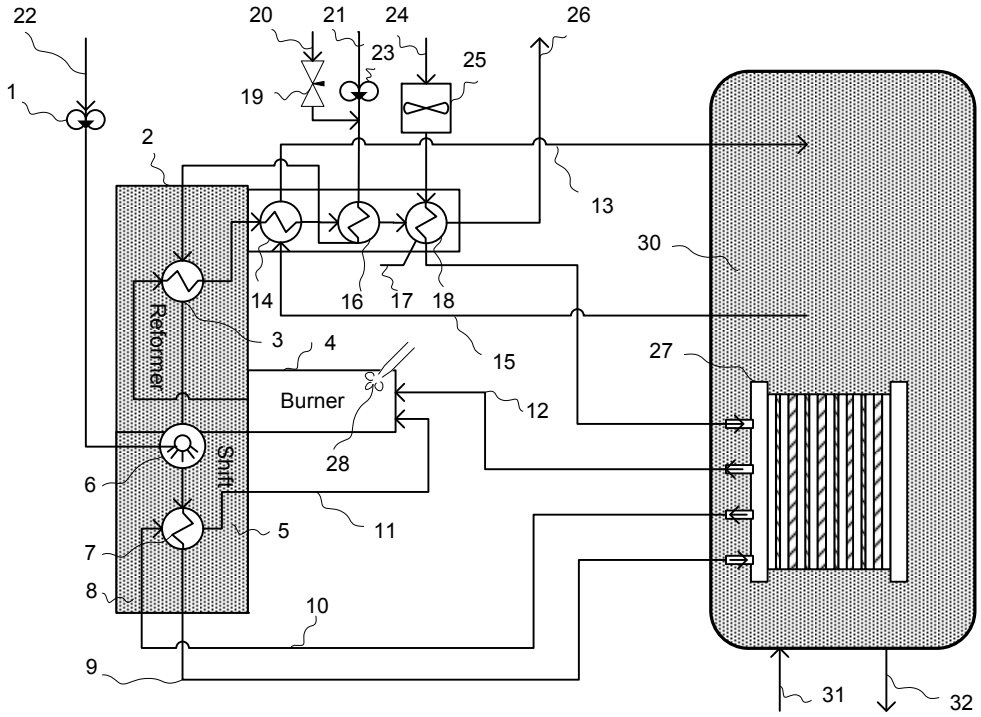

Fig 1: Diagram of the proposed CHP system

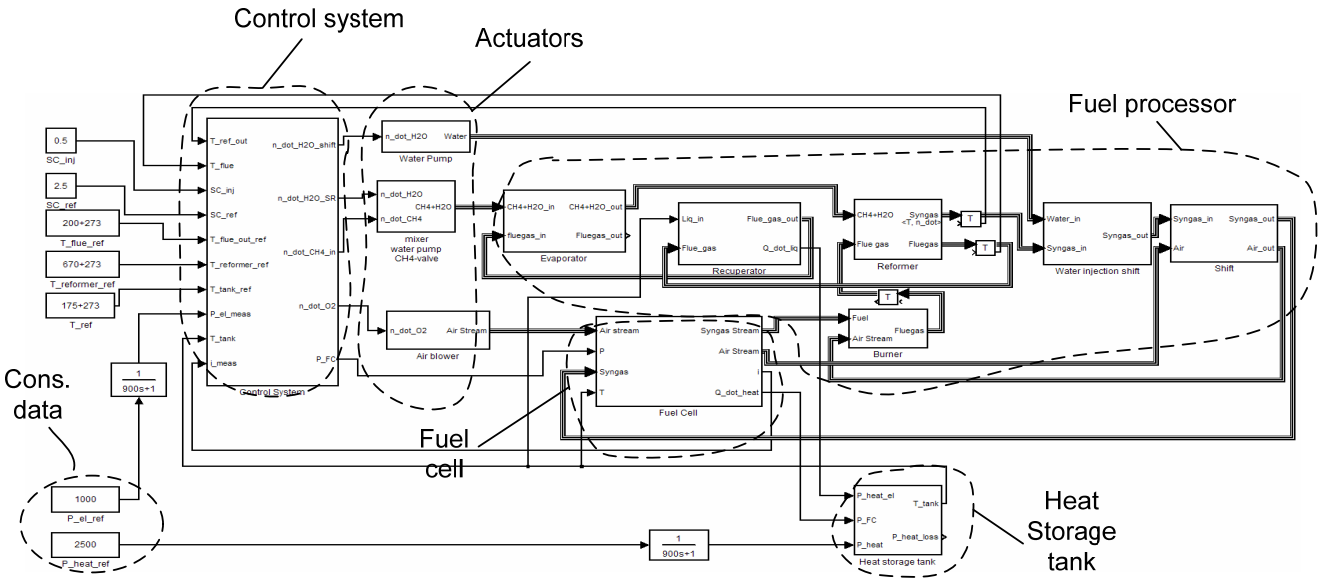

Fig 2: Overall layout of Simulink model.

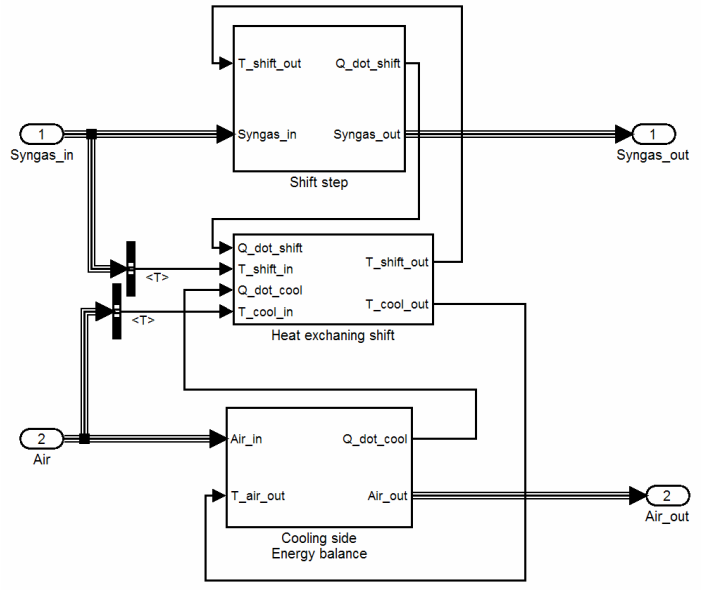

Fig 3: Structure of shift model in Simulink.

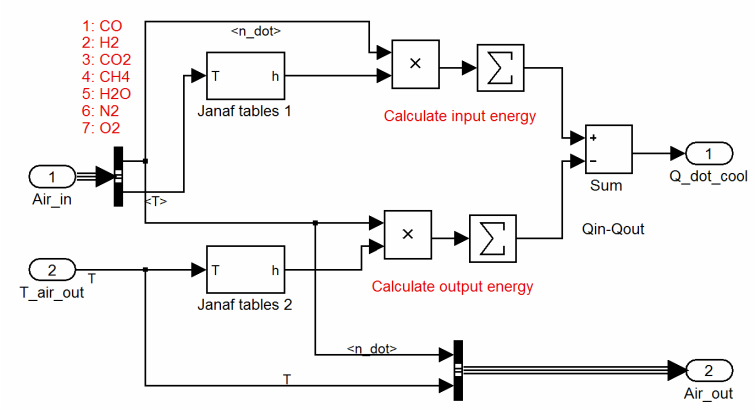

Fig 4: Calculation of change in energy of the air stream in the shift reactor.

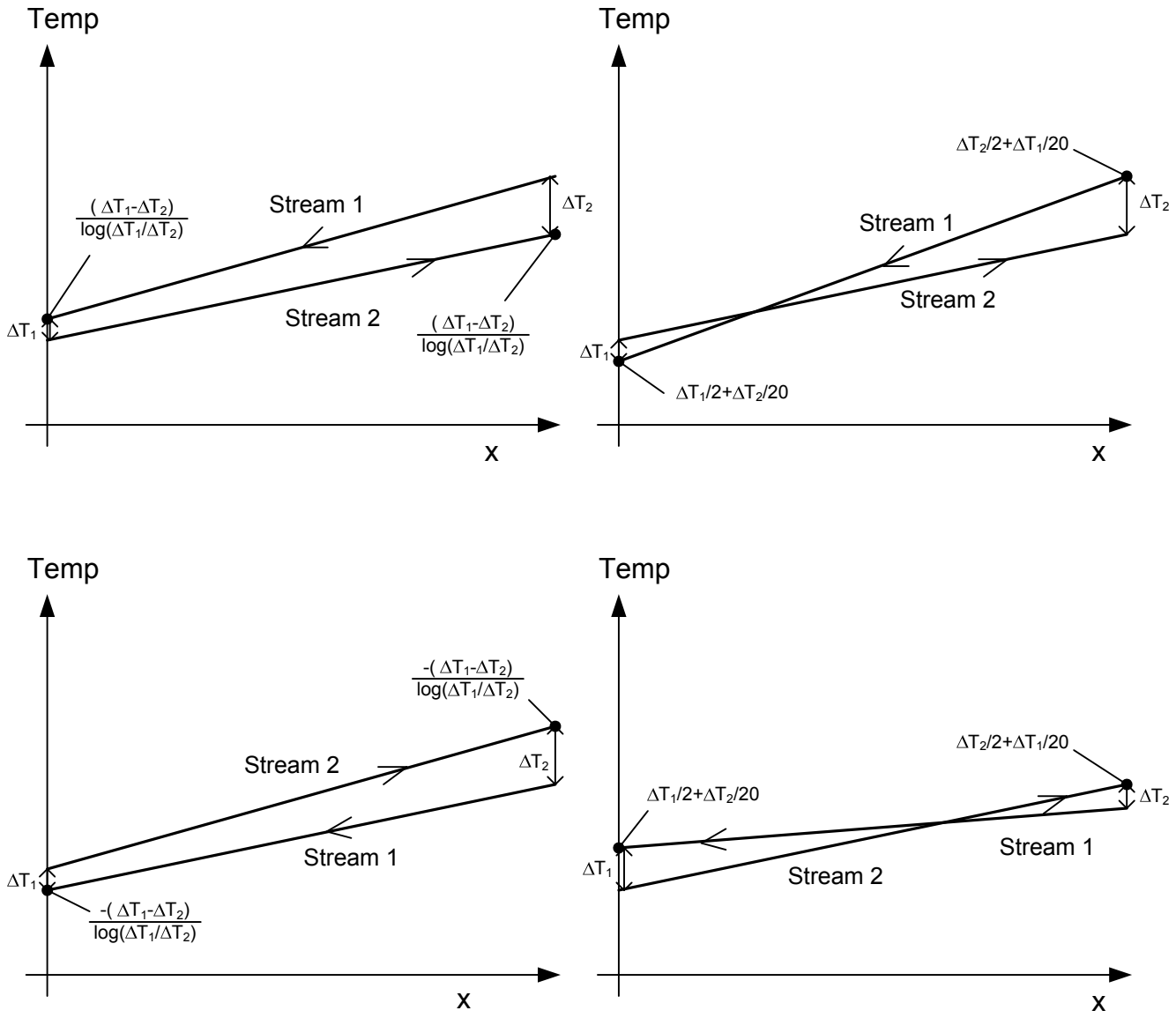

Fig 5: Schemes for calculating the average temperature difference.

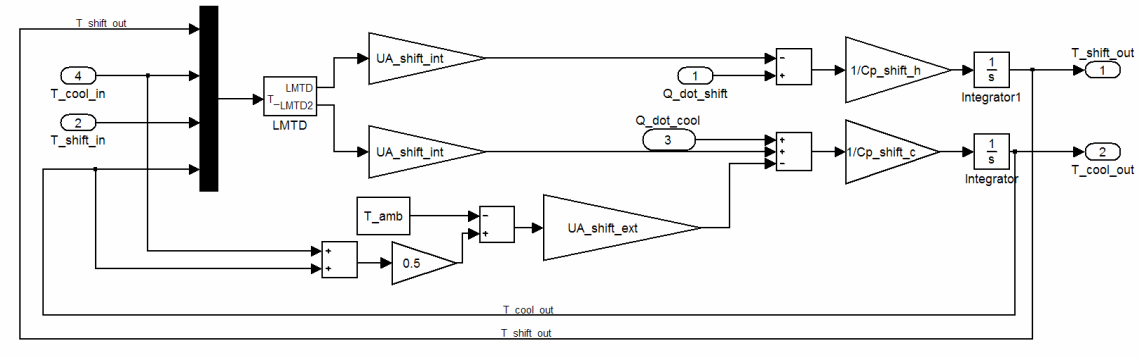

Fig 6: Example of block diagram of heat exchanger model in Simulink.

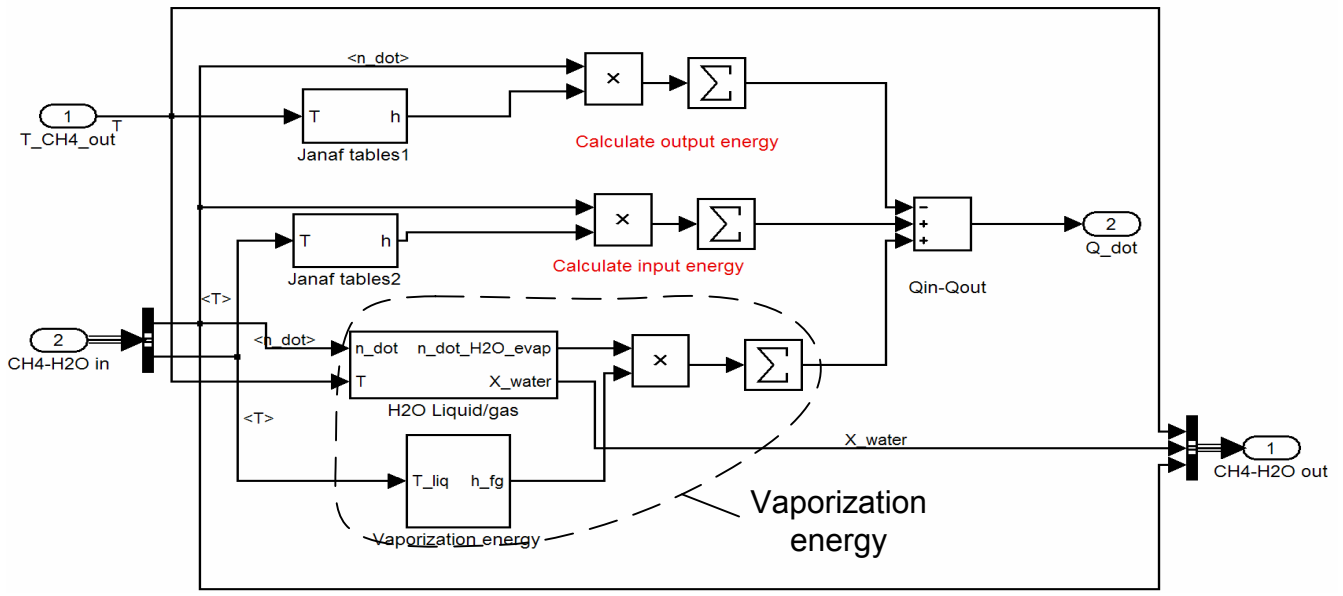

Fig 7: Evaporator/condenser model, calculation of the change in energy flow.

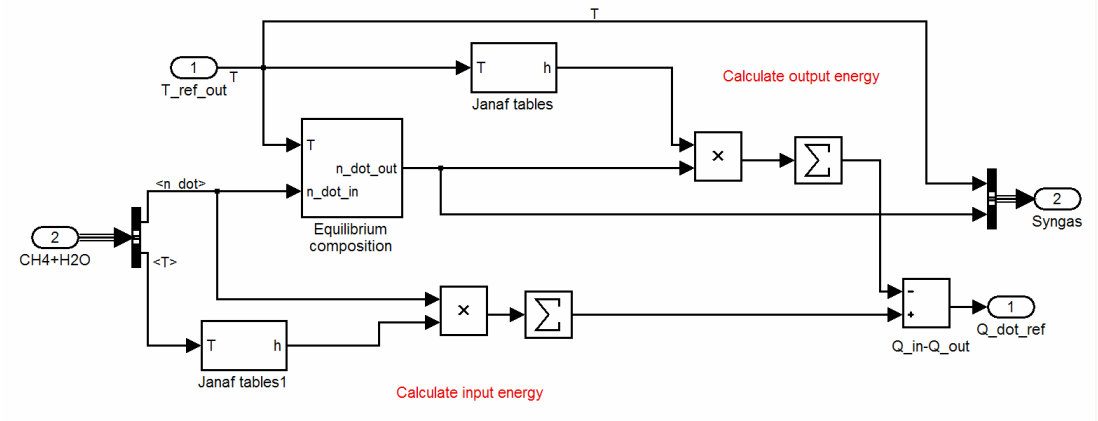

Fig 8: Steam reformer model (reforming side).

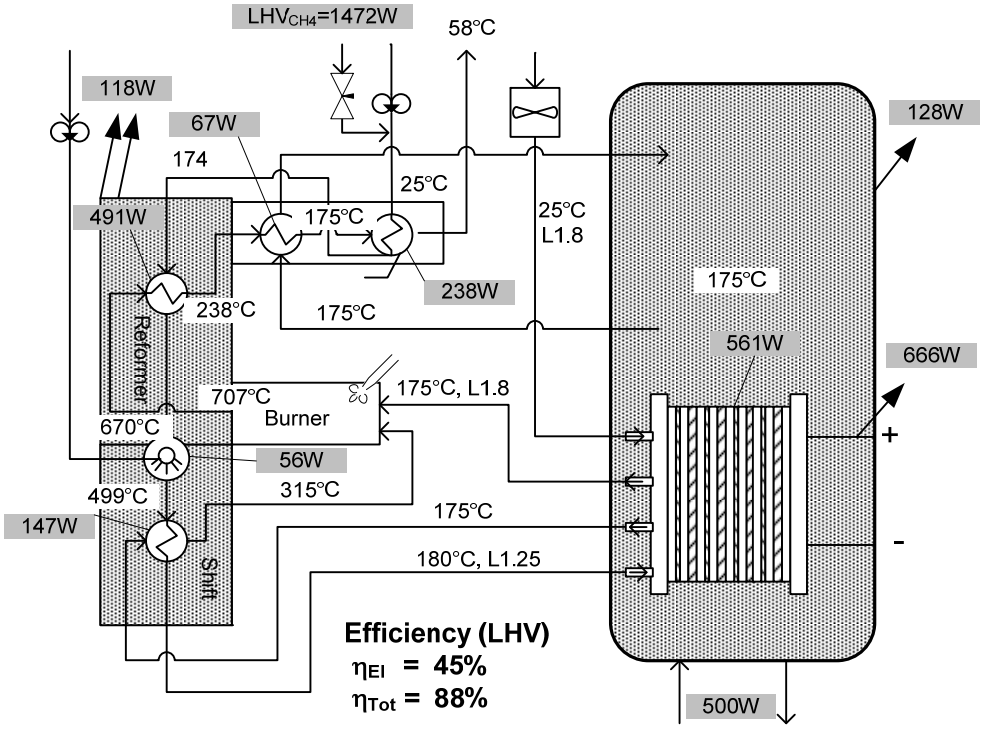

Fig 9: Steady state output scenario based on a typical summertime consumption pattern (heat consumption of 500W and electricity consumption of 666W).

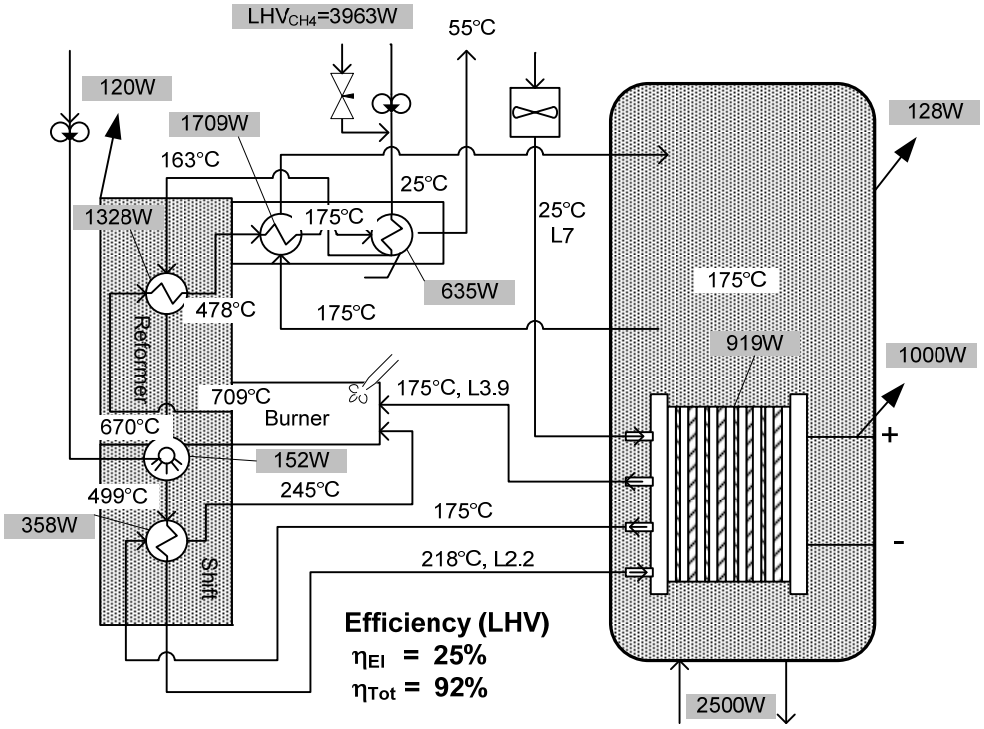

Fig 10: Steady state output scenario based on a high level power production (heat 2500W and electricity 1000W).

Table 1

Numerical values used for the fuel cell model

Membrane		
Membrane thickness, t_{memb}	0.1×10^{-3}	m
Values used for cathode model		
Charge transfer constant, a_0	2.761×10^{-3}	K^{-1}
Charge transfer constant, b_0	-0.9453	-
Ohmic loss constant, a_1	-1.667×10^{-4}	$\Omega\ K^{-1}$
Ohmic loss constant, b_1	0.2289	Ω
Diffusion limitation constant, a_2	-8.203×10^{-4}	$\Omega\ K^{-1}$
Diffusion limitation constant, b_2	0.4306	Ω
Limiting current constant, a_3	33.3×10^{3}	A
Limiting current constant, b_3	-0.04368	-
Open circuit voltage, U_0	0.95	V
Pre-exponential factors used for anode model		
CO desorption rate, b_{fc}	8.817e12	bar
H_2 desorption rate, b_{fh}	2.038e6	bar
CO electrooxidation rate, k_{ec}	3.267e18	A cm^{-2}
H_2 electrooxidation rate, k_{eh}	25607	A cm^{-2}
CO adsorption rate, k_{fc}	94.08	A cm^{-2} bar^{-1}
H_2 adsorption rate, k_{fh}	2.743e24	A cm^{-2} bar^{-1}
Activation energy values used for anode model		
CO desorption rate, E_{bfc}	127513	J $mole^{-1}$
H_2 desorption rate, E_{bfh}	47904	J $mole^{-1}$
CO electrooxidation rate, E_{kec}	196829	J $mole^{-1}$
H_2 electrooxidation rate, E_{keh}	34777	J $mole^{-1}$
CO adsorption rate, E_{kfc}	19045	J $mole^{-1}$
H_2 adsorption rate, E_{kfh}	1.899e5	J $mole^{-1}$
Other constants		
Fuel cell active area, A_{cell}	135	cm^2
Number of cells, n_{cells}	65	-

Table 2

Numerical values used in the fuel processor and heat reservoir model

Internal overall heat transfer coefficients		
Reformer, $UA_{ref,int}$	10	$W\ K^{-1}$
Water gas shift, $UA_{shift,int}$	3	$W\ K^{-1}$
Evaporator/condenser, $UA_{evap,int}$	30	$W\ K^{-1}$
Recuperator, $UA_{rec,int}$	Inf	$W\ K^{-1}$
External overall heat transfer coefficients		
Reformer, $UA_{ref,ext}$	0.1	$W\ K^{-1}$
Water gas shift, $UA_{shift,ext}$	0.1	$W\ K^{-1}$
Evaporator/condenser, $UA_{evap,ext}$	0.1	$W\ K^{-1}$
Recuperator, $UA_{rec,ext}$	0.1	$W\ K^{-1}$
Burner, $UA_{burn,ext}$	0.05	$W\ K^{-1}$
Heat capacities		
Specific heat capacity (AISI316), $c_{p,\ reactors}$	530	$J\ kg^{-1}\ K^{-1}$
Mass of burner, m_{burn}	1	kg
Mass of reformer, m_{ref}	2	kg
Mass of recuperator, m_{rec}	1	kg
Mass of water gas shift, m_{shift}	0.5	kg
Mass of evaporator, m_{evap}	1	kg

Submitted to Journal of Hydrogen Energy, accepted with minor revisions, second revision is being processed.

Part two: Control of a Novel HTPEM based Micro Combined Heat and Power Fuel Cell System

Anders R. Korsgaard[a], Mads P. Nielsen[a], Søren K. Kær[a]

[a] *Institute of Energy Technology, Aalborg University, DK-9220 Aalborg, Denmark*

Elsevier use only: Received date here; revised date here; accepted date here

Abstract

A novel micro combined heat and power system and a dynamic model thereof was presented in a part one of the publication. In the following, the control system and dynamic performance of the system is presented. The model is subjected to a measured consumption pattern of 25 Danish single family houses with measurements of heat, power and hot water consumption every 15th minute during one year.

Three scenarios are analyzed ranging from heat following only (grid compensation for electricity), to heat and power following with net export of electricity during high and peak load hours. Average electric efficiencies above 40% $_{LHV}$ was obtained and beyond 90%$_{LHV}$ in total efficiency.

Keywords: Fuel Cell; PEM; CHP; Intermediate temperature; HTPEM; Control

1. Introduction

Micro combined heat and power (CHP) has been receiving an increasing interest in the recent years due to political requirements for more efficient power production. This has been sought fulfilled using various technologies including internal combustion engines, stirling engines, micro turbines and fuel cells where the latter is believed to have the highest electrical efficiency.

Among fuel cells, a range of different types exist including Proton Exchange Membrane (PEM) and Solid Oxide Fuel Cells (SOFC). In the present publication, special attention will be given to a type of PEM fuel cell operating at slightly higher temperatures (120-200°C) based on phosphoric acid doped Poly-benz-imidazole (PBI) membranes, commonly termed high temperature PEM (HTPEM).

The use of PBI for fuel cell applications was first published by Wainright et al. [1] followed by a number of papers [2][3]. Some of the same authors published data regarding the oxygen reduction reaction [4] and recently they published data on CO coverage [5].

Other research groups also published data regarding development of PBI based MEA's such as the group of Bjerrum et al. [6][7] [8].

Recently Cheddie et al. [9][10] published a model of a PBI membrane but it only included one operating temperature and the stoichiometric ratio was not given.

The authors of this work presented an empirical model of the HTPEM fuel cell ([11][12]).

There has been some activity on modelling the impact of micro CHP from a grid perspective by amongst others El-Sharkh et al.[13], Hawkes et al. [14] and Paepe et al. [15]. Additionally a range of different test results have been presented including [16]. Pukrushpan et al. applied a range of advanced control algorithms to fuel cell systems and provided a dynamic model of a partial oxidation based system [17]. The models are however not suited for performance analysis in terms of efficiency and thermal integration as heat exchanger limitations are not taken into account. Joshua Golbert et al. presented both some models and some advanced non linear control [18].

The present paper is the second of a two part publication. In the first part an extensive model of a complete CHP system was given [19].

In this publication focus will be given to the control system and various overall control scenarios.

To install an increasing amount of renewable energy sources in the energy system these units should additionally be able to perform everything from net production to net consumption during peak and low consumption hours of the day respectively. During weekends it might even be economically feasible to shut them off and use cheap renewable energy from the grid.

To play a major role within grid stabilization the units should be able to respond from 0-100% load within minutes or even seconds imposing hard demands on dynamic system capabilities.

Finally, efficiencies similar to those of large scale central power plants must be obtained for micro CHP systems to play a major role in a future with continuously increasing energy prices.

In this publication a model of a novel system which is able to meet most of these demands is presented along with a number of control strategies. The models used are mostly based on experimental data, and have a fairly good precision in terms of static as well as dynamic performance.

2. Theory

In part one an in depth description of the system and the modelling aspects was given. Hence only a brief introduction to the system modelled is given in the following. Afterwards the model inputs representing the user consumption data and energy prices is given. Finally, the control system and three overall control scenarios are discussed.

2.1. Model and system summary

Fig 1 shows an overview of the system from which a model was created in part one [19]. Generally the system consist of a steam reformer, water gas shift reactor, fuel cell, heat reservoir, burner and some heat exchangers.

Fig 2 shows the overall Matlab®Simulink model created from this system. From right, four system actuators controlled by the control system feeds the system with reactant air, water and methane. These inputs are also shown in fig 1. The steam reformer based fuel processor is provided

with natural gas and water through the evaporator which is fed to the reformer converting the fuel into a hydrogen rich mixture of H_2, CO and CO_2. The water gas shift reactor converts most of the CO to CO_2 using water. This exothermic process is cooled using the reactant air leaving the fuel cell. The heated air is subsequently passed to the burner. The reformate gas is passed to the fuel cell before mixing with cooling air from the shift in the burner. This mixture is catalytically combusted providing the energy for the steam reforming process. After the reformer, the burner flue gas is further cooled in the recuperator supplying heat to the hot water reservoir. As the final step before leaving through the exhaust, the flue gas provides heat to the water evaporator.

The fuel cell itself is placed inside the heat storage reservoir which contains a fluid which remains in liquid form up to 190°C. Hence all heat released from the fuel cell will be efficiently transferred to the heat reservoir without any losses (electrical or thermal).

The advantages of system simplicity are apparent but it puts some challenges on the control system design as the control set points are increasingly coupled.

The model itself is described in detail in part one. Generally, it is based on overall energy considerations of the inlet-outlet gas compositions, LMTD (Logarithmic Mean Temperature Difference) heat exchanger models and chemical equilibrium calculations [20]. The thermal inertia of the components is included using the heat capacity of the solids providing the background for predicting the dynamic response of the system.

The fuel cell is modelled using the empirical model presented in [11] and [12], which is based on extensive series of tests including effects of CO concentration (0.1-10%), temperature 120-200°C and cathode stoichiometry. The anode overpotential is calculated based on the average CO concentration of the reformat gas stream fed to the fuel cell.

Parasitic losses to fans and pumps have not been included but based on the authors experience it is believed that these can be kept as low as 1-3% of the electrical output due to the system simplicity. Additionally, no inverter/converter losses are included.

2.2. Model inputs

An extensive data series for 25 single family houses was available containing quarterly measurements of electric power, heat and hot water consumption yielding a total data set size of 3 x 35,000 points. Fig 3 shows running average (96 points ~ one day) of the data series of house 26, which corresponds to the average consumption of the 25 houses. The consumption is provided by the subsystem in the lower left corner of Fig 2. The simulation input is based on the average consumption of the 25 houses at a given time (house 26). This can be done because the grid will not see the fluctuations of the individual houses from short duration spikes when i.e. thousands of units are coupled in parallel.

To provide some indications of the economical feasibility of using a fuel cell based micro CHP system in place of conventional natural gas furnaces, economical data for fuel and electricity cost is also provided for the model. Even

though the economical conclusions might not be transferred directly to other countries, it is assumed that the trend of the cost is similar in many especially European countries.

Table 1 shows the Danish natural gas price for smal consumers. The energy taxes shown are applied to heat producing units such as conventional gas fired furnaces and it is assumed that micro CHP systems will be treated similarly. In contrast taxes (again from Danish legislation) are not applied to the amount of natural gas which is used for electricity production for the grid (assuming 65%$_{LHV}$ electrical efficiency). This means that if a power plant exports 100 kWh of electricity to the grid tax refunds corresponding to approximately 154 kWh of fuel will be given.

Hence it is assumed that the taxes will be refunded for the part relating to the electricity sold, such that:

$$c_{NG,net} = E_{tot,NG} p_{NG,tot} \cdot -E_{tot,\exp} \cdot (p_{NG,CO2} + p_{NG,energy}) / 0.65 \quad (1)$$

Where $p_{NG,tot}$ [€/kWh] is the total cost of buying natural gas, $p_{NG,CO2}$ and $p_{NG,energy}$ are the taxes [€/kWh] and $E_{tot,NG}$ and $E_{tot,\ exp}$ are the total amount of natural gas consumed in kWh equivalents and the electricity exported, respectively.

The Danish electricity grid already has many unregulated power production units including windmills and smaller CHP plants supplying the heat for domestic heating. Additionally, the power consumption is unevenly distributed throughout the day and year increasing the need for regulating power. To increase the motivation for decentral power production units to vary the power production according to the demand, the electricity payment has been divided into three tariffs. Table 2 shows the time intervals in which the tariff structure is divided into.

Table 3 shows the three electricity price tariffs and the corresponding cost margin when exporting electricity to the grid. As observed, the margin is negative when producing during low tariff period. This may not be the case if lower natural gas prices can be negotiated when used for electricity production. Much higher margins can be obtained during peak (up to 50%) and high load periods. It is still unclear how the electricity production from these units will be regulated, but for the medium to long term it is believed that the tariff structure from Table 3 might be the most likely outcome. For the short term a fixed energy price may be given, where the net annual production is used for price calculations.

Additionally, a standby fee may be given for these units as they offer power to the grid with a quick response time. This has not been included in the calculations of the economics.

For electricity import the standard taxed electricity cost is used which is currently 164€/MWh. VAT is not included in any of the prices/tariffs.

2.3. Control system

The control system is built up based upon classical PI regulators (Proportional-Integral) and feed forward strategies combined with constrained parameters.

Basically, only the reformer outlet and the hot water reservoir temperatures are controlled using the fuel and air supplies, respectively. However, in some cases the reactant

supply to the fuel cell need to be constrained such that starvation does not occur especially during transients.

Fig 4 shows the controller for the reformer outlet temperature which uses the inlet flow of methane as actuator. A standard PI controller is used having the gains shown in the diagram. Additionally, a feed forward of the measured current is added using a gain corresponding to a stoichiometric ratio of 2. The gain is calculated as the number of moles H_2 required for the reaction divided by 4 as one mole of methane ideally produces 4 moles of H_2.

The output is saturated such that the stoichiometric ratio of the reformat in the fuel cell never drops below 1.25 to prevent fuel starvation during transients. To prevent integrator run-away anti windup is implemented.

The control system for the outlet flue gas temperature of the reformer has the same structure. Hence

$$\dot{n}_{O2,ref} = (T_{Flue,out,ref} - T_{Flue,out,meas}) \cdot G_c + I_{FC} K_{feed,air} \quad (2)$$

Where G_c is the PI controller (K_p=40·10^{-9} and T_i=1000 sec) and the feed forward gain is determined by:

$$K_{feed,air} = \frac{\lambda_{air,feed} n_{cells}}{4F} \quad (3)$$

$\lambda_{feed,air}$ is set to 5 resulting in some overshoot but this is needed to maintain the shift outlet temperature sufficiently low.

The output is saturated such that a minimum air flow corresponding to $\lambda_{FC,air}$=1.8 is obtained, with the above mentioned anti windup function.

The water injection at the inlet of the evaporator and after the reformer is always kept relative to the methane inlet flow such that

$$\dot{n}_{H2O,shift} = SC_{shift} \dot{n}_{CH4,ref} \quad and \quad \dot{n}_{H2O,SR} = SC_{SR} \dot{n}_{CH4,ref} \quad (4)$$

2.4. Overall control scenarios

2.4.1. Reference scenario

For comparison of economical figures a reference scenario based on a traditional Danish household with a natural gas furnace is used. The annual consumption of power and heat multiplied by the taxed electricity and natural gas price previously mentioned are used as reference annual expenses. The furnace including heat reservoir is considered having an average efficiency of 90%$_{LHV}$ where losses from the heat reservoir are taken into account. The total variable cost of operating the traditional furnace is held constant during all scenarios giving a total of 1637€/year. This number is used to calculate the relative margin for installing the μCHP unit in the household compared to the traditional natural gas furnace.

2.4.2. Scenario one: Heat following – unbound electric

This is the simplest scenario which allows a straight forward implementation. The fuel cell production is controlled using the temperature of heat storage as set point such that:

$$P_{ref,FC} = (T_{HST,ref} - T_{HST,meas}) \cdot G_c \quad (5)$$

Where G_c is an ordinary PI controller with gains K_p=200 and T_i=3600 sec. The power reference is set to zero if the reformer outlet temperature becomes lower than 550°C as

this would result in high methane concentration in the reformate and insufficient hydrogen for the fuel cell. The set point for the heat storage tank has been set to 168°C. Lower temperatures than 150-160°C would make the fuel cell much more sensitive to carbon monoxide [11].

This is the scenario with the highest obtainable electrical efficiency, as the outlet flue gas temperature of the reformer is minimized, having a set point at 200°C.

The fuel cell output is saturated at a maximum of 2kWe to prevent operation in low efficiency regimes.

2.4.3. Scenario two: Heat and power following

In this configuration all heat and electricity is sought supplied by the fuel cell using only the grid as a buffer during short transients. The power consumption is measured and supplied as a reference value for the fuel cell. The set point for outlet flue gas reference temperature (see Fig 4) is also calculated using a PI controller with saturated output between 200-550°C. The controller is rather slow ($T_i=10^3$ sec) recognizing the slow thermal response of the hot water tank. The gain is higher with a gain ($K_p=30$). An anti windup loop is included as in the previous cases.

Similarly, the load is cut off if the temperature of the reformer drops below 550°C.

The fuel cell output is again saturated at 2kWe.

2.4.4. Scenario 3: Heat and power following, peak power production

In this scenario electricity is exported only when it is desirable according to Table 2. The rest of the time, the system will seek to only produce the heat and power which is needed for the household. The heat storage tank should in this case be larger in order to produce more electricity during the daytime saving the thermal energy to the night (or weekends).

It is likely that the decision to export is made by a central fleet owner. However, for the current scenario it is assumed that the fleet operator is driven by cost perspectives. The motivation for producing electricity is proportional to both the difference between the maximum and the current temperature of the hot water tank and the margin at the current production hour, referring to Table 3. The power control law for the fuel cell would in this case look like:

$$P_{FC,ref} = (T_{HST,\max} - T_{HST})(p_{el} - p_{NG})K_{\exp} + P_{el,cons} \quad (6)$$

Where the maximum temperature of the heat storage tank ($T_{HST,max}=185$°C) and the energy costs (p_{el} and p_{NG}) can be found from Table 1 and Table 3. The constant ($K_{exp}=4400$) can be termed a motivation factor for producing power to the grid and is set empirically. The household electricity consumption is given as $P_{el,cons}$.

As mentioned above, it is assumed that the tax paid for the amount of natural gas used for electricity export will be refunded.

3. Results

In the following all calculations are based on the same size of system to make them directly comparable in terms of pay back time. However it might make sense to increase the size of the fuel cell in scenario one and three due to the net export of electricity (short periods of high power output). The size of the fuel cell is given in terms of active

area and the number of cells in the stack. The size of the reformer is given in terms of weight and over all heat transfer coefficient (UA). The figures used are listed in the part one of the paper and corresponds to a system with maximum electrical output of 2kWe at a current density of approximately 0.4 A/cm^2.

The size of the heat storage reservoir will be varied in the three scenarios. The base size is 60L (with a heat capacity corresponding to water) for the heat following scenario and 250L for scenario two and three where decoupling of heat and power production is desired.

3.1. Electric power cycle

To provide an insight in the dynamics of the system an example of a basic load cycle is given. Fig 5 shows the transient behavior of the system during a 120,000 second cycle based on the heat and power following strategy of scenario two. A constant thermal load of 1700W is applied to the system while step inputs in the power drawn from the system are applied.

The reformer is started from zero and the electrical load is applied in one step to 1400W once the outlet reformer temperature reaches 550°C. This happens within the first few hundred seconds of operation. The load is then cycled through a load pattern (300W, 1600W, 1000W, 500W, 500W) in sharp steps with around one second in rise time. The thermal response is sown on the right axis in the top left figure. The corresponding stack performance is shown in the top right.

In the bottom left the reforming temperatures are shown. Initially, the feed forward gains produce a little overshoot to provide the fast startup. The outlet flue gas temperature drops to about 300°C to limit the thermal output in the recuperator as sufficient thermal energy is available from the fuel cell. In this case the reformer efficiency could have been increased further by lowering the outlet temperature (supplying less air to the reformer). This however, would have violated the minimum fuel cell stoichiometry of 1.8.

The load suddenly drops to 300W for the next interval meaning that the fuel cell cannot provide sufficient thermal energy for the system. Hence the flue gas outlet temperature is increased providing additional energy to the recuperator.

After 40,000 seconds the load is increased to 1600W resulting in an undershoot followed by an overshoot. This is due to the wall temperature which has to be increased to accommodate sufficient heat transfer. The controller reacts fast with a little overshoot before settling at new flue gas temperature of 800°C. At 1000W the inlet and outlet flue gas temperatures are lowered both due to the higher heat transfer capabilities and due to the higher heat production of the fuel cell. The recuperator thus has to produce less energy to the storage tank to satisfy the consumption.

The shift is only indirectly controlled by the other set points. The resulting temperature profiles are shown in the lower right end of the figure. As seen the shift reformate outlet temperature is approximately 200-300°C and the air inlet temperature to the burner is in the same range.

3.2. Snapshots of the performance in scenarios one and three

Fig 6 shows simulation results for the first week of January. In this scenario the electrical power output is controlled only by the temperature of the heat storage reservoir (set point 168°C) which was set to a rather small size (60L). The base plus the $P_{el,imp}$ area gives the total consumption while the base plus $P_{el,exp}$ gives the net produced power by the system. It is observed that large exports during both night and day are dominant and only a minor peak in power consumption gives a fraction of import at this time of year. About 10-20% of the heating demand is supplied by the recuperator, hence lowering the electrical efficiency. If in contrast it had been chosen to increase the size of the reformer (and perhaps fuel cell) to be able to produce higher efficiencies, this would result in a large overcapacity during summertime. During the four days simulated about 160 kWh were produced, where 71 kWh was consumed locally and other 89 kWh was exported to the grid. Unfortunately, only 45% of the power was produced during grid high and peak load hours.

Fig 7 shows the equivalent production/consumption pattern but for the summertime where both the power and heat consumption is significantly lower. Still, due to the high electrical efficiency of the system there is a net export of electricity to the grid. However, in periods some import does exist. The thermal energy is now almost entirely produced by the fuel cell.

Fig 8 shows the simulation of scenario three during the first four days of January with a hot water tank of 250L. It is seen that during daytime there is a net export of electricity, providing more than 1kWe during peak and 0.5-1kW during high load, to the grid. In the night time the fuel cell exactly produced what is needed for the household. In the right figure the heat production is shown, having the main production during the daytime. However, during nighttime, the recuperator produces some heat to keep the heat storage tank around the set point (168°C). This indicates that a larger heat storage tank (and to some extent fuel cell) could make sense. Grid export is only present during high and peak load grid situations whereas in off-peak situations the system is operated in near island mode.

Fig 9 shows a similar case of scenario three but for the 2nd week of August. It is clear that the heat consumption is much lower at this time of year. Hence the motivation for producing electricity is much lower as only little thermal energy is needed. The grid electricity consumption however is also lower than the remaining part of the year, and so a lot of central power plant capacity should be available (even though the central power plants cannot use all the available thermal energy either). It is also observed that the export of electricity only takes place during the morning as the heat reservoir quickly reaches its maximum temperature, and hence electricity export is stopped from around midday.

3.3. Scenario simulations

Table 4 shows the simulations to be performed. Scenario one, which is only heat following, would probably only need a small heat storage tank, since the system would pro-

duce the heat as needed, which is analyzed in scenarios 1.a-1.d. Scenario 1.e analyzes the effect of doubling the fuel cell size. Only one case is tested in scenario two which is the standard fuel cell size (135 cm^2 MEA's and 65 cells) and the 250L hot water tank.

Case 3.a is run on the standard system but with grid export during peak hours. In 3.b the fuel cell size is doubled and the last case (3.c) analyzes the effect of a very large heat reservoir.

Table 5 shows the results of the simulations. Note that the total efficiencies are listed in two ways in the table. The first is given in the way that the system is actually modeled, where the heat loss from the heat storage tank is lost. The second assumes that this energy is supplied to the household by passive heating. The insulation thickness of the heat storage is the same for all the scenarios (100mm), assuming a 2m high cylinder.

It is clear that the heat following scenarios will have the largest efficiency since it seeks only to produce heat with the fuel cell. The electrical efficiency is more or less constant during the first four scenarios at $37\%_{LHV}$ in average. Note that the peak efficiency is much higher. However doubling the fuel cell size in this case results in approximately 4% increase in efficiency from the base scenario. However it does not contribute much to the margin of the system since most of the electricity is produced during low load where the production margin actually is negative.

The second scenario has the lowest electrical production of all the scenarios and hence also the lowest electrical efficiency. Since no import or export is present no positive contributions are made on the margin. Hence this figure reflects exactly the savings in buying the electricity from the grid versus producing it locally. This scenario would be readily implementable since no major political changes or subsidiaries are needed.

Scenario 3.a provides a slightly better electrical efficiency as there is a net export of electricity. The net export during peak and high load is significant in all three sub scenarios taking into account that there is approximately 1300 peak and 2600 high load hours during a year. This corresponds to approximately 1kW average export capacity during peak load and a bit more than 0.5kW during high load. The overall margin is also slightly higher than scenario 1.a which is due to the higher income on sales at high and peak power situations. Installing a fuel cell twice the size provides a 36 € higher margin which may be difficult to justify depending on the fuel cell capital costs. A larger heat reservoir will without doubt increase the peak load export capability. However it seems that it is at the expense of thermal efficiency unless the heat storage tank is heavily insulated.

Concluding, scenario one would be the scenario with the highest thermal and electrical efficiency. However since a still increasing amount of electricity is produced from renewable energy, without positive regulation force, it might make sense to use the strategy of scenario three. In the short term scenario 2.a might be the simplest to implement, only using the grid as a buffer for short electricity spikes.

Fig 10 shows the resulting margins as a bar plot with error bars to reflect +/- 20% changes in the natural gas price.

4. Discussion

4.1. Control system

Future work should include some more advanced strategies where at least some degree of gain scheduling should be performed since the system gains change radically over the range of operation. More advanced strategies such as multivariable, adaptive and maybe even predictive schemes may provide more tight control of the set points. Especially the fluctuations in the reformer and shift outlet temperatures should be minimized. During many of the trials made on the model instability of current control system occurred due to high CO concentrations in the fuel cell. These instabilities are however physical existing when operating the fuel cell at high loads with high CO concentration and low temperatures. This made the fuel cell cross the peak power point of the polarization curve changing the sign of the gain making the controller unstable. This problem is linked directly to the integration of the fuel cell in the heat storage reservoir.

For better performance of the system, variable steam to carbon ratios could have been included, such that the outlet or inlet temperature of the water gas shift is kept within a tighter range. Also the water inlet to the reformer could maybe be reduced during high thermal loads and increased during high electrical loads. However, it has to be noted that this would also increase system complexity.

For the present, water balance has not been sought obtained as this would require large heat exchanger areas of the system to condense sufficient water from the exhaust for the steam reforming. However this is straight forward to accomplish heat exchanging with ambient air. The condenser might even be included in some of the technical systems in the household such as hot tap water supply lines or floor heating systems, and thereby increasing the thermal efficiency.

4.2. Alternative scenarios

During low load grid situations it might make more sense to import electricity for both household heat and electricity consumption (i.e. during summer nights). This option could indeed be a solution but this would require that the tax to be removed during these off-peak situations. This would presumably also have some positive effects on system lifetime.

5. Conclusions

A novel fuel cell based combined heat and power system for residential use was presented. The system is extremely simple with only four actuators for the entire system. A control system was proposed taking as input only the current of the fuel cell, the power consumption of the household and three temperature measurements.

The system was modeled using Matlab®Simulink software to simulate an entire year with a resolution in the range of seconds modeling most thermal dynamics of the system. The instant response capability was demonstrated

making the system capable of taking part in grid stabilization.

Three scenarios were analyzed with additional system parameter variation of the system components used. The first was heat following only (electricity is sold or used by the household). The second provides exactly the amount of heat and power that the household needs operating in near island mode. The last added electricity export during high and peak load grid situations. Average yearly efficiencies were calculated to be up to 41%/92%$_{LHV}$ electrically and thermally respectively (based on LHV of natural gas and excluding balance of plant components). Based on the current Danish energy price structure annual contribution margins from 400-600€ can be obtained compared to the traditional gas fired furnaces.

Acknowledgements

This work was supported by Danfoss A/S, Dantherm Air Handling A/S and American Power Conversion Denmark ApS.

Nomenclature

F	Faraday constant
T	Temperature
I	Cell current
λ	Stoichiometric ratio
R	Universal gas constant
n	Mole
Q	Heat energy
E	Energy (thermal or electric)
SC	Steam to Carbon ratio
p_{xx}	Cost of energy per kWh
G_c	Control transfer function
K_p	Proportional control gain
T_i	Integral control time constant
K_{exp}	Electricity production motivation factor

References

[1] J.S. Wainright, J.-T. Wang , D. Weng, R.F. Savinell, M.Litt, J. Electrochem. Soc. 142 (1995) 121-123.
[2] R.F. Savinell; J.S. Wainright; M. Litt, Electrochem. Soc (1995) 214-215.
[3] J., T. Wang; R. F. Savinell; J.S. Wainright, M. Litt; H. Yu, Electrochimica Acta, 41 (1996) 193-197.
[4] Zhenyu Liu, Jesse S.Wainright, Robert F. Savinell, Chemical Engineering Science, 59 (2004) 4833-4838.
[5] J.D. Holladay, J.S. Wainright, E.O. Jones, S.R. Gano, J. of Power Sources 130 (2004) 111-118.
[6] Qingfeng Li et al., Solid State Ionics 168 (2004) 177–185.
[7] Qinfgeng Li, R. He, J.O. Jensen, N.J. Bjerrum, Fuel Cells Volume 4 Issue 3 (2004) 147-159.
[8] Qingfeng, Li; Hjuler, H.A.; Bjerrum, N.J., Journal of Applied Electrochemistry Vol.31 Issue.7 (2001), 773-779
[9] Denver Cheddie, Norman Munroe, Journal of Power Sources, Vol. 160, (2006), 299-304
[10] Denver Cheddie , Norman Munroe, EnergyConversion and Management, Vol. 47, (2006)1490-1504
[11] Anders R. Korsgaard et al., Proceedings of ASME fuel cell conference 2006 -97214
[12] Anders R. Korsgaard et al., Experimental characterization and modeling of commercial polybenzimidazole-based MEA performance, Journal of Power Sources (2006)
[13] M.Y. El-Sharkh, M. Tanrioven, A. Rahman, and M.S. Alam, Journal of Power Sources , In Press
[14] A.D. Hawkes, and M.A. Leach, Energy, In Press
[15] Michel De Paepe, Peter D'Herdt and David Mertens, Energy Conversion and Management, Vol. 47, Issues 18-19, (2006), 3435-3446
[16] G. Gigliucci, L. Petruzzi, E. Cerelli, A. Garzisi and A. La Mendola, J. of Power Sources, Vol. 131, Issues 1-2, (2004), 62-68
[17] J. Pukrushpan et al, Control Eng. Practice Vol. 14, Issue 3 , (2006), 277-293
[18] Joshua Golbert and Daniel R. Lewin, J. of Power Sources Vol. 135, Issues 1-2 , 3 (2004), 135-151
[19] Anders Korsgaard et al., J. of Hydrogen energy, Part one - Novel model of HTPEM based Micro Combined Heat and Power Fuel Cell System, inpress
[20] A.F. Mills, "Heat and Mass Transfer", 2nd edition, Richard D. Irwin INC, 1995, ISBN-10: 0256114439

Figures

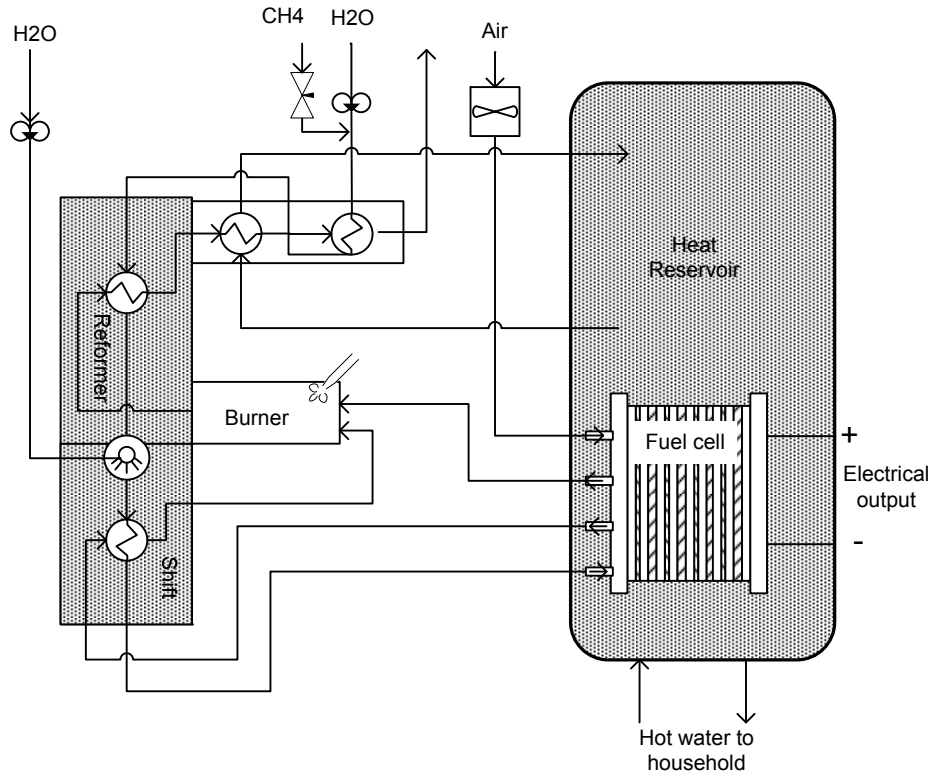

Fig 1: Overview of proposed CHP system.

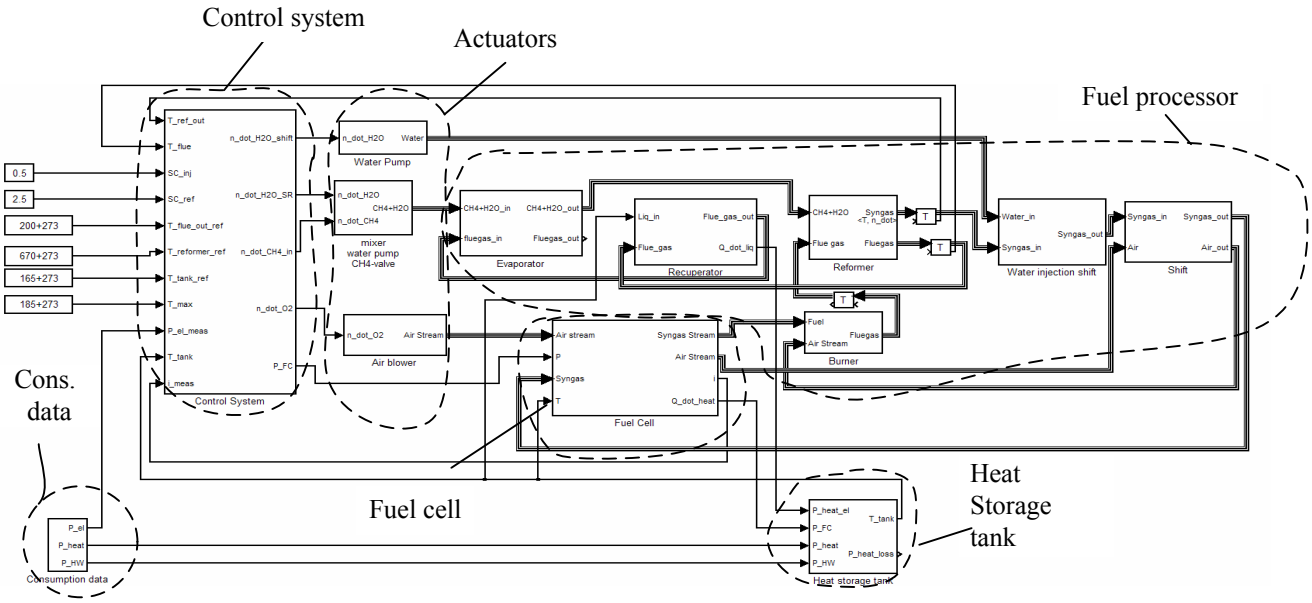

Fig 2: Overall layout of Simulink model.

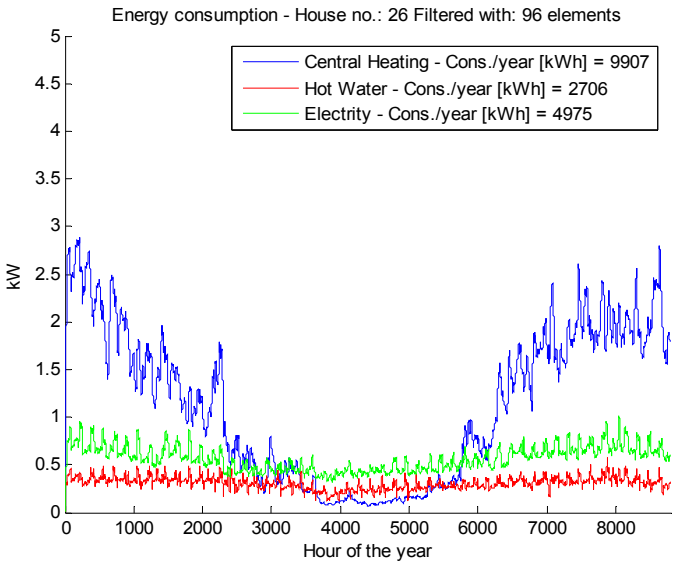

Fig 3: Heat, power and hot water consumption for the average household (house 26) in 1991.

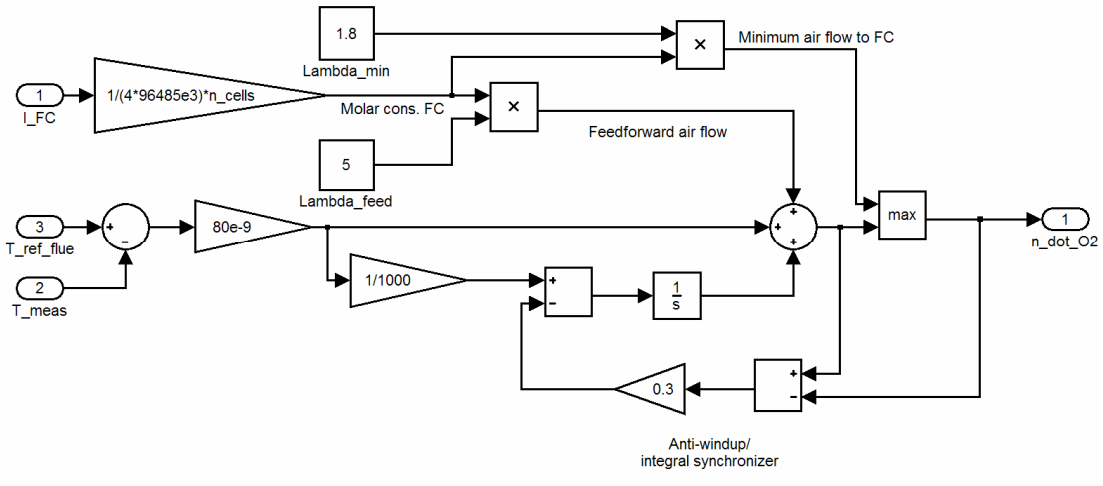

Fig 4: Control of exit flue gas temperature using air inlet flow.

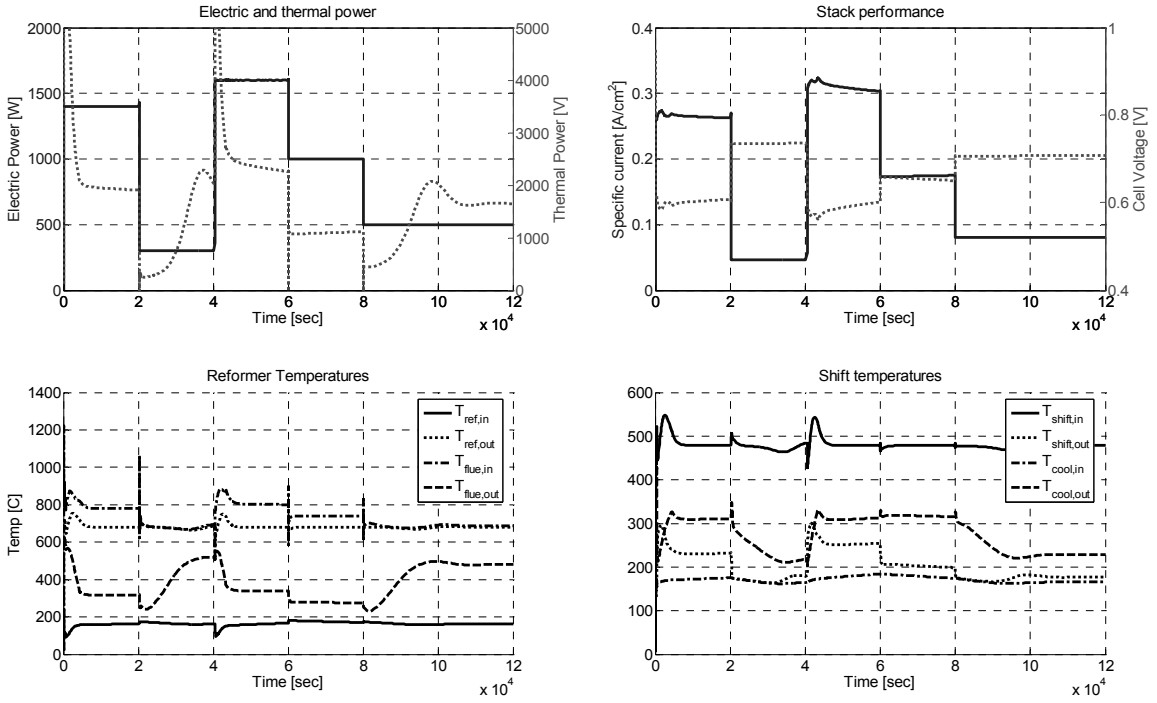

Fig 5: Transient performance of the system. Reformer set point 680°C, SC_{shift}=0.6 and SC_{ref}=2.5.

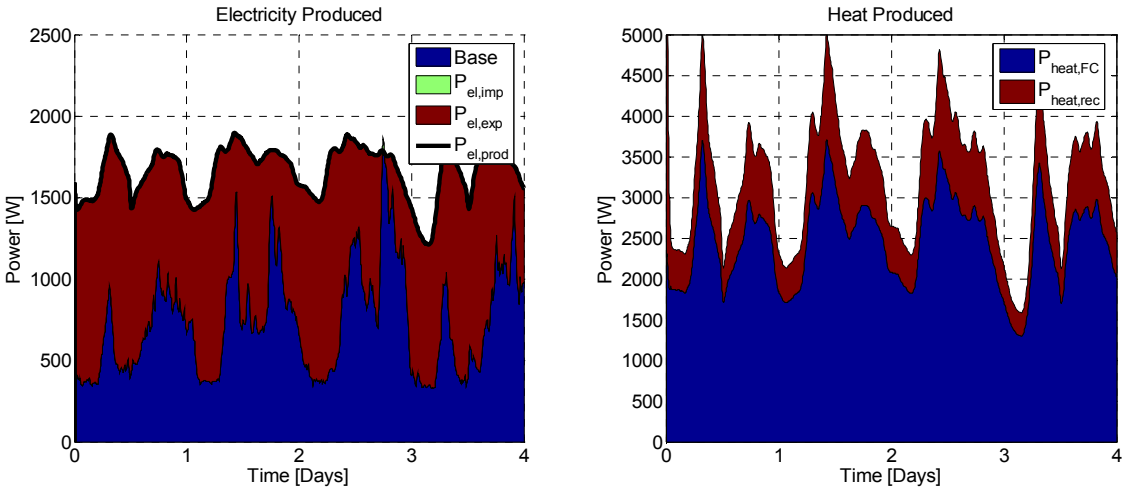

Fig 6: The first 4 days of January (Wednesday to Saturday), Heat following only.

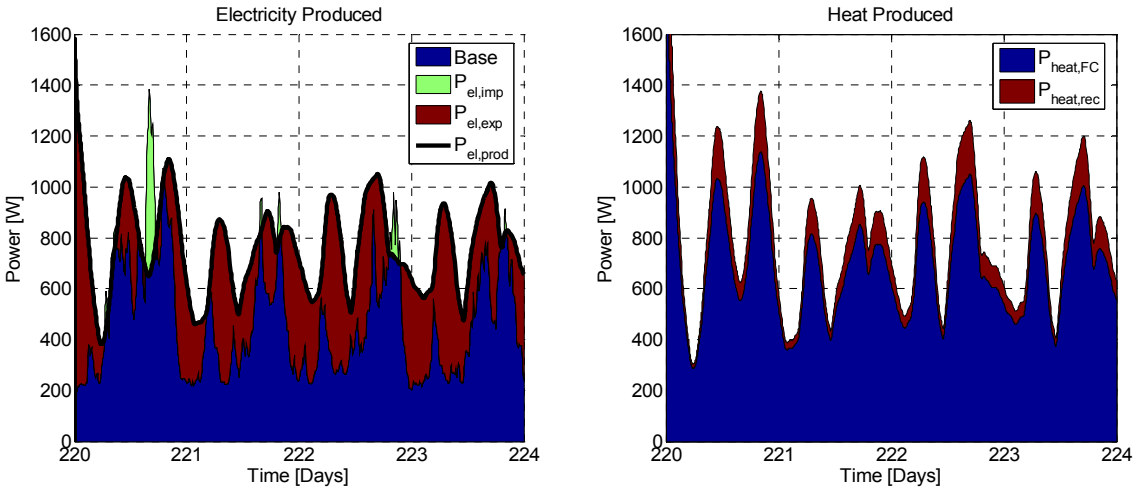

Fig 7: 2nd week of August (Thursday to Sunday), heat following only.

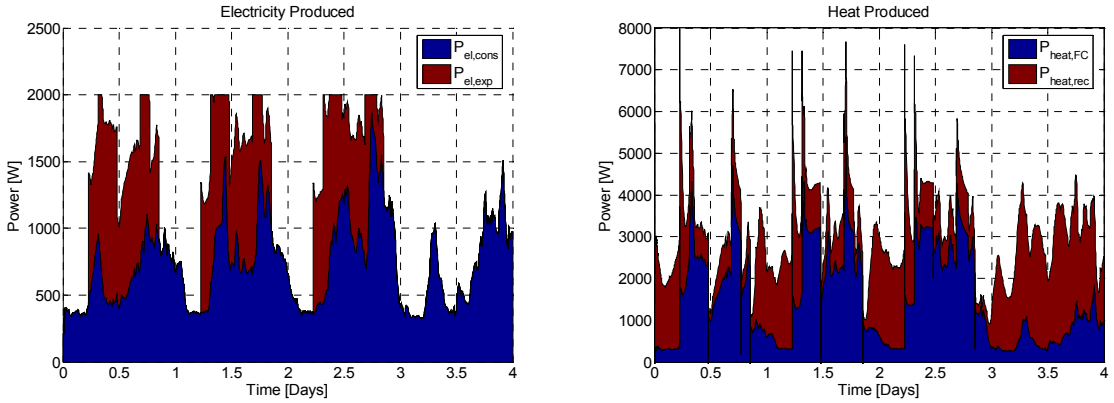

Fig 8: First 4 days of January (Wednesday to Saturday),1991. Scenario 3, heat and power following with net export during high and peak load hours.

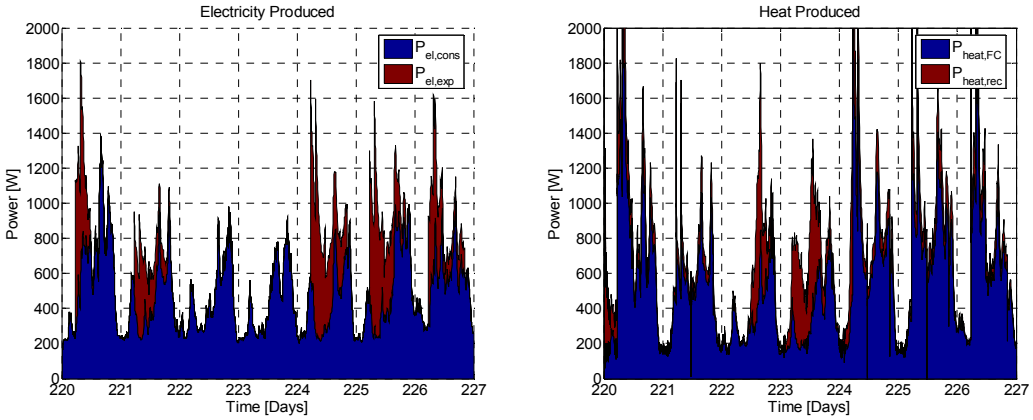

Fig 9: A week in August (Thursday to Wednesday). Scenario 3, heat and power following with net export during high and peak load hours. Note the different y-scale

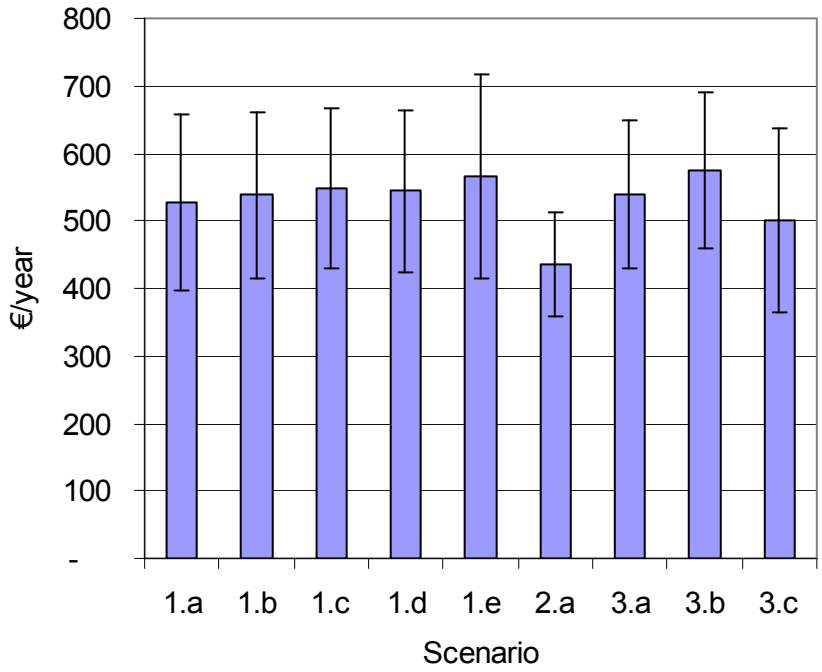

Fig 10: Shows the resulting margins of the analysis. The error bars indicate the sensitivity towards +-20% fluctuations in the natural gas price.

Description	**Price**	**Unit**
Gas price (p_{NG})	31.6	€/MWh
Energy tax ($p_{NG,energy}$)	24.6	€/MWh
CO2 tax ($p_{NG,CO2}$)	2.4	€/MWh
Transport	11.7	€/MWh
Total price, excl. taxes	43.3	€/MWh
Total price, including transport ($p_{NG,tot}$)	70.3	€/MWh

Table 1: Composition of gas price for smaller consumers (<60,000 m^3/year).

Normal working days	Low load	High load	Peak load
Winter (October – March)	21.00– 06.00	06.00 – 08.00	08.00 – 12.00
		12.00 – 17.00	17.00 – 19.00
		19.00 – 21.00	
Summer (April - September)	21.00– 06.00	06.00 – 08.00	08.00 – 12.00
		12.00 – 21.00	

Table 2: Low, high and peak load hours of the year.

	Low load [€/MWh]	High Load [€/MWh]	Peak Load [€/MWh]
C-tariff (0,4 kV-net) (P_{el})	29	65	88
Natural gas price including transport	43.3	43.3	43.3
Margin	-14.3	21.7	44.7

Table 3: Electricity sales prices and margin when exporting to the grid based on the Danish tariff structure [2006].

Scenario	Scenario	FC-factor	HST-size
1.a	HF	1	250L
1.b	HF	1	125L
1.c	HF	1	60L
1.d	HF	1	40L
1.e	HF	2	250L
2.a	H&PF	1	250L
3.a	H&PF, exp	1	250L
3.b	H&PF, exp	2	250L
3.c	H&PF, exp	1	1000L

Table 4: Scenarios to be analyzed (HF; Heat following, H&PH; Heat and power following and H&PF, exp; Heat and power following with export).

Scenario	$E_{el,prod}$	$E_{LHV,in}$	$E_{loss\ HST}$	$\eta_{tot,1,}$[1]	$\eta_{tot,2,}$[2]	η_{el}	$E_{el,imp}$	$E_{el,exp}$	E_{exp_peak}	E_{exp_high}	E_{exp_low}	$c_{ref,\ furnace}$	Margin
	kWh	kWh	kWh				kWh	kWh	kWh	kWh	kWh	€ / year	€ / year
1.a	9,334	25,173	1,075	87.1%	91.4%	37.1%	86	4,449	475	1,101	2,873	1,637	527
1.b	9,082	24,548	725	88.3%	91.2%	37.0%	133	4,245	470	1,025	2,750	1,637	538
1.c	8,978	24,198	506	89.1%	91.2%	37.1%	155	4,163	466	1,001	2,696	1,637	548
1.d	8,937	24,198	409	89.0%	90.7%	36.9%	163	4,130	465	992	2,673	1,637	544
1.e	**11,003**	26,984	1,075	87.4%	**91.4%**	40.8%	50	6,083	685	1,461	**3,937**	1,637	566
2.a	4,970	20,512	1,075	85.6%	90.9%	24.2%	-	-	-	-	-	1,637	**435**
3.a	7,282	23,318	1,075	85.2%	89.8%	31.2%	-	2,312	966	1,319	27	1,637	538
3.b	7,910	23,931	1,110	85.7%	90.3%	33.1%	-	2,940	1,208	1,691	41	1,637	**574**
3.c	8,091	25,636	2,450	80.7%	90.2%	31.6%	-	3,121	1,511	1,578	32	1,637	501

Table 5: Shows the result of scenario simulations. 1) Efficiency (LHV) not taking heat loss from the heat reservoir into account. 2) Efficiency (LHV) including heat loss from the heat reservoir, assuming it will contribute to the heating of the household.

6 Conclusion

From the introduction it is found that the CHP system should have at least the following properties:

- Have a total efficiency equal to or higher than conventional gas furnaces
- Have an electrical efficiency comparable to that of central power plants (taking the omitted transmission losses into account)
- Have a fast transient response to have a load following characteristic in relation to the power consumption of the local household
- Variable heat-to-power ratio
- Provide peak power production capability for the market
- Large turn-down ratio

A novel system concept was introduced and modeled. System level electrical efficiencies as high as 45%, at an electrical output of 666W, was obtained with a nearly instant response supporting the demands listed above. The system complexity is very low with only 4 actuators (fans and pumps) for the entire system. The system was modeled, mostly based on laboratory measurements, taking into account heat losses, limitations in heat transfer and major thermal inertias of the system.

HTPEM was chosen due to several reasons even though LTPEM has some advantages (i.e. slightly better efficiency at stack level when operated on pure H_2). Some of the major problems in the LTPEM technology include the need for humidification and condensation to obtain water balance but most of all the high sensitivity towards carbon monoxide which would need a complicated clean up system. The steam reformer type fuel processor was chosen due to the potentially high efficiency obtainable.

3 different scenarios were investigated based on the consumption pattern of 25 single family houses, the Danish tariff structure for electricity trade to the grid and current natural gas prices for private households.

The first scenario was the purely heat driven scenario where the fuel cell should deliver as much as possible of the thermal energy for the household. Electricity is produced merely as a byproduct, importing and exporting to the grid as needed. An average efficiency during the 1 year cycle was between 37-41%$_{LHV}$ mostly depending on the size of the fuel cell

The second scenario produced heat and electricity for the household on a as needed basis ultimately running in a close to island mode only using the grid as an electrical buffer. This is the scenario with the lowest margin compared to a traditional natural gas fired boiler. However it will be very simple to implement as no political decisions need to be taken.

The last scenario is based on the previous scenario but with net export during high and peak grid load situations. Up to 1kW peak power capacity was obtained in average throughout the year corresponding to 1-2 large central power plants if all 300,000 households, which currently have natural gas boilers installed, obtained micro CHP systems. The margin obtained with this scenario

was the largest of the 3 having more than 500€ reduced variable costs for natural gas than in the reference scenario with the traditional boiler.

The total efficiency was between 85-94% in all of the scenarios.

From the analysis made in this project the fuel cell technology seems indeed promising for residential combined heat and power units. Especially when taking transmission losses into account it looks like it can compete with central natural gas power plants. However there is still a lot of development to be performed to reach that level.

7 References

[1] ”Afprøvning af mikrokraftvarmeanlæg”, Elfor, Elsam, and Techwise, January 2002. Eltra PSO-F&U project

[2] ” Technology Data for Electricity and Heat Generating Plants”, Energistyrelsen, Elkraft System and Eltra, 2005

[3] AKE, sep. 19th 2006, http://www.forsyning.dk/FV/El/Boligkunder/Elpriser+boligkunder/

[4] Dong Energy, sep. 19th 2006, http://www.dong.dk/tridion/Images/dk/Naturgas_tcm49136.pdf#search=%22naturgas%20energiindhold%22

[5] Dong Energy, sep. 19th 2006, http://www.dongenergy.dk/privat/e+shop/naturgas/flexpris.htm

[6] Dong Energy, sep. 19th 2006, http://www.dongenergy.dk/erhverv/produkter/naturgas/listepris.htm

[7] Det Energipolitiske udvalg, 1997, bilag 6

[8] Det Energipolitiske udvalg, bilag 600, July 2000

[9] www.Energinet.dk, Sep. 17th 2006

[10] ADVFN.com, sep. 21st 2006, http://www.advfn.com/p.php?pid=commodities&cc=DK&refredir=1&nopu=lS%2B4mhbmSZt%2Br8NpYcZNVTzpDYDvlvZmvSELNGiM5%2FDvmA7%2F2X0rPhGDAkXakieL

[11] Dong Energy, “Produktplad for naturgas”, sep 21st 2006, https://www.dong.dk/tridion/Images/dk/FLS-032373_1_016_tcm4-12103.pdf#search=%22dong%20sammens%C3%A6tning%20naturgas%20pdf%22

[12] Elsam Engineering, FURIM project report, EU PROJECT NO. SES6-CT-2004-502782, march 2006

[13] “Staus and recent progress in SOFC development at Haldor Topsoe and Risø”, Fuel cell seminar, 2005

[14] Masashi and Tanaka, Osaka gas, 23rd World Gas Conference, Amsterdam 2006

[15] S. Caux, J. Lachaize, M. Fadel, P. Shott, L. Nicod, Journal of Process Control, volume 15, issue 4, 2005;pp 481-491.

[16] Joshua Golbert, Daniel R. Lewin, Journal of Power Sources, Volume 135, Pages 135-151.

[17] J.T. Pukrushpan, A.G. Stefanopoulou, H. Peng, Proceedings of the American Control Conference, Anchorage, Alaska, May 8–10, 2002.

[18] J.C. Amphlett, R.F. Mann, B.A. Peppley, P.R. Roberge, A. Rodrigues, J. Power Sources 61 (1996) 183–188.

[19] J.S. Yi, T.V. Nguyen, J. Electrochem. Soc. 145 (4) (1998) 1149–1159.

[20] Bernardi, D. M. & Verbrugge, M. W. 1992, "A mathematical model of the solid-polymer-electrolyte fuel cell", Journal of the Electrochemical Society Vol.139 Issue.9, pp. 2477-2491.

[21] Springer T.E., Zawodzinski T.A., Gottesfeld S, 1991, Journal of the Electrochemical Society, Vol 138 pp2334-2342

[22] Marr, C. & Li, X. 1998, "An engineering model of proton exchange membrane fuel cell performance", ARI Vol.50 Issue.4, pp. 190-200.

[23] Janssen, G. J. M. 2004, Journal of Power Sources Vol.136 Issue.1, pp. 45-54.

[24] Qi, Z., He, C., & Kaufman, A. 2002, Journal of Power Sources Vol.111 Issue.2, pp. 239-247.

[25] M.Y. El-Sharkh, M. Tanrioven, A. Rahman, and M.S. Alam, Journal of Power Sources , In Press

[26] A.D. Hawkes, and M.A. Leach, Energy, In Press

[27] Michel De Paepe, Peter D'Herdt and David Mertens, Energy Conversion and Management, Vol. 47, Issues 18-19, (2006), 3435-3446

[28] G. Gigliucci, L. Petruzzi, E. Cerelli, A. Garzisi and A. La Mendola, J. of Power Sources, Vol. 131, Issues 1-2, (2004), 62-68

[29] J.S. Wainright, J.-T. Wang , D. Weng, R.F. Savinell, M.Litt, J. Electrochem. Soc. 142 (1995) 121-123.

[30] R.F. Savinell; J.S. Wainright; M. Litt, Electrochem. Soc (1995) 214-215.

[31] J., T. Wang; R. F. Savinell; J.S. Wainright, M. Litt; H. Yu, Electrochimica Acta, 41 (1996) 193-197.

[32] Zhenyu Liu, Jesse S.Wainright, Robert F. Savinell, Chemical Engineering Science, 59 (2004) 4833-4838.

[33] J.D. Holladay, J.S. Wainright, E.O. Jones, S.R. Gano, J. of Power Sources 130 (2004) 111-118.

[34] Qingfeng Li et al., Solid State Ionics 168 (2004) 177–185.

[35] Q. Li, R. He, J.O. Jensen, N.J. Bjerrum, Fuel Cells Volume 4 Issue 3 (2004) 147-159.

[36] Qingfeng, Li; Hjuler, H.A.; Bjerrum, N.J., Journal of Applied Electrochemistry Vol.31 Issue.7 (2001), 773-779

[37] Denver Cheddie, Norman Munroe, Journal of Power Sources, In Press.

[38] Denver Cheddie , Norman Munroe, EnergyConversion and Management, In Press.

[39] Wolfgang Ruettinger*, Oleg Ilinich, Robert J. Farrauto, Journal of Power Sources 118 (2003), pp. 61–65

[40] M. Bovo and M. Mandø, "Characterization of a fuel processing unit" – M.Sc. Thesis, Aalborg University, Institute of Energy Technology, Denmark, 2006

[41] Mads Pagh Nielsen, Anders Korsgaard and Søren Knudsen Kær, "Optimization of the HEN of a reforming system", Conference paper, SIMS 2004